Chemical profiling of anti-Alzheimer's active compounds from the plant *Ficus barclayana*.

BY

Abdirahman Sharey

A thesis submitted in partial fulfilment for the requirements for the degree of Master of Science by Research, at the school of School of Pharmacy and Biomedical Sciences, University of Lancashire, Preston, UK

January 2025

Declaration

Type of Award: Master of Science by Research

School: School of Pharmacy and Biomedical Sciences

1. **Concurrent registration for two or more academic awards**

I declare that while registered as a candidate for the research degree, I have not been a registered candidate or enrolled student for another award of the University or other academic or professional institution.

2. **Material submitted for another award.**

I declare that no material contained in the thesis has been used in any other submission for an academic award and is solely my own work.

3. **Use of a Proof-reader**

The following third-party proof-reading service was used for this thesis Turnitin in accordance with the Policy on Proof-reading for Research Degree Programmes and the Research Element of Professional Doctorate Programmes.

Signature of Candidate: a.sharey

Print name: Abdirahman Sharey

Acknowledgement

First and foremost, I am grateful to my supervisor, Dr Jioji Tabudravu, for his guidance, expertise, and constructive feedback, which helped me improve my writing and complete this project. The insight and critical feedback from the chapter submitted and the research plan helped me significantly improve this project. I am grateful for their time and effort in reviewing my project, always answering my queries regarding practical work immediately, and always offering their support. I am also thankful to Shubham Sewariya, Nathanael Brockbank, Jack Robinson, Jamie Reynolds, Charles Kneale-kaye and Tanvier Khan for their time and effort in helping complete this research with their insight regarding the experimental side of the project.

I also want to thank the University of Central Lancashire for providing me with the resources and facilities to make this project possible through access to the laboratory facilities, countless journals and books. I am also grateful to the institution for allowing me to complete my master's degree during the year I've spent there. I look forward to a successful graduation in July.

I would also like to extend my gratitude to Dr David Horsley of Tau Rx Therapeutics at the University of Aberdeen, who helped screen the anti-Alzheimer bioassay of the isolated compounds from this research and sent back the results for the activity of these isolated compounds. I'd also like to thank Jeanette Andersen's research group at Maribo, UiT, The Artic University of Norway, Tromsø, for their assistance with the anti-cancer screening.

List of figures

Figure 1 shows the risks factors for AD[5]. _____ *14*
Figure 2 shows Traditional cholinesterase inhibitors. The molecular structures of (A) physostigmine, (B) tacrine, (C) donepezil, (D) rivastigmine, (E) galantamine and (F) metrifonate. _____ *18*
Figure 3 shows structures of (A) phenserine, (B) tolserine and (C) eseroline. The circle indicates the active moiety of eseroline. _____ *19*
Figure 4 shows the structure of Psoralen. _____ *21*
Figure 5 shows Acetylsalicylic acid (1), Salicin (2), Morphine (3), Digitoxin (4), Quinine (5) and Pilocarpine (6). _____ *24*
Figure 6 shows the Chemical structures of compounds from *Ficus carica*. _____ *29*
***Figure 7** shows the structure of oleanolic acid.* _____ *30*
Figure 8 shows the strategy of information-based drug discovery of natural products[40]. _____ *31*
Figure 9 shows the stages of structural elucidation strategy on natural products[54].__ *36*
Figure 10 shows the relationship between different spaces involved in natural product[60]. _____ *39*
Figure 11 shows how DEREP-NP works[61]._____ *39*
Figure 12 shows the Kupchan fractionation method[1]._____ *41*
Figure 13a-b shows the LC-MSMS$^+$ total ion chromatogram of WW fraction with 1a (top) shows the total ion chromatogram, 1b (bottom) shows the DAD1(Diode Array Detected wavelength at 330 nm)._____ *48*
Figure 14a-b shows the LC-MSMS$^+$ total ion chromatogram of the WB fraction with 2a (top) shows total ion chromatogram, 2b (bottom) shows the DAD1(Diode Array Detected wavelength is 330 nm). _____ *49*
***Figure 15** shows the structures of the known compounds in the ww fraction.* _____ *49*
Figure 16a-b shows the chromatogram of the FD4 fraction, with 16a (top) shows the LC-MS total ion chromatogram, 16b (bottom) shows the DAD1(Diode Array Detected at 330 nm). _____ *51*
Figure 17a-b shows the chromatogram of the WB4 fraction, with 17a (top) shows the total ion chromatogram, 17b (bottom) shows the DAD1(Diode Array Detected wavelength at 330 nm). _____ *52*
Figure 18a-b shows the chromatogram of FH4, with 18a (top) shows the total ion chromatogram, 18b (bottom) shows the DAD1(Diode Array Detected wavelength at 330 nm)._____ *52*
Figure 19 shows the structure of β-sitosterol identified in the FD4 fraction. _____ *53*
***Figure 20** shows the dereplicated structures of the known compounds in the semi-purified fractions using the LCMS data processed by the ACD labs software.* _____ *54*
Figure 21 shows the TIC of the FM fraction and mass spectrum of the compound eluting at retention time of 6.13 min._____ *57*
Figure 22 shows the TIC of the FH fraction and the mass spectrum of the compound eluting at the retention time of 6.15 min (922.01 is the refence mass as explained in chapter 3.5). _____ *57*

Figure 23 shows the TIC of the FD fraction and the mass spectrum of the compound eluting at the retention of time 6.13 min. _____ *58*
Figure 24 shows the TIC of the WW fraction and the mass spectrum of the compound eluting at the retention time of 12.27 min. _____ *58*
Figure 25 shows the total ion chromatogram (top), retention time at 15.82 min and the mass spectrum of the unknown compound in the FM fraction (bottom)._____ *59*
Figure 26 shows the total ion chromatogram (top), retention time at 15.77 min and the mass spectrum of the unknown compound in the FH fraction (bottom). _____ *59*
Figure 27 shows the total ion chromatogram (top), retention time at 15.81 min and the mass spectrum of the unknown compound in the FD fraction (bottom). _____ *60*
Figure 28 shows the total ion chromatogram (top), retention time at 19.82 min and the mass spectrum of the unknown compound in the WB fraction (bottom). _____ *60*
Figure 29 shows the scatter plot of ion peaks against retention time for unknown compounds in FM, FD, FH, WB and WW fractions eluted on a reversed phase C18 column. The scatter plot shows that most of the unknown compounds in the extract were non-polar (9) in nature with molecular weight between 400-700 Da. _____ *61*
Figure 30 shows the scatter plot of the unknown ion peaks in the FM7 fraction against retention time. The scatter plot indicates that most of the compounds eluted are non-polar in nature with molecular weight between 400-700 Da. _____ *64*
Figure 31 shows the scatter plot of the unknown ion peaks in the FH4 fraction against retention time with most compounds are more non-polar in nature and within the molecular weight of 300-700 Da. _____ *64*
Figure 32 shows the scatter plot of the unknown ion peak in the WB4 fraction against retention time. The scatter plot indicates that all the compounds eluted are non-polar in nature and within the molecular weight range of 300-700 Da. _____ *65*
Figure 33 shows the scatter plot of the unknown ion peaks in the FD4 fraction against retention time. The scatter plot indicates that all the compounds eluted are non-polar in nature within the molecular weight range of 200-700 Da._____ *65*
Figure 34 shows the scatter plot of the unknown ion peaks in all the purified fractions. The scatter plot indicates that majority of the compounds retained are non-polar in nature within the mass range of 400-900 Da. The data can be seen in the appendix sections on Table A5-A8._____ *66*
Figure 35 shows the ^{1}H NMR spectra of the FH4 fraction at 800 MHz in CD_3OD. ____ *67*
Figure 36 shows the ^{1}H NMR spectra of the FH5 fraction at 800 MHz in CD_3OD. ____ *67*
Figure 37 shows the ^{1}H NMR spectra of the FM7 fraction at 800 MHz in CD_3OD.____ *68*
Figure 38 shows the ^{1}H NMR spectra of the FM9 fraction at 800 MHz in CD_3OD.____ *68*
Figure 39 shows the partial structural fragments determined for compound FM7 from the 1D and 2D NMR._____ *73*
Figure 40 shows structural fragments (A-D) elucidated from FH-4 NMR data suggesting presence of glycolipids and/or amino lipids or potentially lipopeptides._____ *75*

Figure A 1 *shows the MS spectrum of the WW fraction of the identified known compound of Ficus. 100*

Figure A 2 *shows the mass spectrum $(M+H)^+$ peak of the identified compound (Rutin) in the WB fraction. 102*
Figure A 3 *shows the MS identified compound of the -sitosterol that was identified in the FD4 fraction..... 104*
Figure A 4 *shows the mass spectrum $(M+H)^+$ peak of the compound (24R)-ethylcholest-4-ene-3,6-diol that was identified in the WB4 fraction..... 105*
Figure A 5 *shows the mass spectrum $(M+H)^+$ peak of the compound Myricetin that was identified in the FH4 fraction..... 105*
Figure A 6 *shows the retention time and the mass spec of the unknown compound in the FM fraction..... 106*
Figure A 7 *shows the retention time and the mass spec of the unknown compound in the WB fraction. 107*
Figure A 8 *shows the retention time and the mass spec of the unknown compound in the WB fraction. 108*
Figure A 9 *shows the retention time and the mass spec of the unknown compound in the WW fraction..... 108*
Figure A 10 *shows the retention time and the mass spec of the unknown compound in the WW fraction..... 109*
Figure A 11 *shows the scatter plot of all the masses in the FH4 fraction of retention time against m/z using the ACD lab software..... 115*
Figure A 12 *shows the scatter plot of all the masses in the FD4 fraction of retention time against m/z using the ACD lab software..... 115*
Figure A 13 *shows the scatter plot of all the masses in the WB4 fraction of retention time against m/z using the ACD lab software..... 116*
Figure A 14 *shows the scatter plot of all the masses in the FM7 fraction of retention time against m/z using the ACD lab software..... 116*
Figure A 15 *shows the ^1H NMR spectrum of the FH4 compound at 800 MHz in CD_3OD. 117*
Figure A 16 *COSY spectrum corelations between the CH_2 group (S2) and the vinyl proton (r). 117*
Figure A 17 *COSY spectrum showing anomeric proton correlations to neighbouring proton..... 118*
Figure A 18 *HSQC spectrum showing chemical shifts of protons possible associated to peptides/amino acids..... 118*
Figure A 19 *HMBC spectrum corelations showing correlations between the methyl group (L2) and the CH_2 group (S), and the quaternary carbon to both the methyl group and the CH_2 group confirming this existence of this substructure..... 119*
Figure A 20 *HMBC spectrum showing correlations between neighbouring alkene protons to the alkyne bond. 119*
Figure A 21 *shows the ^1H spectrum of FM7 compound at 800 MHz in CD_3OD. 125*
Figure A 22 *shows the COSY of FM7 compound. 125*
Figure A 23 *shows the HSQC spectrum showing chemical shifts of protons possible associated to the five membered sugar ring..... 126*
Figure A 24 *shows the HSQC-DEPT of FM7 compound..... 126*

Figure A 25 *shows the selected HMBC correlations for proposed structure of the partial structure of FM7.* *127*
Figure A 26 *shows the ROSEY of FM7 compound.* *127*

List of Tables

Table 1 *shows the samples that were active for the anticancer screening.* _____ *77*
Table 2 *shows the results of the fractions for the B50 assay.* _____ *79*
Table 3 *shows the reference compounds used for the B50 assay* _____ *81*

Abbreviations

Solvents

Methanol	MeOH
Deuterated methanol	MeOD
Dichloromethane	DCM
Acetonitrile	ACN

Analytical techniques

Nuclear magnetic resonance	NMR
Ultraviolet	UV
Heteronuclear single bond quantum	HSQC
Heteronuclear multiple bond coherence	HMBC

Abstract

This research project involves the chemical profiling of anti-Alzheimer's active compounds from the Fijian plant, *Ficus barclayana* using advanced chromatography, mass spectrometry and NMR techniques. A potentially new compound with possible anti-Alzheimer's properties has been previously isolated from *Ficus barclayana*, which has been shown to reduce tau protein aggregation. Tau protein aggregation in the brain is a hall mark of Alzheimer's disease. The compound which has never been identified was initially extracted and isolated from the plant using methanol and dichloromethane, and semi-purified using a modified Kupchan[1] liquid-liquid partitioning scheme, with further purifications by HPLC and analysed by HR-LCMS and NMR. Due to low amount of sample, the compound could not be identified. This work is a follow up of that initial project where extracts from the same plant genus have been received from the Fiji Islands and was repurified using bioassay guided fractionation to get the target compounds in good yield so that structural analysis and tau-aggregation inhibition assays can be completed. Tau aggregation inhibition assay was carried out at Tau Rx Therapeutics, Aberdeen. There was a total of 382 masses found from the Kupchan fractions of FH, FD, FM, WW and WB, and 88 masses found in the pure compounds, which had a quality score of more than 40%, as shown in the appendix section Table A16-A19. Six compounds showed activity for the anti-cancer and anti-Alzheimer's screening, as shown in Chapter 4 in Tables 3 and 4, with compound FH5 being the most active. Two compounds were dereplicated through 1D and 2D NMR analysis with a partial structure proposed as shown in Chapter 4 as Figures 33 & 34. Further purification methods, such as HPLC, need to be performed to determine the complete structures of these compounds.

Table of Contents

Declaration 2

Acknowledgement 3

List of figures 4

List of Tables 7

Abbreviations 8

Abstract 9

CHAPTER ONE 13

1.0 Introduction 13

1.1 What is Alzheimer's disease 13

1.2 Symptoms/diagnosis of AD 14

1.3 Treatments of AD 16

1.4 Bioassay 19

1.5 Research statement 20

1.6 Aim and Objectives 21

CHAPTER TWO 22

2.0 Literature review of Ficus 22

2.1History of natural products for drug discovery 22

2.2 Challenges of natural products drug discovery 25

2.3 Advantages of natural products for drug discovery 25

2.4 Anticancer screening 26

2.5 Historical background of Ficus 27

2.6 Historical background and research of *Ficus barclayana* 29

2.7 Strategies for drug discovery in natural products 30

2.7.1 Berberine 32

2.7.2 High throughput screening (HTS) 32

2.7.3 High-content screening 33

2.7.4 Computer-aided drug development 33

2.8 Structural elucidation techniques 34

2.8.1 Spectroscopic analytical techniques 34

2.8.2 Natural product database 36

2.9 Dereplication of natural products 37
CHAPTER THREE 40
3.0 Methods 40
3.1 Sample collection and extraction 40
3.2 Kupchan fraction 40
3.3 Size exclusion chromatography (SEC) fractionation and isolation 41
3.4 Nuclear magnetic resonance (NMR) 42
3.5 Liquid Chromatography-mass spectrometry (LC-MS) 43
3.6 Data processing 44
3.7 Dereplication process 44
3.7 Bioassay 45
3.8 ACD Labs 45
CHAPTER FOUR 46
4.0 Results and Discussion 46
4.1 In-house library 46
4.2 Data processing and dereplication 46
4.2.1 Dereplication of the crude extracts 47
4.2.2 Elucidation of the pure compounds 50
4.2.3 Identification of compounds isolated from the Kupchan fractions 55
4.2.4 Elucidation of unknown compounds of the pure compounds 62
4.3 Dereplication by NMR 66
4.3.1 Dereplication through 1D-NMR and 2D-NMR for structural determination of compound FM7 69
4.3.2 Dereplication through 1D-NMR and 2D-NMR for structural determination of compound FH4 74
4.4 Bioassay results 76
4.4.1 Anti-cancer screening 76
4.4.2 Anti-Alzheimer's screening 78
CHAPTER FIVE 83
5.0 Conclusion 83
5.1 Limitations 84
5.2 Future wok 85
References 87
Appendix 93
1.0 In-house library of known compounds of Ficus. 93

2.0 Bioassay _____97
2.1 Anti-Alzheimer's bioassay _____97
2.2 Anti-cancer screening _____99
3.0 LCMS _____100
4.0 NMR _____117
4.1 1D and 2D NMR spectrum of compound FH4. _____117
4.2 1D and 2D NMR spectrum of compound FM7 _____125

CHAPTER ONE

1.0 Introduction

This chapter will cover what Alzheimer's disease (AD) is, the symptoms and diagnosis of Alzheimer's disease, and the treatment of Alzheimer's disease. It will also cover what bioassay is and why it is important.

1.1 What is Alzheimer's disease

Alzheimer's disease is a brain disorder that gets worse over time. It is characterised by changes in the brain that lead to deposits of specific proteins, causing the brain to shrink and brain cells to die. Alzheimer's disease is the most common cause of dementia, which causes a gradual decline in memory, thinking, behaviour and social skills[2]. Alzheimer's disease is defined by the formation of intraneuronal neurofibrillary tangles, which the tangles are formed by tau protein, which accumulates in neurodegenerative disorders. Alzheimer's is defined by the formation of intraneuronal neurofibrillary tangles, which accumulate to form paired helical filaments (PHF) or related straight filaments [3]. The Tau protein is a microtubule-binding protein accumulating in neurodegenerative disorders like frontotemporal dementia and Alzheimer's. The accumulation of tau protein correlates with neuron loss and memory deficits, which are called tauopathies[4]. There are currently 50 million AD patients around the world, with this figure projecting to double every 5 years, reaching 150 million AD patients by 2050[5]. The economic and human costs of AD represent a global burden costing around 1 trillion US dollars annually, whilst being a burden on the individuals affected AD and their families[5].

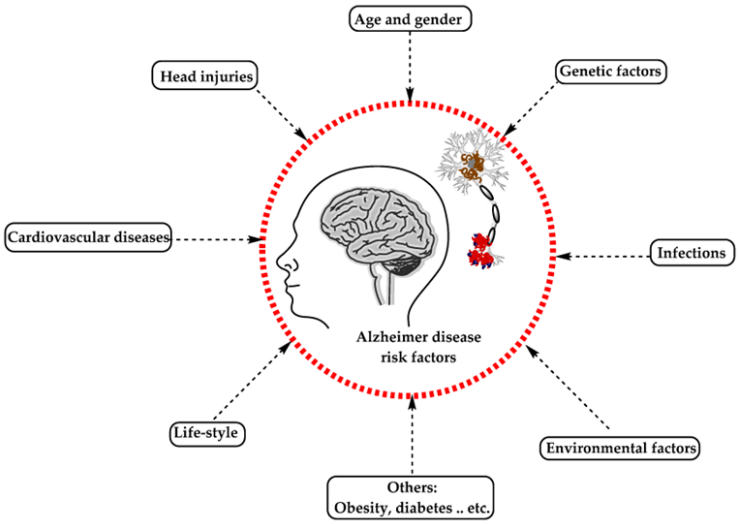

Figure 1 shows the risks factors for AD[5].

1.2 Symptoms/diagnosis of AD

Diagnosing a patient with Alzheimer's Disease (AD) involves a series of assessments, including magnetic resonance imaging (MRI) to assess neurons, neurological examinations, and laboratory tests such as complete blood count, thyroid function tests, and vitamin B12 levels. Optional laboratory examinations, such as sedimentation rate or urine drug screening, may be performed[6]. Studies suggest that vitamin B12 deficiency is strongly associated with neurological disorders and an increased risk of AD. Diagnosing B12 deficiency involves measuring serum B12 levels, serum homocysteine, and an extensive blood count[4]. The clinical diagnostic criteria for AD were introduced in 1984 by the National Institute of Neurological and Communicative Disorders and Stroke (NINCDS), which formed a workgroup with the Alzheimer's Disease and Related Disorders Association (ADRDA) (NINCDS-ADRDA)[5]. This criterion was updated in 2011 with two categories of AD biomarkers. The first category contains

markers of brain amyloids, detected by positron emission tomography (PET) and cerebrospinal fluid (CFS) analysis. The second includes markers of neuronal damage such as cerebrospinal fluid tau, magnetic resonance imaging (MRI) to measure atrophy and fluorodeoxyglucose (FDG) to measure metabolic activity[4]. Alzheimer's Disease is clinically classified into four stages: (1) pre-clinical, (2) the mild/early stage of AD, (3) moderate AD stage, and (4) severe AD or late stage[5]. The pre-clinical stage can last several years and is characterised by mild memory loss and early pathological changes in the hippocampus and cortex[5]. At this stage, daily activities, clinical signs, and symptoms of AD are unaffected. Symptoms show up during the early or mild stage through disorientation of place and time, loss of memory, loss of concentration, and the development of depression in a patient's daily life[5]. As AD progresses to the moderate stage, the disease spreads to the cerebral cortex area, which causes increased memory loss, impaired impulse control, and challenges with reading, speaking, and writing. This causes a cognitive impairment in which the AD patient cannot recognise family members, thus leading to the patient's death because of difficulties in swallowing, urinating, and becoming bedridden[5].

AD involves two types of neuropathological changes, positive and negative lesions, which both provide symptoms and disease progress. The positive lesions are caused by an accumulation of neurofibrillary tangles, amyloid plaques, dystrophic neurites, neuropil threads, and other deposits found in the brains of AD patient[7]. The negative lesions are characterised by the loss of neural, neuropil, and synapses found in AD patients. The synaptic loss is a result of axonal transport defects, oxidative stress, and mitochondrial damage, which contribute to minor fractions such as the build-up of Aβ and tau at the synaptic sites[8]. Therefore, dendritic spines, pre-synaptic terminals and

axonal structures are eventually lost. While the underlying causes of pathological changes in AD are still unknown, two primary hypotheses have been proposed, the first suggesting that there is an impairment in the cholinergic function, a risk factor in AD. In contrast, the second hypothesis is an alteration in amyloid β-protein production and processing[9].

1.3 Treatments of AD

The treatment of AD includes two classes of drugs, which are antagonists to *N*-methyl d-aspartate (NMDA) and inhibitors to cholinesterase enzymes, which are both effective at treating AD symptoms but not good enough to cure or prevent them. The cholinergic hypothesis states that AD is primarily caused by a decrease in acetylcholine (Ach) synthesis, as this can be used to enhance the cholinergic levels in the brain by suppressing the biological activity of acetylcholinesterase (AChE)[10]. Therefore, these drugs inhibit AChE, breaking down Ach, allowing the AChE inhibitors to increase the concentration of ACh, which increases the function of neural cell[10]. The four commonly prescribed drugs to treat AD are Donepezil, galantamine, rivastigmine, and memantine as they have been developed from cholinesterase enzyme (ChE) [10]. At higher doses, the effectiveness of the drugs becomes limited and dose-associated side effects are shown. Donepezil is used to treat mild to moderate AD and was approved in 1996, whilst presenting side effects such as insomnia, diarrhoea, muscle cramps and muscle weakness[10]. Donepezil works at the molecular and cellular levels in all the pathogenesis stages of AD and the neurotransmitter level. This includes inhibiting glutamate-induced excitotoxicity and reducing oxidative stress-induced effects[10]. The key issue with donepezil is its inability to interact with the oxyanion hole or the catalytic triad. Phenserine, tolserine, and eseroline are derived from Physostigmine and

are the next-generation ChE inhibitors. Phenserine showed moderate success when tested for AD, as it improved memory and learning in aged dogs and rats during initial phase clinical trials[10]. Phenserine was used to treat AD because of its dual anti-Aβ and anti-AChE effects. It was also used to treat cognitive impairments induced by traumatic brain injury in mice in 2016 [11].

The difference in structure between phenserine and tolserine is the presence of the 2-methyl group in its phenylcarbamoyl moiety, as shown in Figure 3. Tolserine has a higher potency against hAChE than phenserine or Physostigmine, with the side effects or benefits of tolserine unclear in clinical and preclinical models[12]. Eseroline is a metabolite of Physostigmine, and its effects on AChE inhabitation are limited and reversed compared to physostigmine[12]. The cyclic alkyl carbamate derived from eseroline, shown in Figure 3, is effective against AChE with higher selectivity than BChE[13].

The other treatment for AD is N-methyl d-aspartate (NMDA) antagonists as it has a role in the pathophysiology of AD, with its stimulation resulting in Ca^{2+} influx that activates signal transduction, and the gene transcription is triggered for the formation of long-term potentiation (LTP) [14]. Long-term potentiation (LTP) formation is important due to synaptic neurotransmission, plasticity, and memory formation. The major component of neurofibrillary tangle (NFT) is tau, which has a role in the pathological of AD, as tau (axonal protein) is engaged in the stability of microtubules and the regulation of synaptic functions[14]. Tau is needed for the induction of long-term depression (LTD) and the activation of the postsynaptic density (PSD) for Fyn-mediated NMDAR[14]. Overactivation of NMDARs leads to overstimulation of glutamate and abnormal levels of Ca^{2+}, which leads to a decline in cognitive functions and the death of

neural cells[14]. The glutamate-induced excitotoxicity is inhibited by the reduction of tau, as confirmed by the study, whereas it is exacerbated by overexpression of tau [15]. Most of the NMDAR uncompetitive antagonists sent to trials have mostly been failures because of their lower efficacy and side effects, with memantine the only approved drug used to treat AD from this category[14].

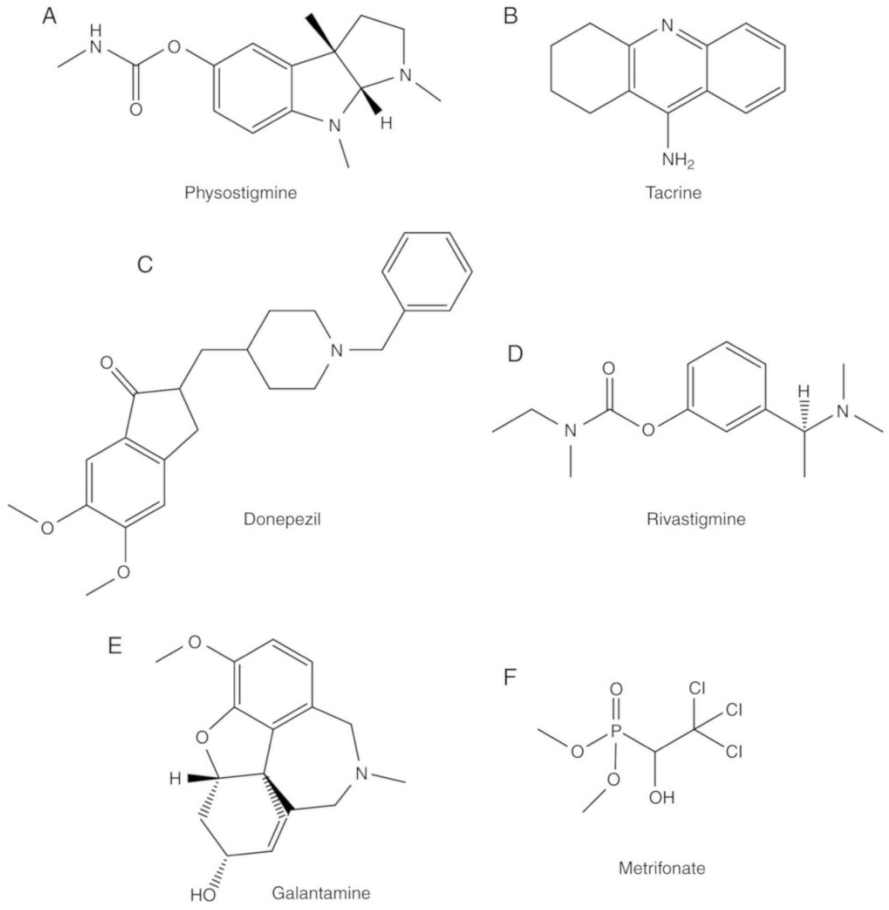

Figure 2 shows Traditional cholinesterase inhibitors. The molecular structures of (A) physostigmine, (B) tacrine, (C) donepezil, (D) rivastigmine, (E) galantamine and (F) metrifonate.

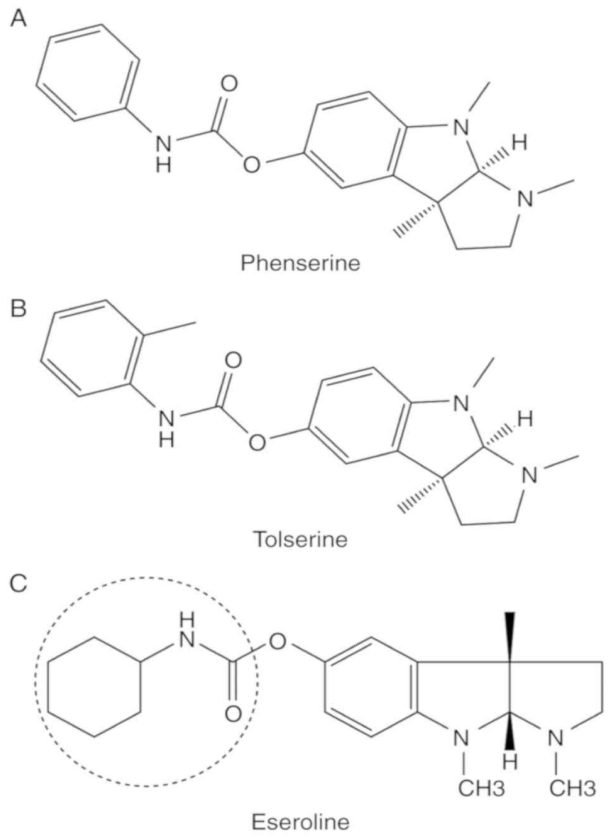

Figure 3 shows structures of (A) phenserine, (B) tolserine and (C) eseroline. The circle indicates the active moiety of eseroline.

1.4 Bioassay

Biological assay or bioassay is defined as "Analysis (of a drug) to quantify the biological activity or activities of one or more components by determining its capacity to produce an expected biological activity on a culture of living cells (in vitro) or on test organisms (in vivo), expressed in terms of units" [16]. The bioassay can be performed directly or indirectly; as with the direct assay, the response must be distinct and unambiguous, with the exact amount of the substance required for a response that can be measured and recorded[16]. As for the indirect bioassays, the magnitude of responses for nominally

equal reference concentration and test preparations are compared instead of just testing the reference concentration required for a specific response[16]. In-vivo, *in-vitro*, and ex-vivo are some of the employed bioassay methods. In vivo, study involves testing living subjects such as animals, plants, or cells, whereas *in vitro* refers to experiments with one on cells, tissues or biological components removed from the living organism(s) of interest[17]. Ex-vivo is the medical procedure where an organ, cells, or tissues are taken away from a living body for treatment, which is then returned to the living body[18].

The biological activity or potency is the specific ability of a product to achieve a defined biological effect, which is considered a critical quality attribute (CQA) [19]. The potency assay is crucial for the development of registration[19]. The IC_{50} is the half-maximal inhibitory concentration used for *in-vitro* measures to evaluate the therapeutic potential of a monoclonal antibody or ligand trap[20]. This means it shows how much of a specific pharmacologic agent is required to inhibit a given biological activity by half, relying on whole cell systems to obtain IC_{50} values[20]. The IC_{50} values give potency information, which is required for evaluating therapeutics that target pathways with few components[20].

1.5 Research statement

Natural products hold many attractive properties for pharmaceutical use, such as being a starting point for further drug development or the creation of new medicines. *Ficus barclayana* is a species of the Fig tree, native to tropical regions of Asia, particularly in Fiji, and belongs to the Moraceae family. Some examples of compounds previously isolated are psoralen (Figure 4), isoflavonoids, flavonoids, tannins and terpenoids. *Ficus barclayana* is a tree-like plant from Fiji, belonging to the Moraceae family, and it has

medicinal properties, such as relieving stomach pains and treating sore legs, swellings, and inflamed eyes. *Ficus barclayana* extract and compounds have been shown to inhibit tau aggregation in unpublished previous works. This project will review all the samples worked up before and new samples received from Fiji to identify active components. The project involves close collaboration with TauRx Therapeutics (industrial partner) for biological assays and testing of extracts, fractions, and individual components to identify the active compounds and their potential activity mode.

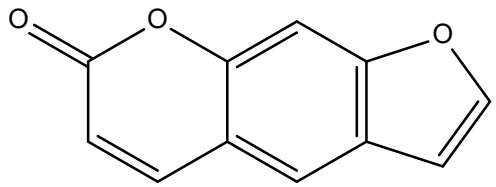

Psoralen

Figure 4 shows the structure of Psoralen.

1.6 Aim and Objectives

The aim of this research is to chemical profile the anti-Alzheimer active compounds from the plant *Ficus barclayana*. The objective of this research is to:

1. To fractionate crude extracts of *Ficus barclayana* using liquid-liquid partitioning techniques

2. To chemically profile compounds in fractions using ^{1}H NMR and high-resolution mass spectrometry

3. To determine chemical structures of pure compounds using LC-HRMS/Ms and 1D and 2D NMR if compounds deemed pure enough

4. To screen extracts and pure compounds for tau-aggregation inhibition activity

CHAPTER TWO

2.0 Literature review of Ficus

The aim of this chapter is to review the literature on medicinal plants in general and on Ficus, as well as the work that has already been carried out.

2.1History of natural products for drug discovery

The background of the uses of natural products for medical uses was discovered through natural sources, such as plants, animals or micro-organisms, and precedes recorded human history by thousands of years[21]. Natural products for medicine and health have been vital for humans since their early ancestor's days, as they chewed on herbs to relieve pain[21]. There are six classes of new chemical entities (NCEs): botanical sources, fungi, bacteria, and marine sources[22]. Modern pharmaceutical chemists added two categories of man-made substances: synthetic chemistry and combinatorial chemistry[22]. One of the most used pain relief drugs in the world is Acetylsalicylic acid (Aspirin), which is found in the bark and leaves of the willow and many other popular trees[23]. The ancient Sumerians and Egyptians, along with Hippocrates, Celsus, Pliny the Elder, Dioscorides, and Galen, utilised natural products as remedies for pain, fever, and inflammation[23]. In 1763, Edward Stone reported the first successful clinical trial of the treatment of malarial fever with the willow bark[23]. Aspirin, when synthesised from salicylic acid through acetylation with acetic anhydride, appears odourless and colourless to white crystals [24].

After the synthesis of Aspirin, Salicin (2) is isolated from the bark of the willow tree Salix alba L[25]. Morphine (3) was derived from the plant *P. somniferum*, which was boiled in acetic anhydride to yield diacetylmorphine (heroin) and converted to codeine

[25]. Digitoxin (4), derived from the plant *Digitalis purpurea* L. (foxglove), is used in this method for the management of congestive heart failure and improving the strength of cardiac contractibility[25]. The antimalarial drug quinine (5) is also isolated from the bark of *Cinchona succuba* Pav. Ex Klotsch has been used for centuries to treat malaria, fever, and cancer[25]. Pilocarpine (6), found in *Pilocarpus jaborandi* (Rutaceae), is an L-histidine-derived alkaloid used to treat glaucoma for over 100 years[25].

Another example of a natural product used for drug discovery comes from the work carried out by Friedrich Wilhelm Sertürner, a German pharmacist who isolated morphine from opium as it was the first pure, naturally derived medicine in1805 [21]. Purified natural products are preferred over crude extracts as ingredients to make drugs, and the elucidation of the molecular structures is preferred over isolating them from natural sources, which reduces the cost of drug production[21]. Because of Friedrich's work, 60% of the readily available drugs, such as "s.artemisinin, camptothecin, lovastatin, maytansine, paclitaxel, penicillin, reserpine and silibinin", were derived from natural products directly or indirectly[26]. Many natural products contribute to human health due to the long history of co-evolution within biological communities, which is the "interacting organisms that evolved in close proximity to one another developed compounds that could influence the biological processes of neighbouring species" [21]. The advantage of these compounds is that they can become a trait that natural selection could act on, thus improving and retaining throughout evolution. For example, certain plant chemicals have evolved to defend against herbivores, and they are now utilised in humans as laxatives, emetics, cardiotonic, or muscle relaxant [27].

Figure 5 shows Acetylsalicylic acid (1), Salicin (2), Morphine (3), Digitoxin (4), Quinine (5) and Pilocarpine (6).

2.2 Challenges of natural products drug discovery

Natural products have problems such as molecular complexity, poor water solubility, poor absorption, poor distribution, poor metabolism, low bioavailability, and poor stability. Natural products have complex and highly intricate structures that can be difficult to synthesize or modify chemically; for example, the bulk stability of isolated products may be inadequate[28]. Another limitation is that isolating a natural product from its natural source, purifying it, and performing subsequent bioassay is expensive and time-consuming [29]. A further limitation would be that the stability of natural products within their source organism may affect the identification, isolation and purification of bioactive molecules for application in drug discovery [29].

2.3 Advantages of natural products for drug discovery

The advantages of natural products in drug discovery outweigh their limitations. They provide both chemical diversity and biological potency, with the resources remaining unexplored from the marine environment[30]. As recent reviews have shown, natural products have a hit rate that is 100 times higher than that of synthetic compounds[30]. Natural product databases contain more scaffolding, which has a proportion of ring systems not found in other drug databases. This promises new starting points in drug discovery[30]. Additionally, combining biotransformation techniques, combinatorial biosynthesis, and combinatorial chemistry further improves the structural diversity of natural product libraries[30]. The manipulation of natural product biosynthesis can yield new derivatives with good qualities and quantities, which impacts our understanding of natural product production[30].

Natural products have contributed to discovering and understanding the targets and pathways involved in disease processes. For instance, the protein-protein complexes β-catenin in the WNT pathway and HIF-1/p300 have been validated as anticancer targets and pathways[30]. Natural products present additional drug targets that can be identified and exploited in these pathways. For example, the discovery of aspirin's anti-inflammatory mechanism of action led to the identification of the cyclooxygenase isozymes COX-1 and COX-2[30].

Many microbial natural products have entered the market without needing any chemical modifications[30]. Examples include the antibacterial agents erythromycin A, vancomycin, penicillin G, streptomycin, and tetracycline, as well as the antifungal agents amphotericin B and griseofulvin[30]. These examples show the capability of microorganisms to produce small molecules that resemble drugs[30].

2.4 Anticancer screening

Historically, anticancer screening strategies were used in vitro assays to identify agents with nonspecific growth-inhibitory or cytotoxic activities. In contrast, modern approaches screen for specific pharmacological properties using high-throughput technologies[31]. This means that drugs are now selected based on their pharmacological mechanism of action, such as molecular targets specific to cancer cells, which are not present in normal tissues and can be identified and used to screen drug libraries[31]. The advantage of the MTT assay is its accuracy, rapidity, and relative simplicity, which makes it commonly used in cytotoxicity studies [32]. The MTT assay used in this experiment is a colorimetric viability assay based on enzyme reduction the MTT molecule to formazan when it is exposed to viable cells[32]. There is a colour change of the MTT molecule when the outcome is a reduction, and absorbance measurements

relative to a control determine the percentage of remaining viable cancer cells[32]. The treatment has varying concentrations of a tested compound that is translated to the compound anticancer activity and its IC_{50} values[32].

The MTT colorimetric assay is conducted in a 96-well plate format, as the cells may require preincubation depending on cell line properties, which can vary from 0-24 hours before the addition of the tested drug[32]. The MTT solution is then added to the treated cells, where the yellow MTT is reduced to purple formazan by mitochondrial and cytosolic enzymes that are active in viable cells. The absorbance indicates the amount of viable cells which remained after treatment with the drug and is compared to the absorbance of control cells not exposed to the drug, with the drug analysed by software that provides the IC_{50}[32].

2.5 Historical background of Ficus

The Genus *Ficus* has about 900 species of trees, shrubs, and vines that belong to the family of Moraceae, primarily native to tropical areas of East Asia[33]. There are 500 Ficus species in the Asian–Australasian region, whereas the Ficus species are fewer in Africa and the Neotropics, with approximately 110 and 130 species, respectively[34]. *Ficus carica Linn* is the most popular member of the genus *Ficus*, which is native to the Sub-Himalayan tract, Bengal, and central India. It is known by more than 135 names[34]. It's used to cure diabetes and respiratory, gastrointestinal, reproductive, and infectious diseases[34].

Phytochemicals are chemicals that plants produce, and they contain coumarins, flavonoids, sterols, triterpenoids, and anthocyanins in various parts of the plan[35]. The phytochemical research of *Ficus carica* led "to the isolation of phytosterols,

anthocyanins, amino acids, organic acids, fatty acids, phenolic components, hydrocarbons, aliphatic alcohols, and volatile compounds", as shown in Figure 6[35]. The phytoconstituents of *Ficus carica* are used in producing sunscreen and colouring agents as they also show pharmacological properties such as antioxidant, anticancer, and anti-inflammatory [35]. Rubnov et al. 2001 reported that a mixture of 6-O-acyl-β-D-glucosyl-β-sitosterol found in *Ficus carica Linn* resin was the potent cytotoxic agent for anticancer activity[36]. The natural and synthetic compound in vitro inhibitory affected various cancer cell lines[36].

Extracts from the fruits, roots, and leaves of *Ficus* have been widely used in traditional medicine as they are biologically active against metabolic, gastrointestinal, respiratory, inflammatory, and cardiovascular disorders, as reported in studies[35]. Yang et al., 2010 developed a method from the leaves of *Ficus carica Linn.* to study the ultrasonic-assisted extraction of total flavonoids for activities against the hydroxyl and superoxide anion free radicals[37]. Also, Yang et al., 2010 took figinI and figinII from the leaves of the fig with an antifungal activity using ion exchange chromatography from the lower molecular weight extract of *Ficus carica Linn* leaves, which had antibacterial and antifungal activities against different types of microorganism[37].

In the study of Patil et al. 2011, he reported that the extracts from the leaves of *Ficus carica Linn* showed anti-inflammatory effects for the petroleum ether (PEE), chloroform (CE), and ethanol (EE) extracts[38]. The study used carrageenan-induced rat paw edema and cotton pellet granuloma that exhibit maximum anti-inflammatory effects of "75.90% in acute inflammation, and chronic studies showed a 71.66% reduction in granuloma weight"[38]. The petroleum ether (PEE), chloroform (CE), and ethanol (EE) extracts showed more anti-inflammatory effect than the standard drug Indomethacin,

as these extracts showed “reduced carrageenan-induced paw edema and cotton pellet granuloma in rats[38].

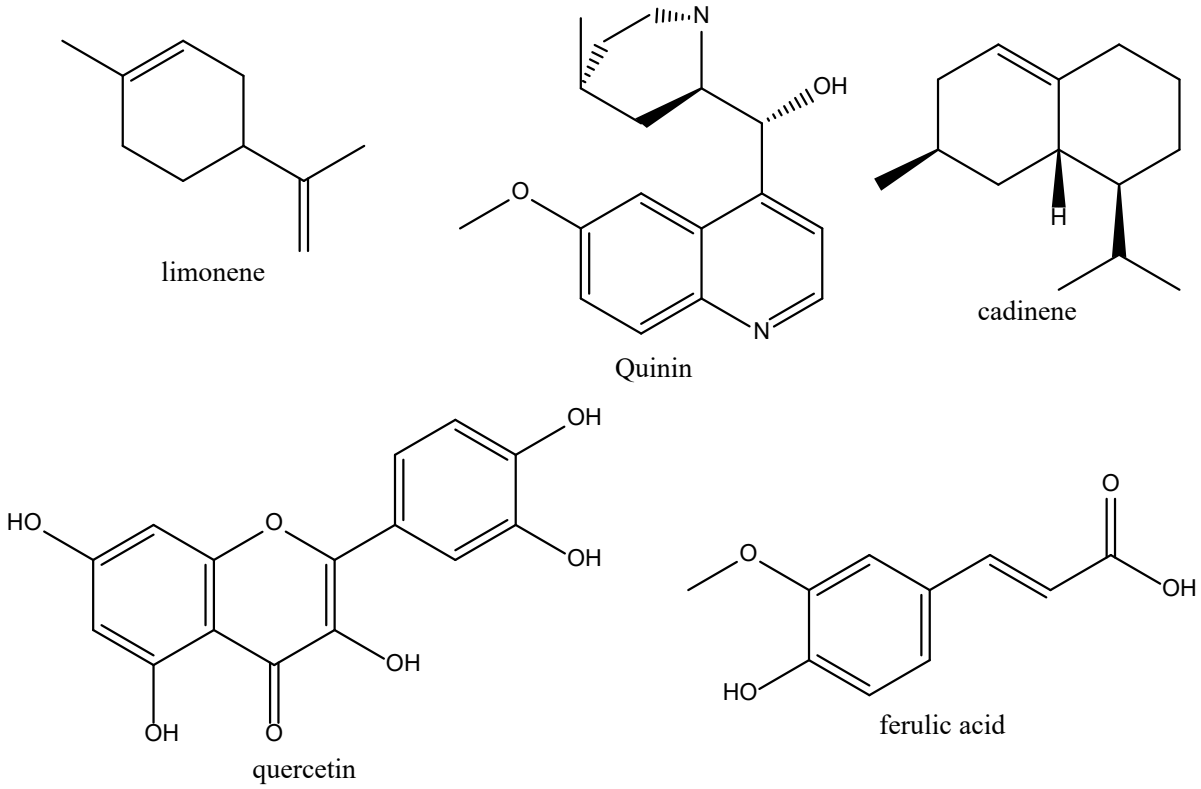

Figure 6 shows the Chemical structures of compounds from *Ficus carica*.

2.6 Historical background and research of *Ficus barclayana*

Ficus barclayana is a species of the Fig tree, native to tropical regions of Asia, particularly in Fiji and it belongs to the Moraceae family. Some examples of compounds previously isolated are psoralen which has shown moderate to strong inhibitory activity against AChE, isoflavonoids, flavonoids, tannins and Triterpenoids such as oleanolic acid as shown in figure 7.

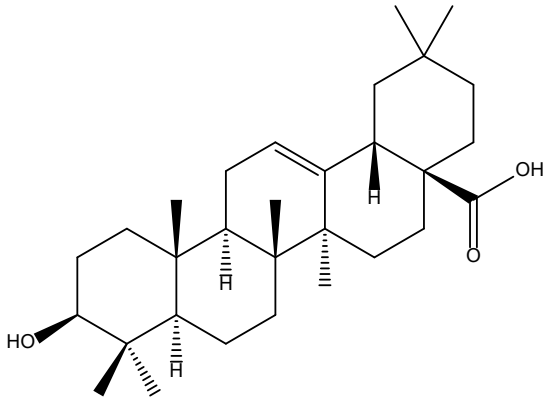

oleanolic acid

Figure 7 shows the structure of oleanolic acid.

Ficus barclayana is a tree-like plant from Fiji, belonging to the Moraceae family which has medicinal properties, such as relieving stomach pains and treating sore legs, swellings, and inflamed eyes. *Ficus barclayana* extract and compounds has been shown to inhibit tau aggregation in unpublished previous works. This project will relook at all the samples worked up before and new samples received from Fiji to identify active components. The project involves close collaboration with Tau Rx[39] Therapeutics (industrial partner) for biological assays and testing of extracts, fractions, and individual components to identify the active compounds and their potential mode of activities.

2.7 Strategies for drug discovery in natural products

The primary strategy for drug discovery is to isolate, extract, and purify the samples, as it happened for the first time in 1806, which was the beginning of natural products of the chemical stage when the monomer of morphine was isolated for the first time from the poppy [40]. Firstly, the samples are to be collected and then extracted using solvents that depend on the type of compound based on solvent polarities. Next is the

fractionation step, where samples with similar polarities or molecular sizes from the extracts are grouped using techniques such as column chromatography, solid phase extraction (SPE), liquid-liquid extraction such as Kupchan method[1] and size exclusion chromatography (SEC)[41]. The extracts are then tested for pharmacological activity, with positive results, leading to isolating the lead compound from the extract for further drug development[40]. More natural products have been isolated from medicinal plants, such as caffeine in 1821, nicotine in 1828, and atropine in 1831 [40]. In the 1940s, Robert Burns was the first to introduce a physical means of identifying the structure of natural products, as this significantly improved the future work done for researching the structure of compounds[42]. He was also responsible for synthesising quinine, cholesterol, cortisone, chlorophyll and reserpine, which helped the total synthesis of organic natural products, as shown in Figure 5[43].

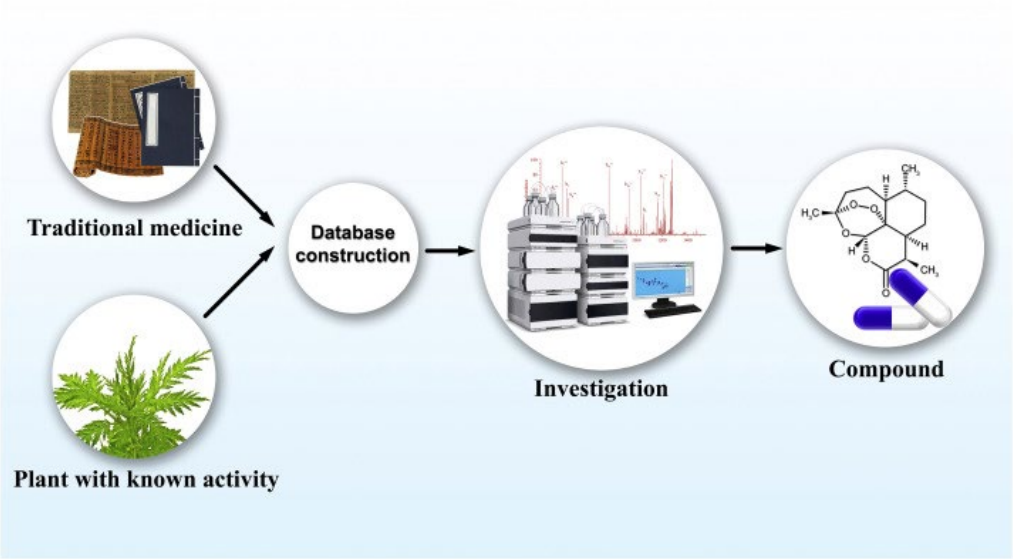

Figure 8 shows the strategy of information-based drug discovery of natural products[40].

2.7.1 Berberine

Berberine (BRB) is used as an antibacterial drug for treating infectious enteritis and bacillary dysentery, as Birdsall found that BRB is the primary practical component of *Coptis chinensis*[44]. Modern pharmacology research on BRB shows that it exhibits good activity for treating cardiovascular diseases, Alzheimer's disease, and cancer [44]. During a screening for novel cholesterol-lowering agents, BRB was found to increase low-density lipoprotein receptor (LDLR) expression in HepG2 cells, with further research confirming its potential to effectively reduce blood lipid lipids[45]. Berberine can protect the central nervous system by reducing Aβ deposition, as it alleviates AD by decreasing Tau hyperphosphorylation and increasing Tau autophagy clearance[46].

2.7.2 High throughput screening (HTS)

High throughput screening (HTS) technologies are currently being used because of the smaller masses (micrograms) of the compound needed for testing, as this is important for compounds of natural products that are difficult to isolate and purify[40]. The first successful drug discovery using HTS technology is the protein tyrosine phosphatase 1B (PTP1B) inhibitor from *Broussonetia papyrifera*[40]. HTS uses the microplate for the experimental tool carrier, with an automated operating system for the experimental process, as data is collected at molecular and cellular levels using instruments that are sensitive and rapid for detection[47]. HTS is performed in 96-well or 384-well plates, which makes it effective for gene function because it injects the gene directly into the gene expression products or the cell[40].

2.7.3 High-content screening

Following the rise of HTS technology, High-content screening (HCS) uses a high-resolution cell imaging system that fully "integrates sample preparation technology, automation equipment, data management system, and detection reagents"[48]. It is a technology that uses cells as detection objects, records the images of cells using multi-well plates using the microscopic imaging method, and analyses the activity of intracellular components[49]. From a single experiment, HCS technology can obtain information from pharmacological activity about the potential toxic effects of drugs and new techniques for drug effects [40].

2.7.4 Computer-aided drug development

For the development of drug designs and methods, the tools and software used are virtual screening, bioinformatics, and artificial intelligence [40]. Examples of structure-based drug designs are HIV protease inhibitors, Indinavir and Darunavir[40]. Donepezil is discovered as a ligand-based drug design, which is used for the treatment of Alzheimer's disease (AD) [40]. Natural products have multi-functional and multi-target characteristics, which make the target protein challenging to determine. Thus, bioinformatics is used to solve this problem[40]. Virtual screening (VS) improves the efficiency of lead compounds that are discovered due to the fact that it reduces the cost of screening and the number of compounds that are screened[50]. The technology uses the database of small molecules to match compounds and is based on the three-dimensional structure of target enzymes, receptors or ion channels[40].

2.8 Structural elucidation techniques

2.8.1 Spectroscopic analytical techniques

After the isolation process of natural products, as explained in Chapter 2.7, the next step is the spectroscopic analytical techniques of the obtained pure compounds. The molecular structures are elucidated using techniques such as liquid chromatography-mass spectrometry (LC-MS), high-resolution mass spectrometry (HRMS), gas chromatography-mass spectroscopy (GC-MS), nuclear magnetic resonance (NMR), infrared spectra (IR), X-ray crystallography, and CD spectroscopy[51]. LC-MS and GC-MS predict the molecular mass and purity of the isolated metabolites. In contrast, the high-resolution mass spectrometry data analysis gives you the molecular formula and the predicted structure of the metabolites using software tools such as SIRIUS and MetaboScape[51]. The final confirmation of the predicted structure is analysed using the NMR data from ^{1}H NMR, ^{13}C NMR, COSY, HSQC, HMBC, NOESY, and TOCSY[51]. The ^{1}H NMR and ^{13}C NMR can detect the types of protons and carbon. At the same time, two-dimensional NMR is used for larger and more complex molecules as it has more resolution to assign the structure of natural compounds compared to 1D NMR[52]. The ^{1}H NMR and ^{13}C NMR spectra show information about an unknown compound's qualitative and quantitative composition, which is used to determine the molecular formula[53]. The Heteronuclear Single Quantum Coherence (HSQC) spectrum shows the resonance of ^{1}JCH couplings between ^{13}C nuclei and protons attached to the corresponding atoms, which allows for the detection of all the CH, CH_2 and CH_3 groups with the chemical shift assignments[53]. The Correlation Spectroscopy (COSY) shows the homonuclear correlations (spin couplings) between vicinal hydrogens separated by

three bonds (3JHH), which makes it possible to identify the neighbouring carbon atoms connected by a chemical bond[53]. The Total Correlation Spectroscopy (TOCSY) allows you to obtain one sub-spectra for different coupled proton sequences in a molecule[53].

The Heteronuclear Multiple-Bond Coherence (HMBC) shows the heteronuclear correlations between ^{1}H and ^{13}C (15N) nuclei separated by two or three bonds, which allows for detecting fragments around a given carbon or nitrogen atom[53]. No method will help show which of the ^{1}H and ^{13}C are separated by two bonds and which by three bonds, which is why the HMBC information is fuzzy[53]. The NOESY/ROESY shows the coupling between hydrogen atoms separated in space by a distance of <5 Å. This is used to determine the stereochemistry of an elucidated structure and to clarify the positions of substituents if the data from HMBC and COSY does not allow to do so[53]. The NOESY/ROESY spectra data is not used to assemble the structure[53]. The *standard* correlation is the COSY and HMBC correlation that does not exceed three bonds, with correlations longer than the three bonds referred to as *non-standard* correlation (NSCs) [53]. It is difficult to detect the NSCs in their number and lengths in HMBC and COSY spectra, which makes their information contradictory[53].

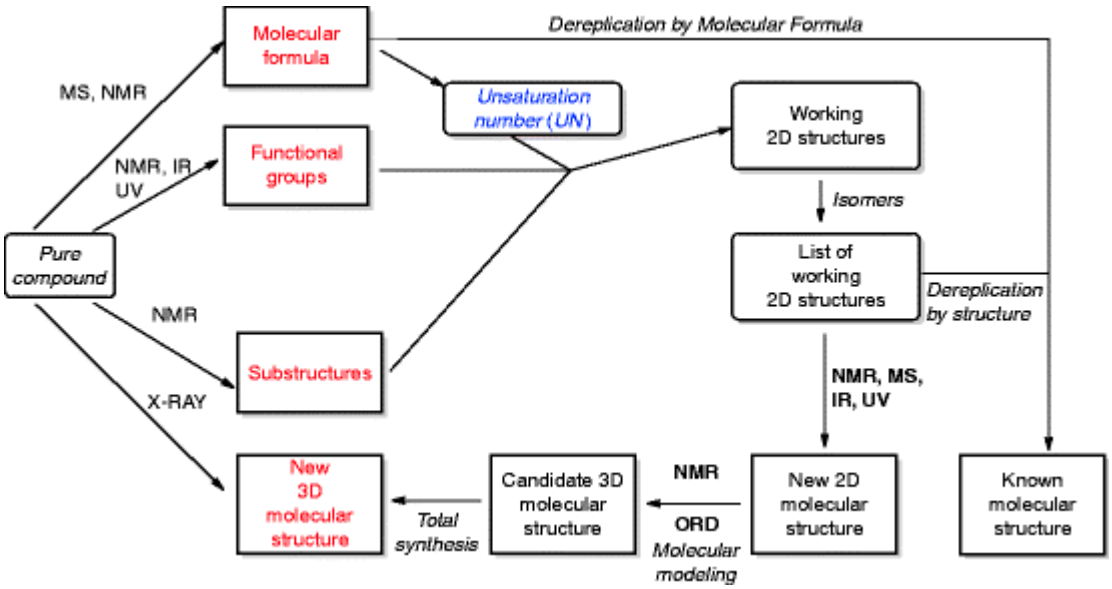

Figure 9 shows the stages of structural elucidation strategy on natural products[54].

2.8.2 Natural product database

The natural product database provides information about natural products and their derivatives, including their structure, source, and mechanism of action, which is helpful for modern drug discovery[55]. There are four ways of searching for natural products from the database: by name/ID, properties, similarities, and substructure [56]. The search by name requires the name of the compound, the Supernatural ID or a natural product supplier ID, which will allow you to access that compound on the database[56]. When searched by the property of the compound, this includes "the molecular weight, the topological polar surface area (TPSA), logP, hydrogen bond acceptor (HBA), hydrogen bond donor (HBD), types of bonds (rotatable bonds, amide bonds), types of atoms (hetero atoms, heavy atoms), stereocenters, and different ring types (aromatic, saturated and aliphatic)" [56]. It also allows you to search for the toxicity classification of each compound using the ProTox-II method when the compound is searched for by its properties [56]. When the compound is searched for by its similarities, there are four ways in which users can search by using the PubChem name to search for a small

molecule structure, as PubChem has 60 million unique chemical structures and 157 million depositor-provided chemical substance descriptions[57]. Another source where you can upload molecules to search for similarities is SMILES (Simplified Molecular-Input Line-Entry System), where the corresponding molecular structure will be displayed and integrated into ChemDoodle structure viewer [56]. This allows for modifying the structure by adding or deleting atoms, and it is possible to draw out the molecular structure using the tools provided[56]. Also, the Tanimoto coefficient allows you to measure the similarities between a Tanimoto similarity of natural compounds from the database and the identical structures of compounds [56]. Lastly, the search by the substructures through the database shows all the specified substructures with a Tanimoto similarity of 1.0, with one being most similar and 0 being dissimilar[56].

2.9 Dereplication of natural products

Dereplication uses chromatographic and spectroscopic analysis to recognise previously isolated substances in an extract. It can identify ubiquitous interfering compounds such as fatty acids or saponins[58]. Dereplication has three pillars: molecular structures, spectroscopy, and taxonomy[59]. Furthermore, dereplication can be used to identify multiple extracts or fractions that contain the same active profile, as this will help prioritise the extracts and fractions for chemical isolation[58]. Dereplication relies on analytical methods such as Mass spectrometry (MS) and Nuclear Magnetic Resonance (NMR) in natural products[60]. Mass spectrometry is highly sensitive but gives limited information for structure elucidation. In contrast, NMR is poorly sensitive but is quantitative and gives detailed structural features, as no analytical technique would combine both advantages of NMR and MS [60].

Dereplication in natural products is carried out using a combination of High-Performance Liquid Chromatography and Mass spectrometry, which allows the measurement of the mass spectra from the isolation of pure compounds of the LC-MS sequence[60]. Specialised databases allow molecular structures to be proposed from the mass spectral data in the research field of marine products[60]. Centrifugal partition chromatography (CPC) is a preparative separation method that allows for the isolation of pure compounds compatible with 13C NMR spectroscopy and biological activity research, as these require milligrams of the pure compound[60].

DEREP-NP is a database that uses 65 structural fragments that are present in 229 358 natural product structures, which are derived from plants, animals, and microorganisms, as shown in Figure 7[61]. It was published in 2013 and is available in the non-proprietary Universal Natural Products Database (UNPD)[61]. It works through the analysis of NMR or MS data by counting the number of times one or more structural features occur in an unknown compound, which it then matches and confirms through a literature comparison of the spectroscopic data to the matching structure if it is the same compound[61]. ChemSpider is another database for the dereplication of natural products using NMR data. It has 22 million diverse compounds, of which Williams and his co-workers created [61].

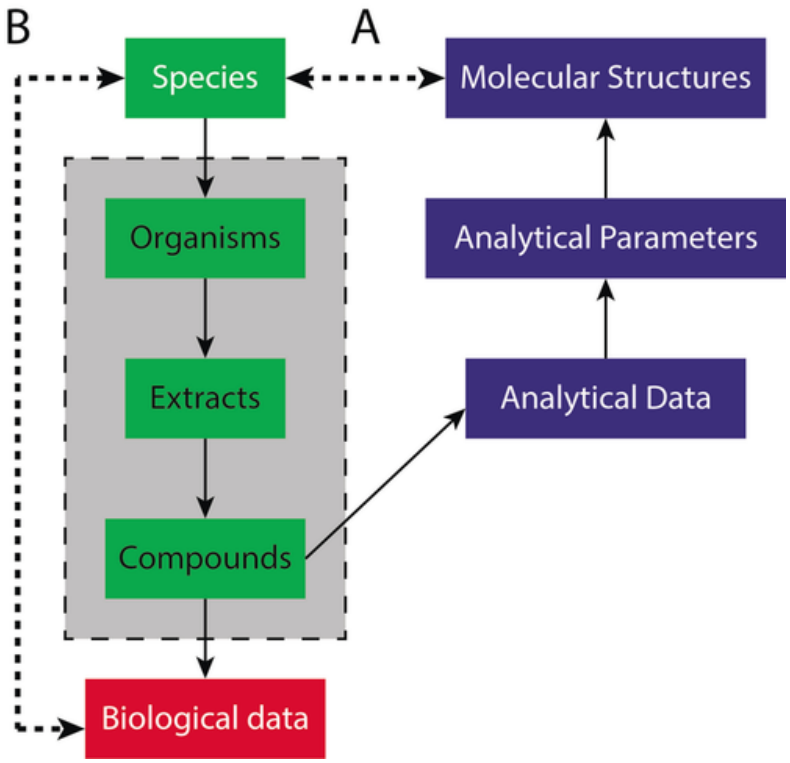

Figure 10 shows the relationship between different spaces involved in natural product[60].

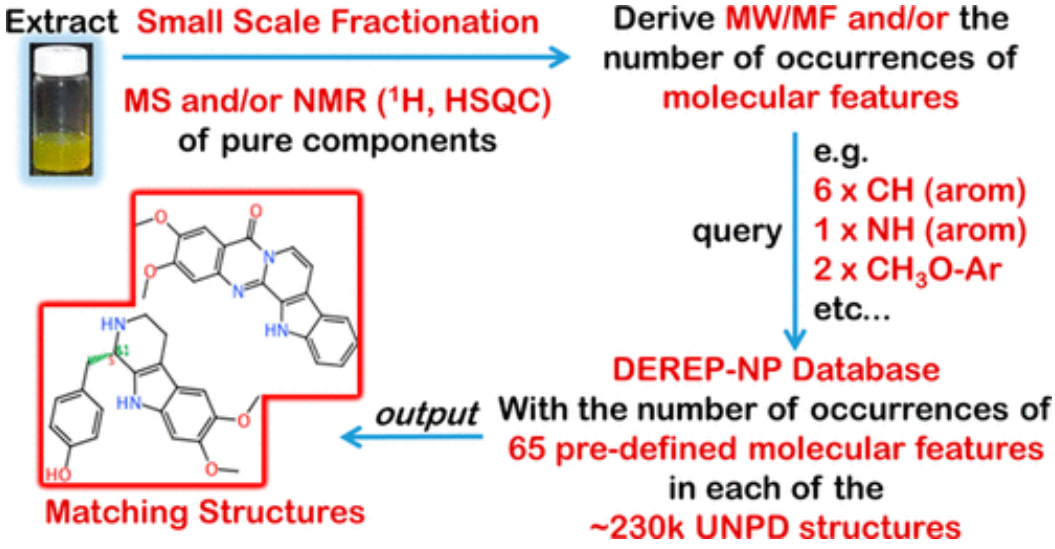

Figure 11 shows how DEREP-NP works[61].

CHAPTER THREE

3.0 Methods

3.1 Sample collection and extraction

Plant samples used in this project were collected and taxonomically identified at the University of the South Pacific, Fiji. They were then soaked in methanol (3x) followed by dichloromethane (3x), dried using a rotary evaporator, packed, and sent to UCLan, UK. At UCLan, this sample was semi-purified using a combination of wet chemistry methods, including liquid-liquid partitioning, size exclusion, and solid-phase extraction techniques. These methods helped simplified the complexity of the sample based on polarity and molecular sizes.

3.2 Kupchan fraction

The modified Kupchan method[1] involves dissolving the crude extract with water and partitioning it with dichloromethane (DCM) in a 100 mL separating funnel. Deionised water was be added to the sample so the polar molecules can dissolve into it. The funnel was then to be closed and mixed. This created a separation between the more polar and nonpolar compounds. The DCM fraction containing the more nonpolar solvents was then be extracted from the funnel into a 250 mL round bottom flask for rotary evaporation at 39^{o}C and 180 rpm, then used for later partitioning. The partition extraction was repeated twice with DCM. Secondary butanol was then be added to the water fraction. The two fractions separated into 250 mL round bottom flasks and labelled as FW for the water fraction and FB for the secondary butanol fraction. The remaining solid from the DCM was then dissolved in 90% methanol-water (50 mL) and partitioned with hexane. The hexane fraction was removed into a 250 mL round

bottom flask and labelled FH. The 90% MeOH-water fraction was then phase-adjusted to 50% methanol-water and partitioned with DCM, as the remaining fractions were extracted and labelled as FD for the DCM fraction and FM for the 50% methanol-water fraction. All fractions were analysed by proton nuclear magnetic resonance spectroscopy (NMR) and high-resolution mass spectrometry (LC-MS/MS).

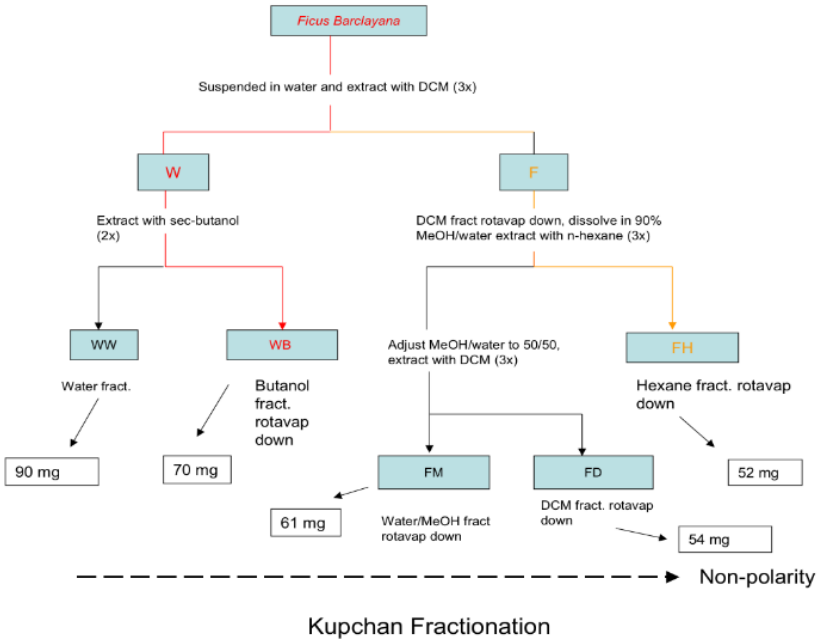

Kupchan Fractionation

Figure 12 shows the Kupchan fractionation method[1].

3.3 Size exclusion chromatography (SEC) fractionation and isolation

Sephadex LH-20[62] size exclusion chromatography (SEC) was applied to fractions FM, FD, FH, WW, and WB using different solvent systems. After cleaning the gel, the first step was to clean up the column and condition the Sephadex LH-20[62] with 100% MeOH. The next step was to prepare the solvent system for FM; it was a 1:1 ratio of CH_3CN and MeOH. Load the gel into the column using 100% MeOH, then load the sample dissolved in 100% MeOH. Elute the sample using 1:1 MeOH/CH_3CN and the flow rate

adjusted to 1 mL per minute. The WB and WW fractions were purified using the same solvent system as the FM fraction. The FD fraction was purified using a 60:40 solvent system of MeOH/CH_3CN, and the FH fraction was purified using a 70:30 solvent system of MeOH/CH_3CN. Each eluted fraction was collected into a plastic vial of 5 mL labelled s1-s14, depending on how many were collected, and similar fractions were then pooled together based on UV absorbance and colour. All fractions were dried and analysed using proton nuclear magnetic resonance spectroscopy (NMR) and high-resolution mass spectrometry (LC-MS/MS).

Further size exclusion column chromatography was done on samples that showed promising ^1H NMR resonance peaks that weren't 100% pure, using the same procedures as described here.

3.4 Nuclear magnetic resonance (NMR)

Nuclear magnetic resonance spectra (1D and 2D) allow the construction of the proposed structure with data generated by sets 1D NMR experiment: ^1H, ^{13}C, DEPT-135 followed by 2D experiments: Double Quantum Filtered COSY (DQF-COSY), Edited Heteronuclear Single Quantum Correlation (HSQC), and Heteronuclear Multiple Quantum Correlation (HMBC). The proton NMR spectra were collected on the 400MHz Bruker at the UCLan main campus, with Methanol D4 used as the solvent. The 2D NMR data were measured at the University of Edinburgh using the 800MHz Bruker, and the result was sent back to UCLan. The chemical shift values were referenced with the CD_3OD solvent. The experimental analysis for the 2D NMR for compounds FH4, FH5, FM7 and FM9 were as COSY (10 min), HSQC-Edited (20 min), HSQC-TOCSY (40 min), ROESY (30 min), and HMBC (60 min) ran on each compound. The samples were prepared in the NMR tube with a volume of 300uL. The 1D and 2D NMR spectra were

analysed using the Advanced Chemistry Development (ACD/Labs)[63] software and the Mestrelab (Mnova)[64] software for the structural analysis.

3.5 Liquid Chromatography-mass spectrometry (LC-MS)

Liquid Chromatography-mass spectrometry (LC-MS) analysis allows the determination of molecular mass and formula and the elucidation of the molecular structures through mass fragmentation data. The process occurred at the University of Central Lancashire (UCLAN) in the JB Firth building, Lab number JBF014 Analytical Service Lab. All LC-HRMS analysis were carried out on an Agilent 1290 LC system with a DAD coupled to an Agilent 6546 LC-QTOF equipped with dual spray jet stream technology electrospray ion source (AJS). The Kupchan[1] fractions (FM, FH, FD, WB and WW) were prepared by diluting them to 100x by dissolving them in LCMS grade MeOH. For instance, the weight of the FH compound was 52mg; this was dissolved in 1 uL of MeOH to make it 52mg/uL. This was then further diluted to 100x by taking 10uL of the sample and adding 990uL of MeOH, which makes this 0.5mg/uL. This is the required concentration so that the compound is detected and not to saturate the detector. The solvent composition system used was 100% water as A and 100% acetonitrile as B at a pressure of 1100 bar and a flow rate of 0.4 mL/min. The standard conditioning at 0 min started with 80% of solvent A and 20% of solvent; at 20 and 25 min, it was 0% for solvent A and 100% for solvent B and at 27 and 32 min, the conditioning of solvent A was 80% and 20% for solvent B. The instrument parameters were 320^{o}C for the gas temperature, gas flow at 8 l/min, and Nebulizer at 35 psi. The temperature control mode was set to 40^{o}C, and the reference masses used in the positive mode were 121.05087300, 322.04812100 and 922.00979800. The blank sample was first injected into the LCMS, followed by reserpine, and then, the compound was injected last. The data for the

LCMS analysis was processed using the Agilent MassHunter Qualitative Analysis[65] software and the ACD/Spectrus Processor 2023[63] software, which will be explained in Chapter 3.6.

3.6 Data processing

The raw data of all the LCMS compounds and blanks were exported to Microsoft Excel as CSV (Comma-Separated Values), allowing the files to be processed. For the Agilent software[65], the parameters used for the data processing is that the relative height was 2.5%, the absolute height was set to 500000, and the quality score used was equal to or above 70%. The retention time was restricted to only between 2.00-20.00 minutes. A combination of four blank libraries was pooled into a single Excel spreadsheet file, which was used to exclude masses within five ppm tolerance in the isolated fractions. The remaining masses of the fractions were divided into known and unknown compounds.

3.7 Dereplication process

An in-house library was created containing 18 known compounds previously isolated from *Ficus* and reported in the literature and accessed via the National Library of Medicine (PubMed Central) database. Database is important for dereplication purposes so that I could focus only on the unknown compounds after identifying the known compounds. To illustrate relationship between molecular mass and polarity a scatter plot was drawn for various Kupchan[1] fractions. Chemical formulas were generated for the unknown masses using the ACD labs[63] software, which are important information for identification of chemical structures of the compounds from the 1D and 2D NMR analyses. All the known and unknown masses are shown in the appendix section as Figures A12-19.

3.7 Bioassay

The fractions obtained from the Kupchan[1] fractionation method, and the size exclusion chromatography were sent for bioassay screening for anti-Alzheimer's and anti-cancer. Dr David Horsley performed the anti-Alzheimer screening for TauRx[39] assay at the University of Aberdeen. The extracts were dissolved at 10 mg/mL of DMSO, with Methyl 3,4,5-trimethoxycinnamate (MTC) used as controls and diluted in water for cell-free immunoassay and in PBS for tau aggregation assay to the required concentrations immediately prior to used[66]. Cellular toxicity was determined using the Cytotox 96-well kit (Promega) as described by Rickard et al.[66]. B_{50} assay and EC_{50} assay (cells) were run on the fractions sent for the anti-Alzheimer screening.

The anti-cancer screening was performed by Jeanette Andersen's research group at Maribo, UiT, the Artic University of Norway, Tromsø[67]. The fractions were tested against three cell lines: A2058_MTT (human melanoma cell line), MRC5_MTT (human lung fibroblast cells), and MCF7_MTT (human breast cancer cell line). The Cell lines were seeded in 96-well-microtitre plates, at 2000 cells/well in RPMI medium with 10% fetal bovine serum (FBS) and 10 µg/mL gentamicin and were incubated for 24 hours before microalgal extracts (50 µg/mL)[68].

3.8 ACD Labs

Advanced Chemistry Development[63] (ACD Labs) is software which provides analytical data handling and management solution, and molecular property modelling as it is used globally by scientists in the pharmaceutical, biochemical, and chemical industries[63].

CHAPTER FOUR

4.0 Results and Discussion

4.1 In-house library

A copy of the in-house library is seen in the appendix section as Table A1, containing compound mass, chemical formula, $[M+H]^+$, $[M-H]^-$ and chemical structure. The high-resolution masses generated from the LC-HRMS of the extracts was used to compare with the masses of the known compounds of *Ficus* from this in-house database for their identification. All the matched masses were within 5 ppm tolerance for the already known compounds in the database indicating possible identity of the unknown compounds.

4.2 Data processing and dereplication

Dereplication uses chromatographic and spectroscopic analysis to recognise previously isolated substances in an extract. It can identify interfering compounds such as fatty acids or saponins[58]. It has three pillars: molecular structures, spectroscopy, and taxonomy[59]. Dereplication relies on analytical methods such as Mass spectrometry (MS) and Nuclear Magnetic Resonance (NMR) in natural products, as mass spectrometry is highly sensitive but gives limited information for structure elucidation. In contrast, NMR is poorly sensitive but is quantitative and gives detailed structural features[60]. The LC-HRMS data were processed using the Agilent MassHunter Qualitative Analysis software[65] and the ACD/Spectrus Processor 2023 software[63]. Using the ACD lab software there were a total of 49 masses in the WW fractions, 40 masses

in the WB fraction, 190 masses in the FD fraction, and 103 masses in the FM fraction that had a quality score of more than 40% (as shown in appendix as Table A12-A19).

4.2.1 Dereplication of the crude extracts

The FM, FH, FD, WW, and WB fractions were obtained from the crude extracts of *Ficus barclayana* using the modified Kupchan as shown in Figure 12. They were profiled using liquid chromatography high-resolution mass spectrometry (LC-HRMS). There was a total of 382 masses found from the Kupchan fractions of FH, FD, FM, WW and WB, which had a quality score of more than 40%. The WW fraction got two hits for the masses of the known *Ficus* compounds from the in-house database, and these were: 610.1536 Da at the retention time of 3.486 min and 318.0386 Da at the retention of 22.891 (as shown in figure A1 and A1.2 and in the appendix). The mass at 610.1536 corresponds to the compound rutin[69] with the chemical formula of $C_{27}H_{30}O_{16}$, and the mass at 318.0386 is the compound myricetin[70] with the chemical formula of $C_{15}H_{10}O_8$. The chromatogram of the WW fraction is shown in Figure 13a-b.

A known compound of *Ficus* was identified in the WB fraction with m/z of 430.3762 and the retention time at 14.68 min (as shown in Figure A2 appendix). This compound is (24R)-ethylcholest-4-ene-3,6-diol[71] and has the chemical formula $C_{29}H_{50}O_2$. Furthermore, the m/z at 610.1536 at the retention of 3.588 min (as shown in Figure A2 appendix) is the compound rutin[69], which has the chemical formula $C_{27}H_{30}O_{16}$ and has been identified in the WB fraction. The chromatogram of the WB fraction is shown in Figure 14a-b.

Figure 15 shows the structure of the known compounds in the WW fraction. No known compounds were identified from the in-house database using liquid chromatography

high-resolution mass spectrometry (LC-HRMS) from the FM, FD, and FH fractions indicating that these fractions potentially contain new compounds.

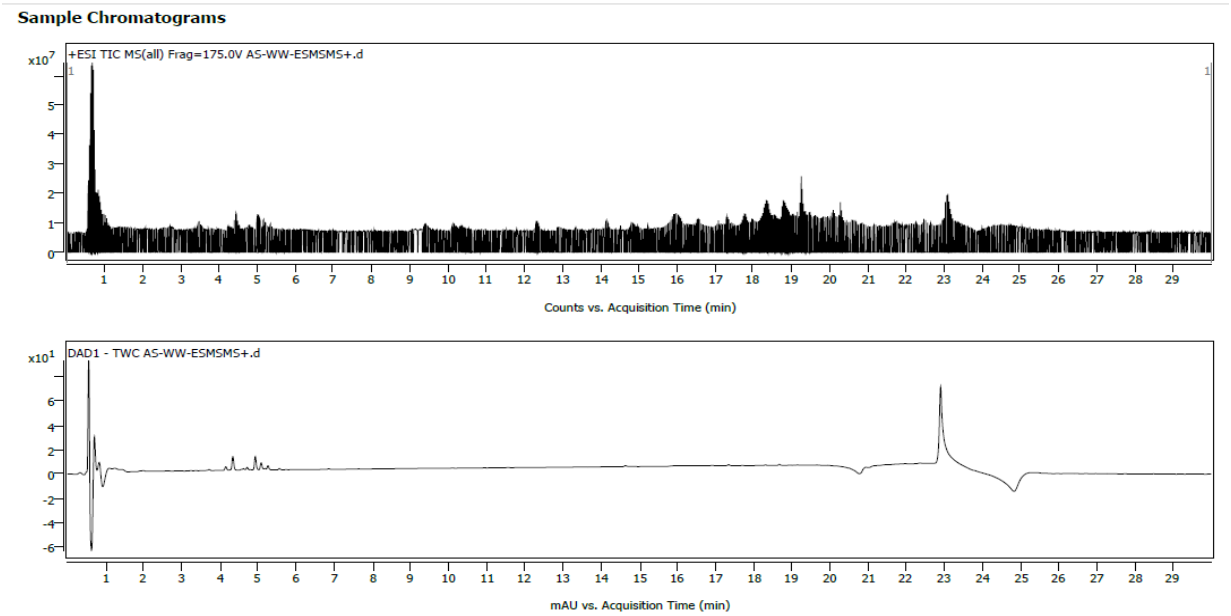

Figure 13a-b shows the LC-MSMS$^+$ total ion chromatogram of WW fraction with 1a (top) shows the total ion chromatogram, 1b (bottom) shows the DAD1(Diode Array Detected wavelength at 330 nm).

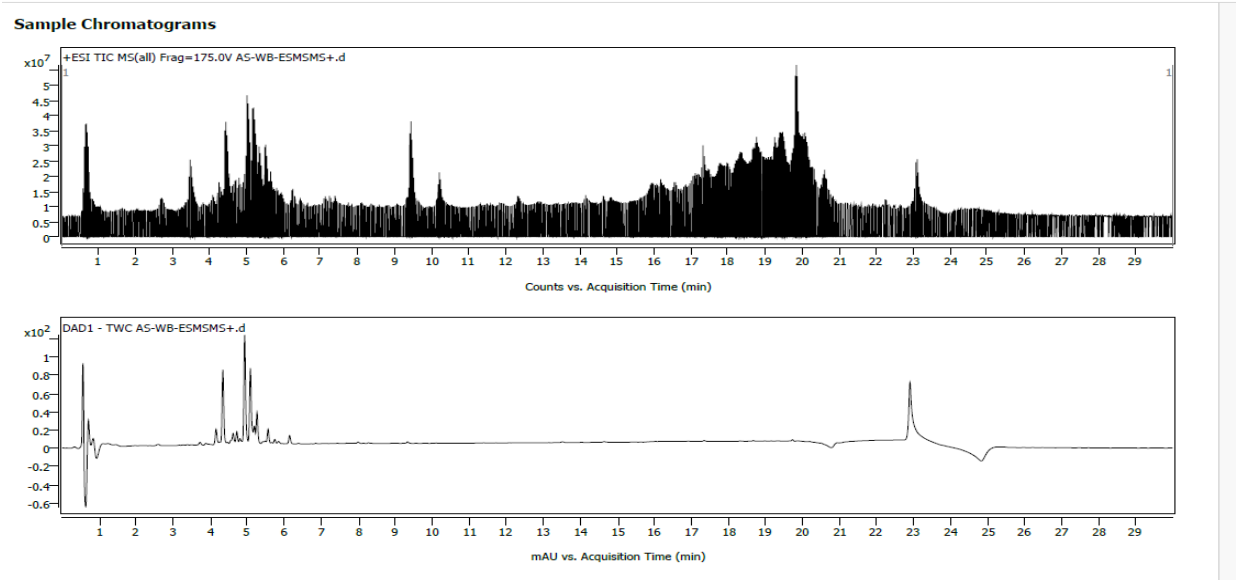

Figure 14a-b shows the LC-MSMS$^+$ total ion chromatogram of the WB fraction with 2a (top) shows total ion chromatogram, 2b (bottom) shows the DAD1(Diode Array Detected wavelength is 330 nm).

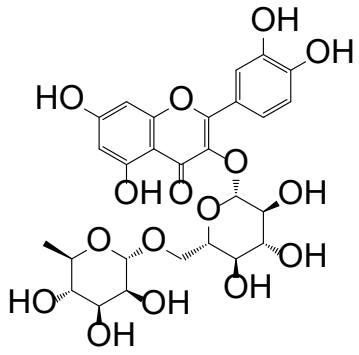

rutin

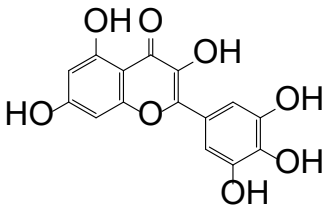

myricetin

Figure 15 shows the structures of the known compounds in the ww fraction.

4.2.2 Elucidation of the pure compounds

Compounds from the crude extracts of FM, FD, FH, WW and WB were profiled using LC-HRMS for known compounds using an in-house library. These dereplicated compounds were purified and isolated by size exclusion chromatography using the LH-20 Sephadex[62] as explained in chapter 3.3. The pure compounds FD4, FH4, FM7 and WB4 were isolated from their respective Kupchan[1] extracts. Two known compounds were identified in the FD4 fraction with masses of 414.3919 at the retention time of 17.30 (Figure A3 in appendix) min and 430.3767 at the retention of 14.68 min (Figure A3.1 in appendix). The mass at 414.3919 is β -sitosterol and has the chemical formula $C_{29}H_{50}0$, and the mass at 430.3767 was identified as (24R)-ethylcholest-4-ene-3,6-diol[71], which has the chemical formula of $C_{29}H_{50}O_2$. The complete chromatogram of the FD4 is shown in Figure 16. The compound identified in the WB4 fraction at the retention time of 14.68 min and a mass of 430.3767 is (24R)-ethylcholest-4-ene-3,6-diol[71] (Figure A4 in appendix), which has the chemical formula of $C_{29}H_{50}O_2$. The compound identified in the FH4 fraction at the retention time of 26.46 min with a mass of 318.0395 is myricetin[70] (Figure A5 in appendix), which has the chemical formula $C_{15}H_{10}O_8$. The complete chromatogram of the FD4 is shown in Figure 16, WB4 is shown in Figure 17, and FH4 is shown in Figure 18. The structure is β-sitosterol is shown in Figure 19.

Using the ACD lab software, four masses were identified as known compounds common in all the 'pure' fractions (FD4, FH4, FM7 and WB4), and their structures are shown in Figure 20. The mass at 365.2 had the chemical formula of $C_{23}H_{26}NO_3$ and the IUPAC name of 1-propyl-2-[(*E*)-2-(2,4,6-trimethoxyphenyl) ethenyl] quinolin-1-ium

(Figure 8A). The mass at 712.2 had the chemical formula of $C_{35}H_{35}O_{16}$ with the IUPAC name of [3-(3,4-dihydroxyphenyl)-7-(4-hydroxyphenyl)-4-[(2*S*,3*R*,4*S*,5*S*,6*R*)-3,4,5-trihydroxy-6-[[(2*R*,3*R*,4*R*,5*R*,6*S*)-3,4,5-trihydroxy-6-methyloxan-2-yl]oxymethyl]oxan-2-yl]oxy-2,8-dioxatricyclo[7.3.1.05,13]trideca-1(12),3,5(13),6,9-pentaen-11-ylidene]oxidanium (Figure 8B). The m/z value at 413.2 had the chemical formula of $C_{27}H_{26}NO_3$ and the IUPAC name of propan-2-yl 2-[[3-(4-methoxyphenyl) isoquinolin-2-ium-2-yl] methyl] benzoate (figure 8C). The m/z value 453.2 generated two potential chemical formulas within the error (Da) of 0.00 to the m/z value. The first chemical formula generated is $C_{22}H_{30}NO_9$ and had the IUPAC name of 2-(diethylamino) ethyl 2-(2-ethylphenyl) acetate;2-hydroxypropane-1,2,3-tricarboxylate (figure 8D). The other chemical formula generated for the mass at 453.2 is $C_{21}H_{24}N_8O_4$ which had the IUPAC name of 2-methyl-*N*-(2-morpholin-4-yl- [1,2,4] triazolo[1,5-a] pyridin-7-yl)-4-(2-oxa-6-azaspiro[3.3]heptane-6-carbonyl)pyrazole-3-carboxamide (Figure 8E).

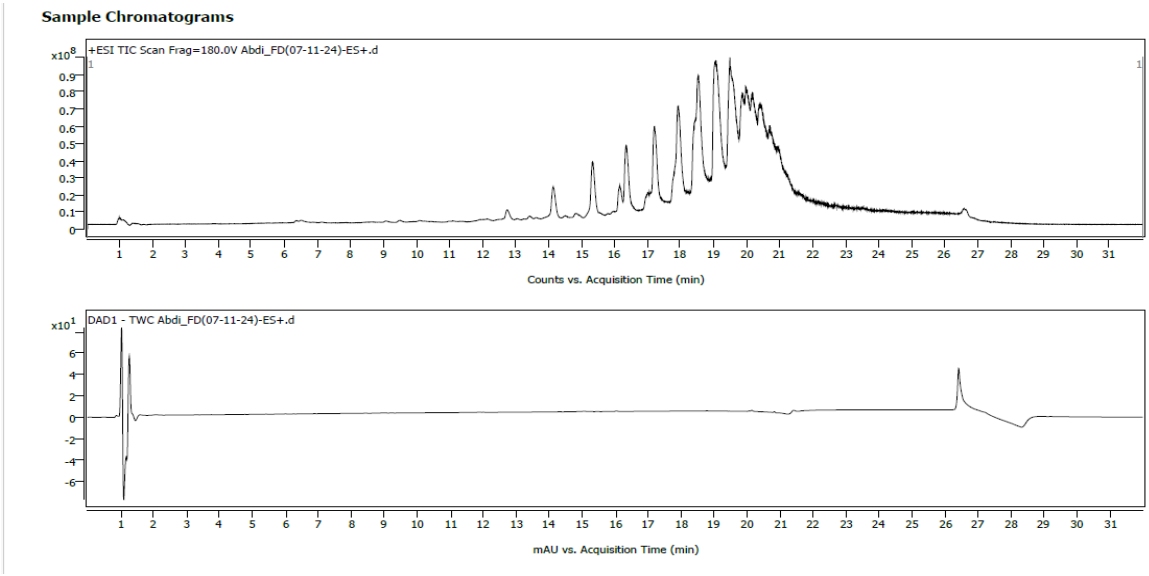

Figure 16a-b shows the chromatogram of the FD4 fraction, with 16a (top) shows the LC-MS total ion chromatogram, 16b (bottom) shows the DAD1(Diode Array Detected at 330 nm).

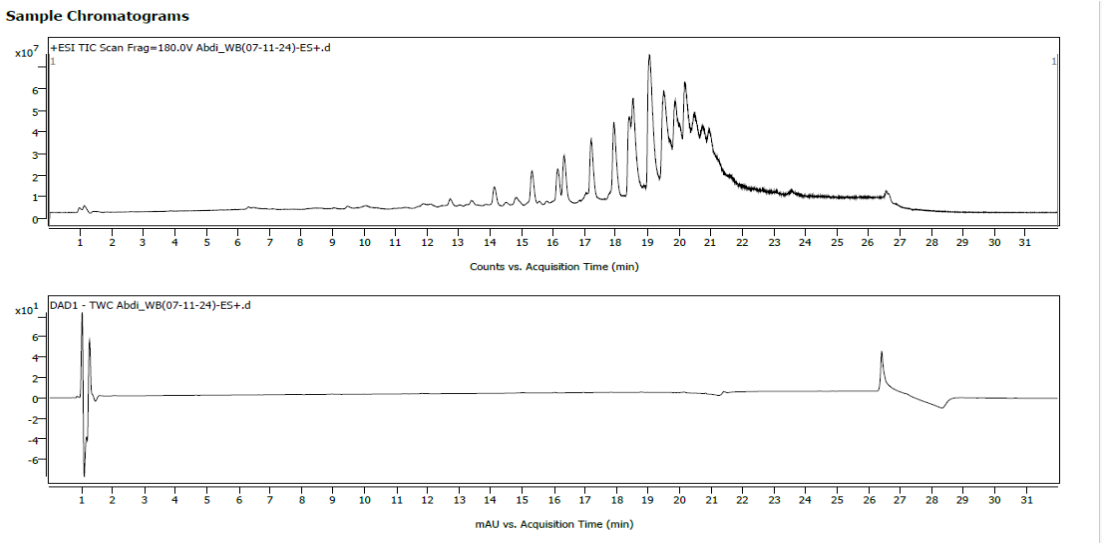

Figure 17a-b shows the chromatogram of the WB4 fraction, with 17a (top) shows the total ion chromatogram, 17b (bottom) shows the DAD1(Diode Array Detected wavelength at 330 nm).

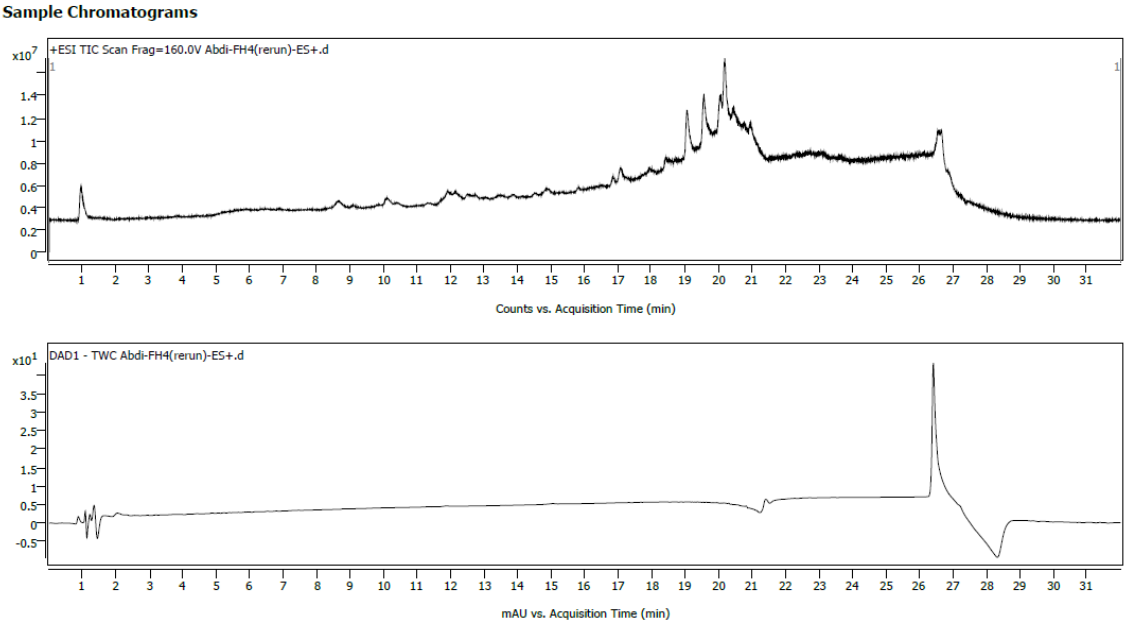

Figure 18a-b shows the chromatogram of FH4, with 18a (top) shows the total ion chromatogram, 18b (bottom) shows the DAD1(Diode Array Detected wavelength at 330 nm).

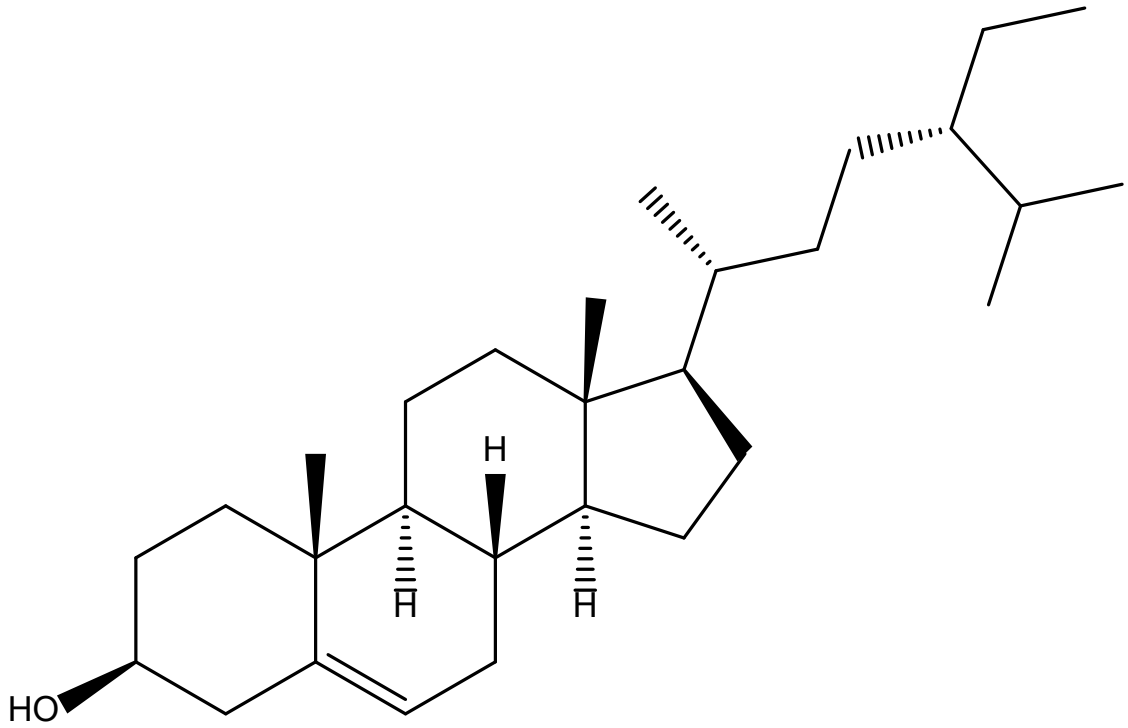

ß-sitosterol

Figure 19 shows the structure of β-sitosterol identified in the FD4 fraction.

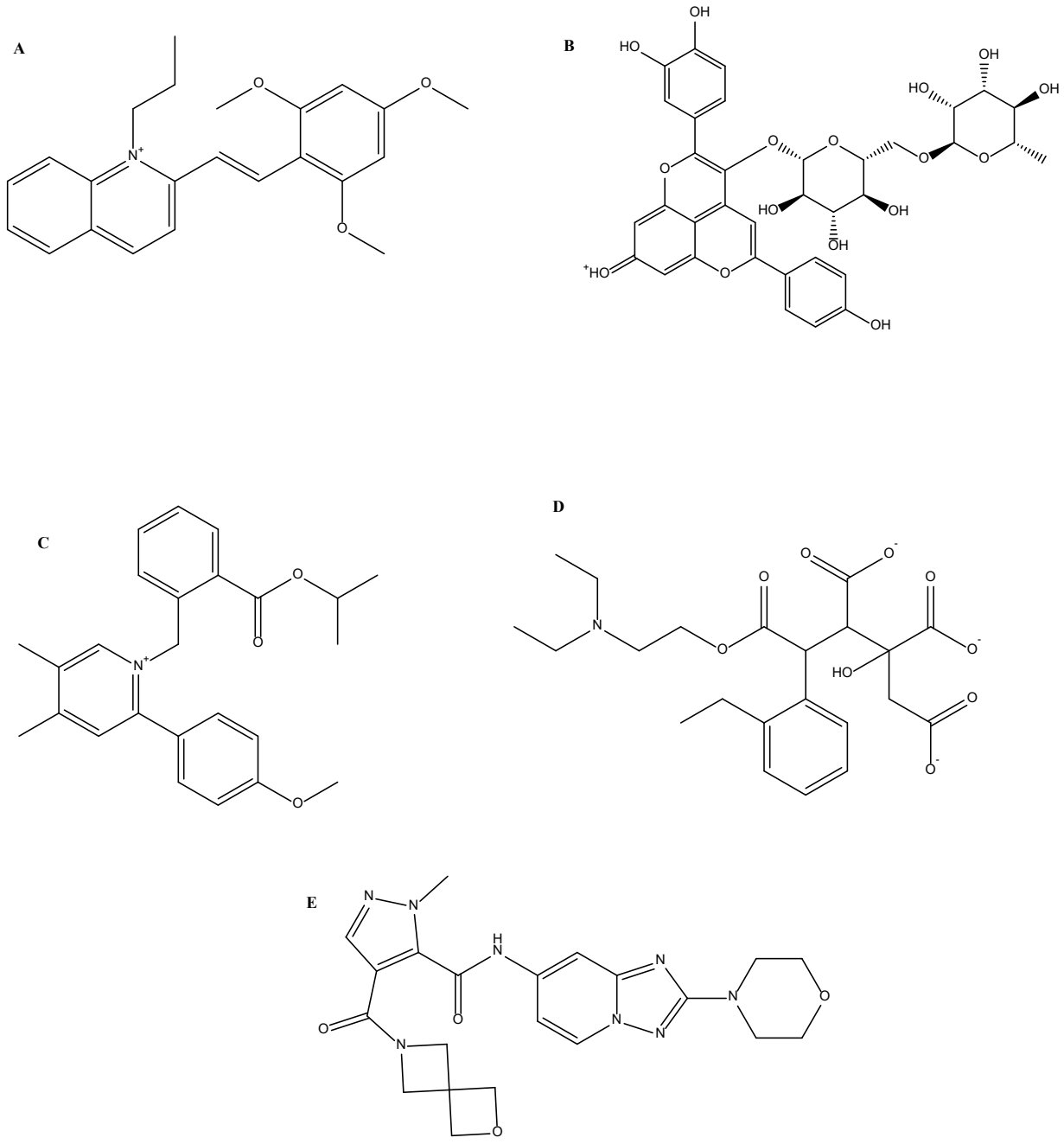

Figure 20 shows the dereplicated structures of the known compounds in the semi-purified fractions using the LCMS data processed by the ACD labs software.

4.2.3 Identification of compounds isolated from the Kupchan fractions

The unknown $[M+H]^+$ peak at 387.18 and the $[M+Na]^+$ peak at 409.162 were found in crude extractions FM, FH, FD, and WW, as shown in Figure A9. The $[M+K]^+$ peak at 425.136 in FM, FD, and WW. This mass was at 8.1 min in the FM fraction, 6.15 min in the FH fraction, 6.13 min in the FD fraction, and 12.27 min in the WW fraction. If the masses are the same but eluted at different times, it means that these compounds are structural isomers. The only fraction this mass was not found was in the WB fraction. A potential chemical formula of $C_{22}H_{27}O_6$ was generated for this mass using the tools on the ACD software.

The $[M+H]^+$ m/z at 623.286 and $[M+Na]^+$ peak at 645.268 were common in fractions FM, FH, FD, and WB. In FM, FD, and WB fractions, the $[M+K]^+$ ion peak was observed at 661.243. The retention time for these masses from the FM fraction were 15.82 min, 15.77 min from the FH fraction, 15.80 min from the FD fraction, and 19.74 min from WB. WW is the only fraction in which the ion peak at 623.286 was not identified its LCMS data. The potential chemical formula for this ion peak at 623.286 generated by the ACD software was $C_{35}H_{43}O_{10}$.

The unknown mass at 653.297 was found in FM, FH and FD, with the $[M+Na]^+$ the ion peak 657.279 was found in the FM, FH and FD fractions (as shown in Figures A6-A8 in the appendix). The $[M+K]^+$ ion peak at 691.253 can be spotted in FM, FH and FD fractions. The mass was eluted at 16.39 min from the FM fraction, 16.35 min from the FH fraction, and 17.23 min from the FD fraction. The unknown mass was not present in either WW or WB fractions. The chemical formula generated by the ACD software for the unknown ion peak at m/z $[M+H]^+$ was $C_{36}H_{45}O_{11}$.

In WW and WB fractions, there was a common unknown ion peak at m/z [M+H] at 565.155 and its $[M+Na]^+$ at 587.138, with both masses eluted at 4.36 min. The chemical formula generated for this unknown ion peak at m/z $[M+H]^+$ at 565.155 is $C_{26}H_{29}O_{14}$ using the ACD software. Furthermore, the unknown ion peak at m/z $[M+H]^+$ at 535.141 was also common in the WW and WB fractions with the $[M+Na]^+$ peak at 557.123 and eluted at 4.94 min in the WW fraction and 4.99 in the WB fraction. The chemical formula generated for this unknown ion peak at m/z $[M+H]^+$ at 535.141 is $C_{25}H_{27}O_{13}$ using the ACD software. These ion peaks were absent in the FM, FH and the FD fractions.

Out of all the crude fractions of *Ficus barclayana*, only the WW fraction had the most interesting peak, as the $[M+NH_4]^+$ ion peak identified at 654.332 eluted at 19.13 min. The $[M+H]^+$ ion peak for the unknown ion peak at m/z $[M+H]^+$ is 637.305, and the $[M+Na]^+$ ion peak is 659.288. Two potential chemical formulas were generated for the unknown compound using the ACD software with an error (Da) of 0.00, which are $C_{27}H_{47}N_3O_{13}$ and $C_{26}H_{41}N_{10}O_9$.

All the unknown ion peaks obtained from the Kupchan[1] fractions (FM, FH, FD, WB and WW) were plotted into a scatter graph of the unknown mass against retention time for all the fractions, as shown in Figure 29. The scatter plot only shows the common unknown masses in all the fractions and where they were retained. For example, the FM and FH have the same unknown masses and retention time, so they are only shown as single point on the scatter graph. As shown in the scatter graph, most of the unknown ion peaks were eluted towards the end of the chromatographic run, thus indicating they are non-polar compounds.

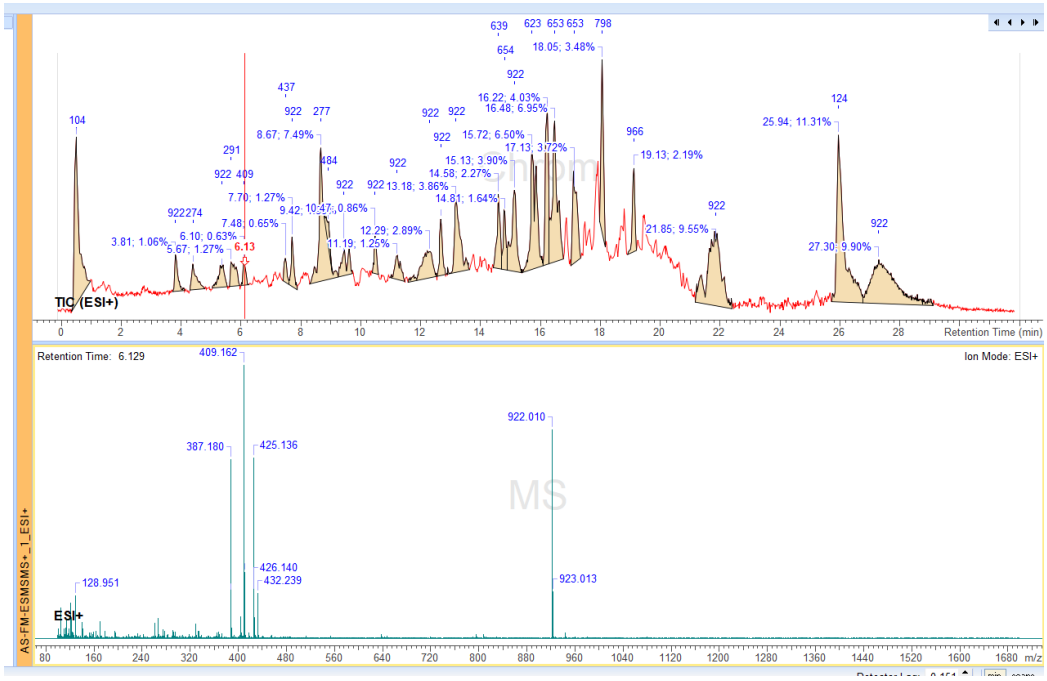

Figure 21 shows the TIC of the FM fraction and mass spectrum of the compound eluting at retention time of 6.13 min.

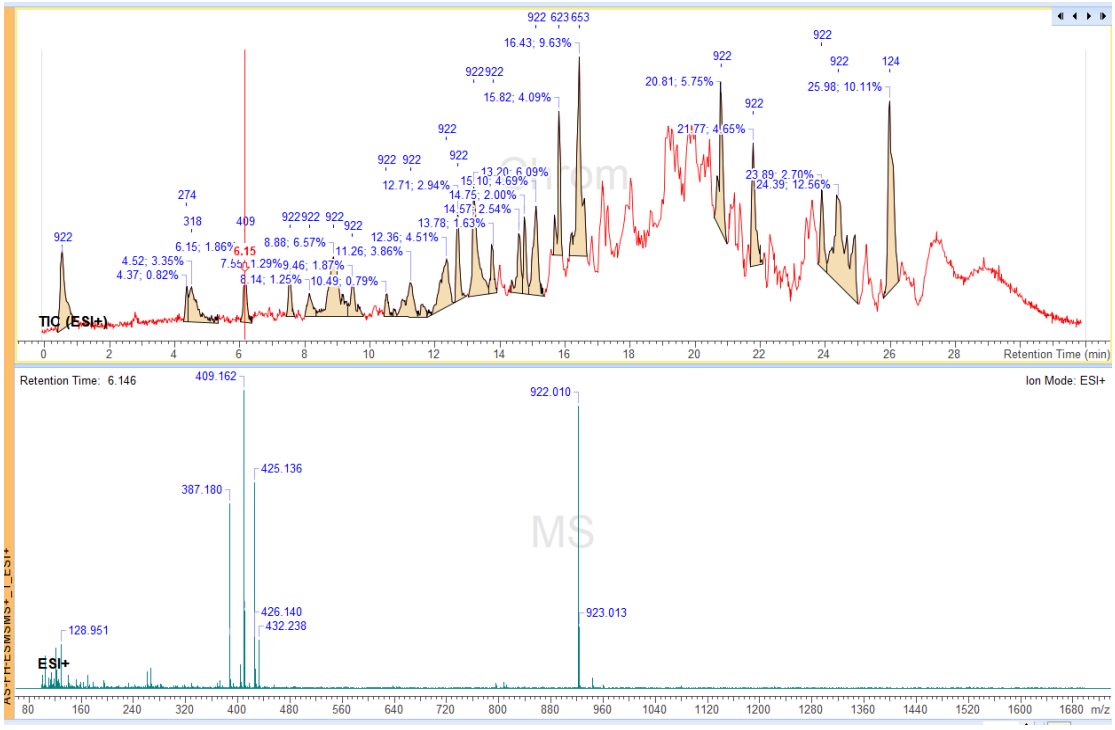

Figure 22 shows the TIC of the FH fraction and the mass spectrum of the compound eluting at the retention time of 6.15 min (922.01 is the refence mass as explained in chapter 3.5).

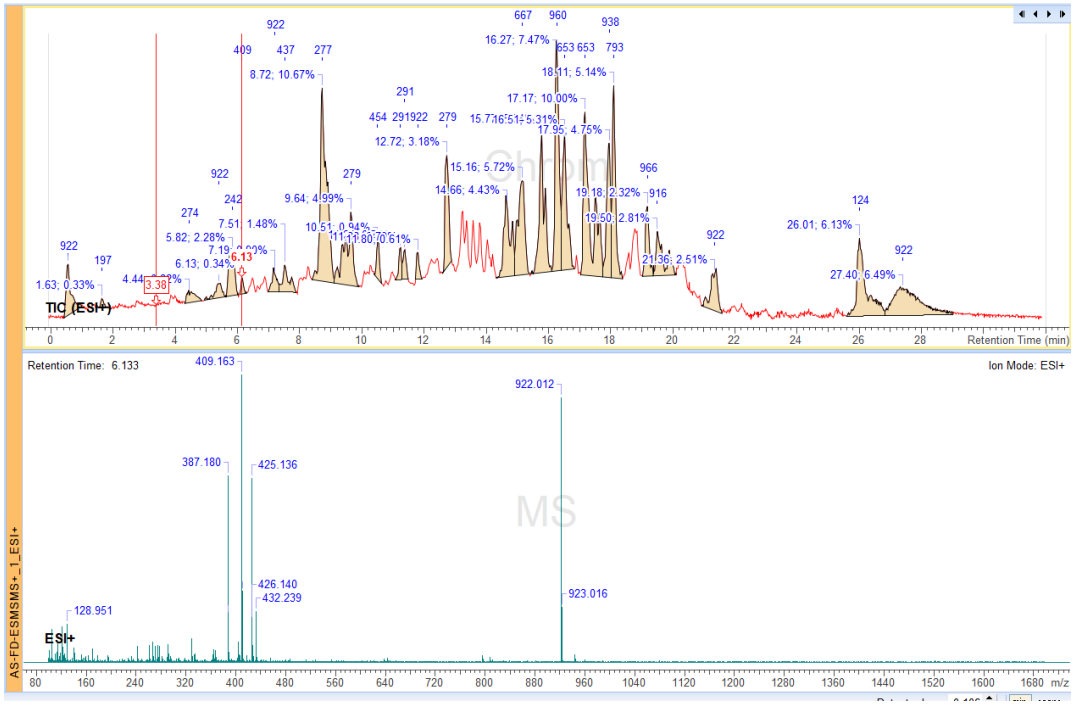

Figure 23 shows the TIC of the FD fraction and the mass spectrum of the compound eluting at the retention of time 6.13 min.

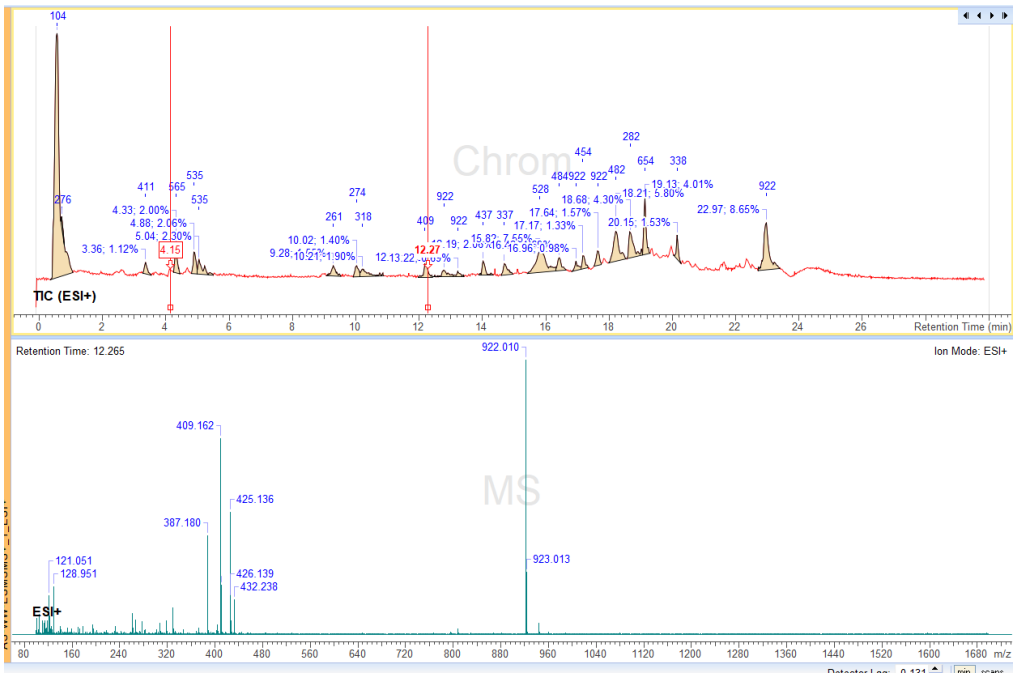

Figure 24 shows the TIC of the WW fraction and the mass spectrum of the compound eluting at the retention time of 12.27 min.

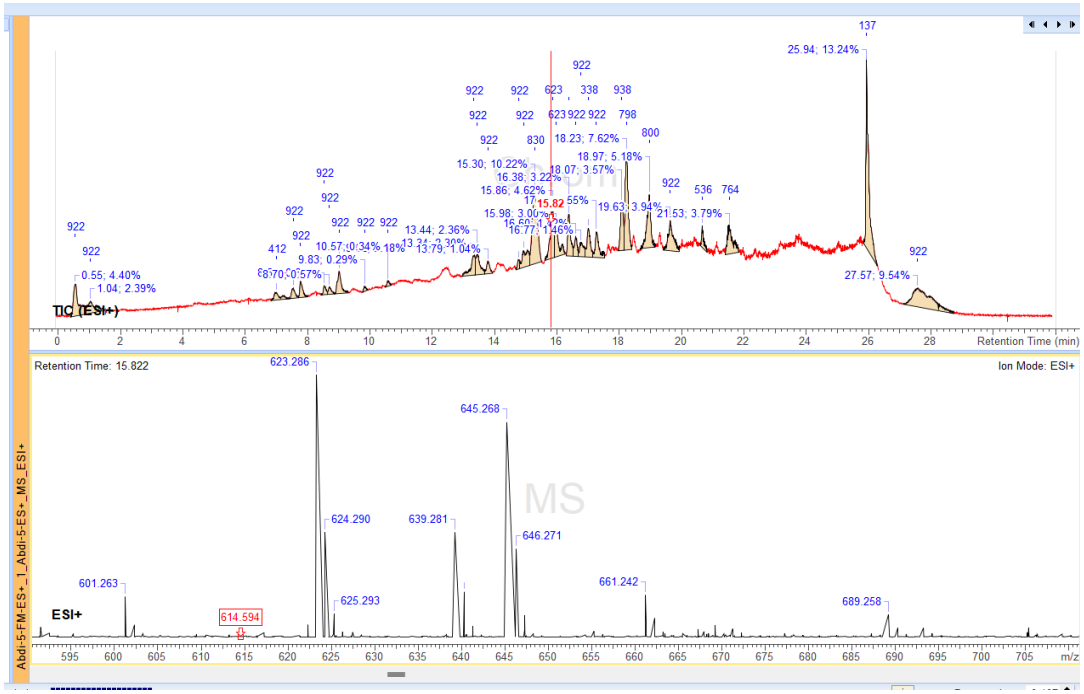

Figure 25 shows the total ion chromatogram (top), retention time at 15.82 min and the mass spectrum of the unknown compound in the FM fraction (bottom).

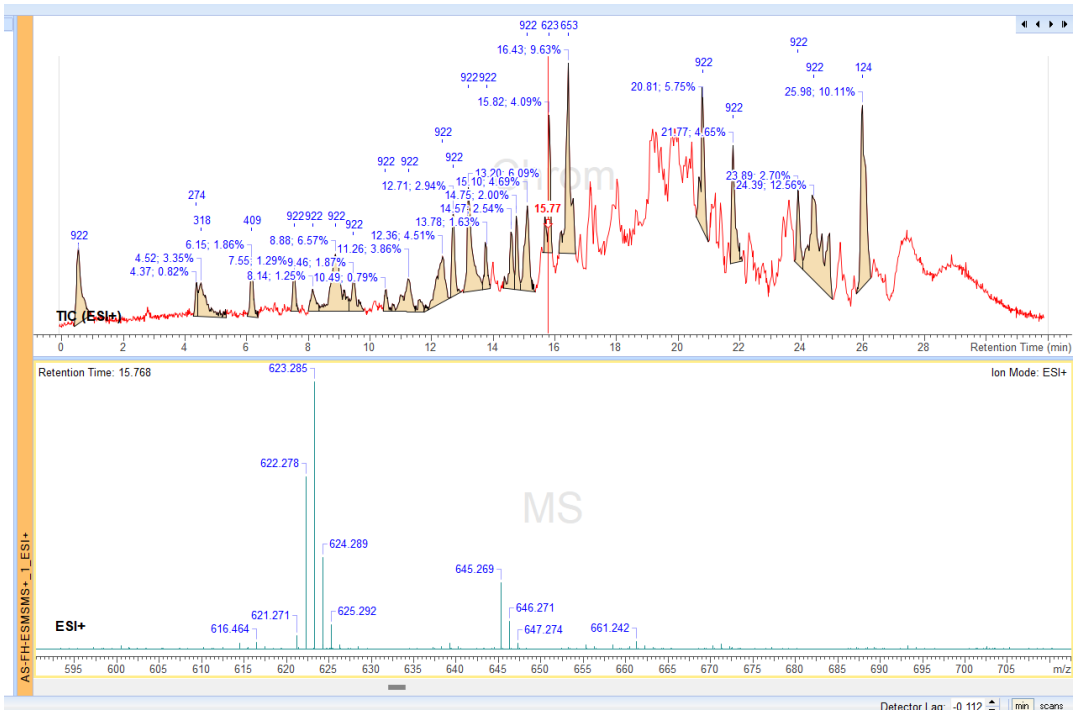

Figure 26 shows the total ion chromatogram (top), retention time at 15.77 min and the mass spectrum of the unknown compound in the FH fraction (bottom).

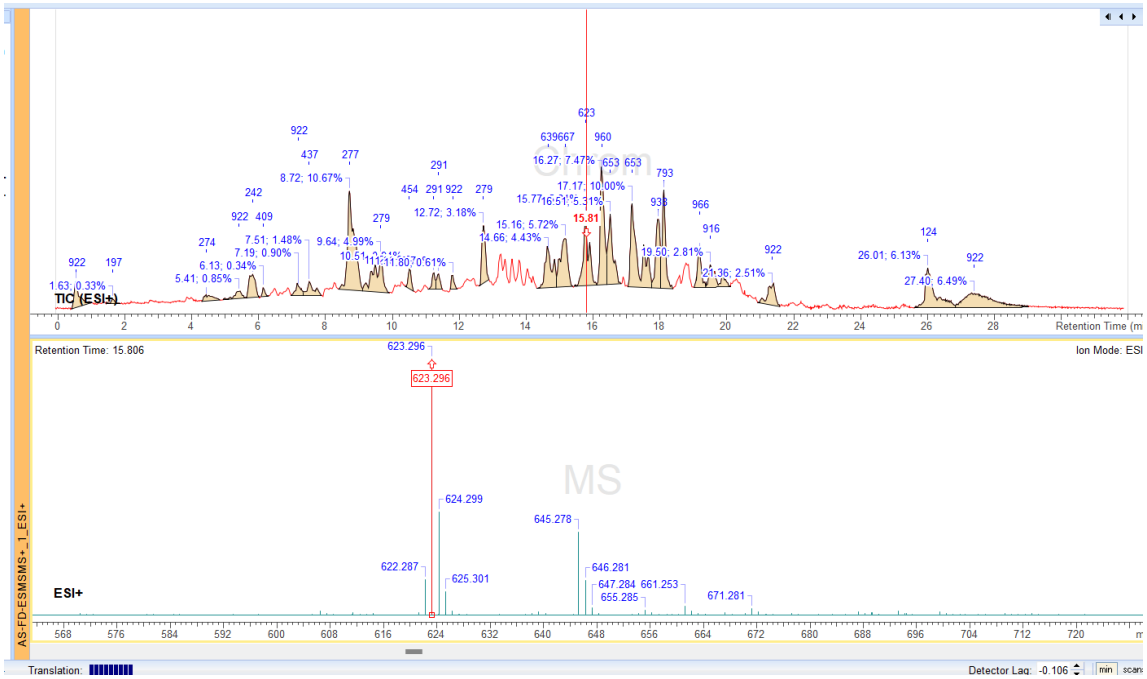

Figure 27 shows the total ion chromatogram (top), retention time at 15.81 min and the mass spectrum of the unknown compound in the FD fraction (bottom).

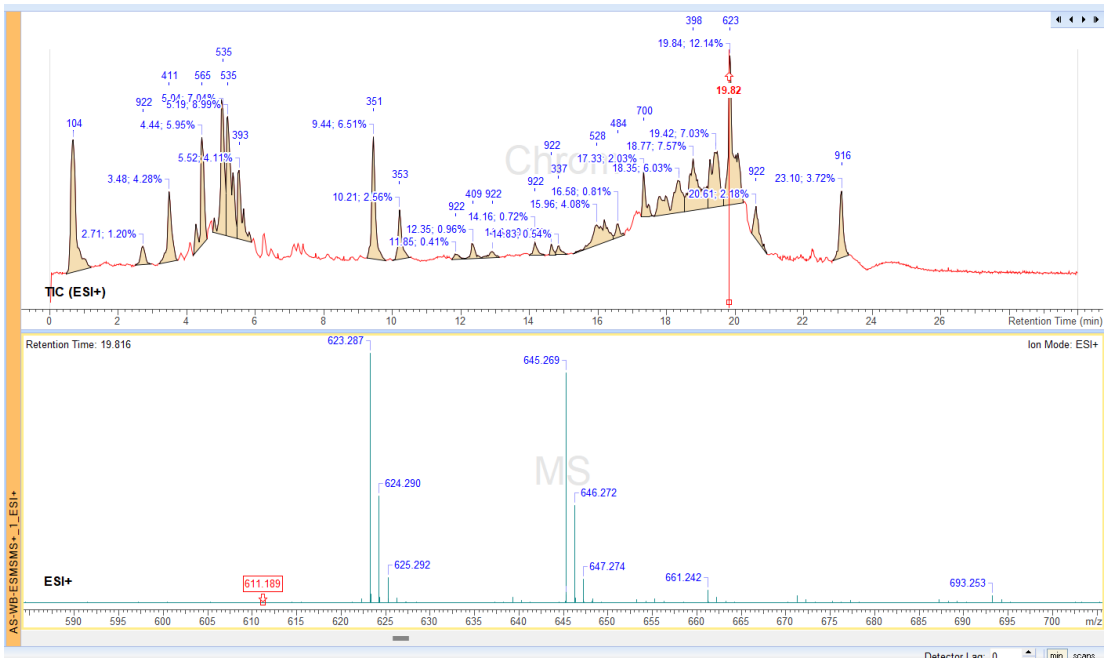

Figure 28 shows the total ion chromatogram (top), retention time at 19.82 min and the mass spectrum of the unknown compound in the WB fraction (bottom).

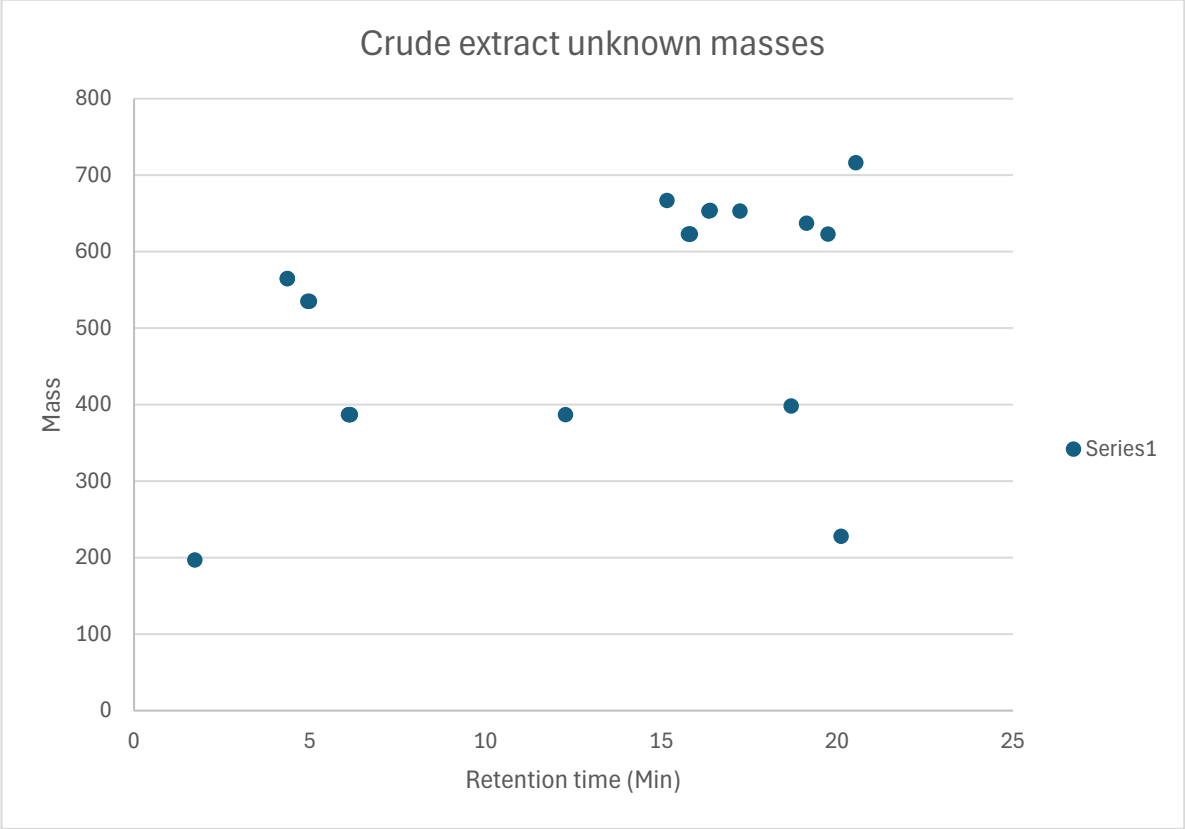

Figure 29 shows the scatter plot of ion peaks against retention time for unknown compounds in FM, FD, FH, WB and WW fractions eluted on a reversed phase C18 column. The scatter plot shows that most of the unknown compounds in the extract were non-polar (9) in nature with molecular weight between 400-700 Da.

4.2.4 Elucidation of unknown compounds of the pure compounds

A combination of 4 blank libraries were pooled into a single spreadsheet, and the masses of the blank database were used to exclude the masses in the fractions of FM7, FH4, WB4, and FD4. The LC-HRMS of the FM7 fraction resulted in 12 masses, suggesting 12 unknown compounds. The same was done for the FD4 fraction, resulting in 45 masses, followed by 30 in the FH4 and 26 in the WB4 fraction. The unknown masses in FM7, FH4, WB4, and FD4 are shown in the appendix in Figures A12, A13, A14, and A15, respectively. A scatter plot of all the unknown masses was plotted against the retention for the FM7, FH4, WB4 and FD4 fractions, as shown in Figures 30, 31, 32 and 33, respectively.

After applying the parameters with the Agilent software where the relative height was set to 2.5%, the absolute height to 500000 and the quality score to equal or above 70%, there were six masses found in the FM7 fraction, seven masses found in the WB4 fractions, 11 in the FD4 fractions and 2 in the FH4 fraction. The two masses found in the FH4 fraction were 609.1794, which was eluted at 19.07 min, and 683.1975, which was eluted at 19.57 min. The mass at 609.1794 can also be identified in the FM7, WB4 and FD4 fractions. The mass at 683.1975 can be identified in the FM7 and FD4 fractions. The chemical formula generated for the mass at 683.1975 is $C_{45}H_{32}O_7$, whereas the chemical formula for the mass at 609.1794 is $C_{21}H_{38}O_{20}$.

The masses at 320.31, 518.13, 775.22, 849.24, 923.26 and 1071.3 can be identified in both the WB4 fraction and FD4 fraction. The chemical formula generated for the mass of 320.32 is $C_{22}H_{44}NO$, $C_{22}H_{32}O_{15}$ for the mass of 518.13, and $C_{40}H_{40}O_{16}$ for the mass of 775.22. Two potential chemical formulas were generated for the mass at 849.24, which were $C_{37}H_{44}N_3O_{20}$ and $C_{36}H_{38}N_{10}O_{15}$, with an error (Da) of 0.00. The mass at 923.26 had

a chemical formula of C48H46NO18, and the chemical formula for the mass at 1071.3 is $C_{47}H_{48}N_{10}O_{20}$.

Three masses in the FD4 fraction were not identified in any of the other fractions: 610.15, 683.196 and 684.155. The chemical formula generated for the mass at 610.16 is $C_{35}H_{32}O_{11}$, $C_{34}H_{36}O_{15}$ for the mass at 683.196 and $C_{41}H_{33}O_{10}$ for the mass at 684.155. All the masses from FM7, FH4, FD4 and WB4 were plotted onto a scatter plot of mass against retention time, as shown in Figure 34. Most of the masses were eluted towards the end, indicating that the compounds are non-polar.

Out of all the 110 masses in the pure fractions (FH4, FD4, WB4 and FM7), four unknown masses were identified in all the pure fractions using the ACD labs to process the data. The masses of the FM7, FD4, FH4 and FM7 are shown in the appendix section as Tables A5, A6, A7 and A8, along with a scatter plot for each fraction (Figures A11, 12, 13 and 14 in the appendix section). The chemical formula generated for the mass at 610.2 is $C_{35}H_{29}O_{10}$, as for the mass at 666.2, the chemical formula generated is $C_{27}H_{37}O_{10}$, and the chemical formula generated for the mass at 929.2 is $C_{43}H_{36}N_4O_{20}$. The chemical formula generated for the mass at 337.2 is $C_{23}H_{28}S$.

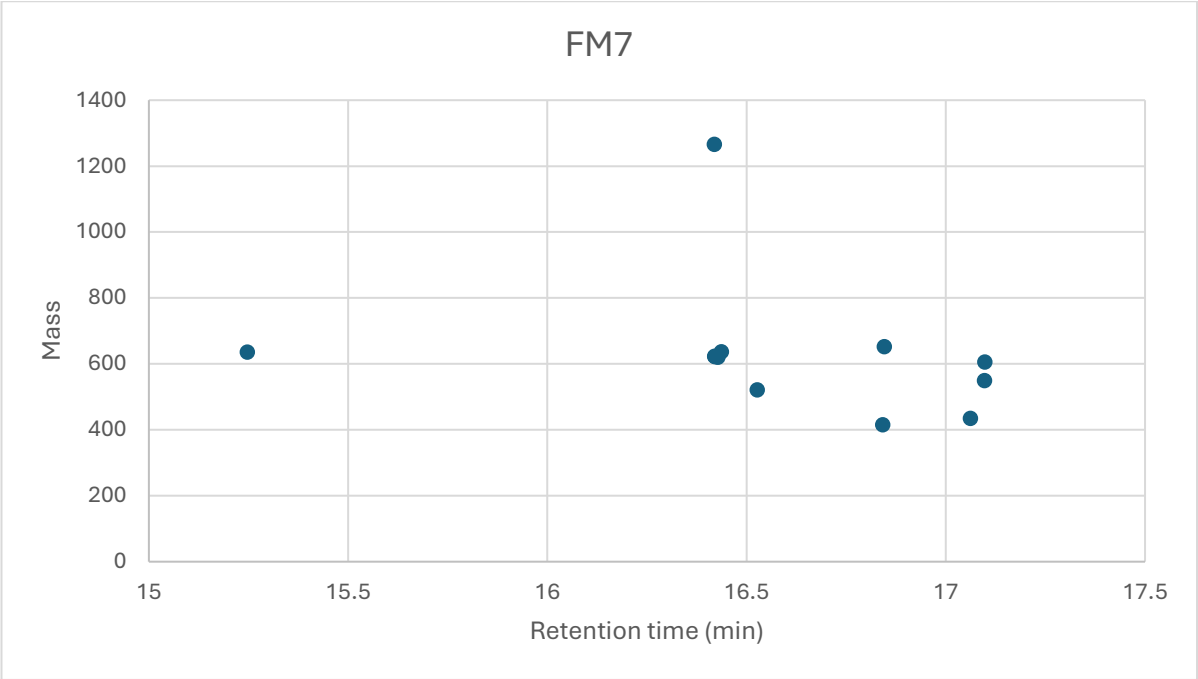

Figure 30 shows the scatter plot of the unknown ion peaks in the FM7 fraction against retention time. The scatter plot indicates that most of the compounds eluted are non-polar in nature with molecular weight between 400-700 Da.

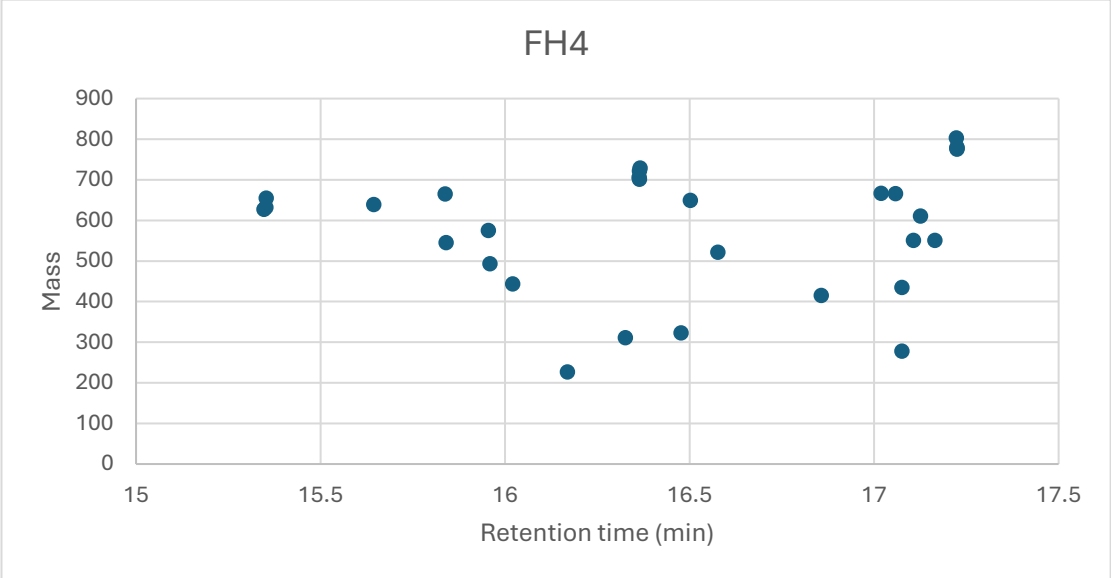

Figure 31 shows the scatter plot of the unknown ion peaks in the FH4 fraction against retention time with most compounds are more non-polar in nature and within the molecular weight of 300-700 Da.

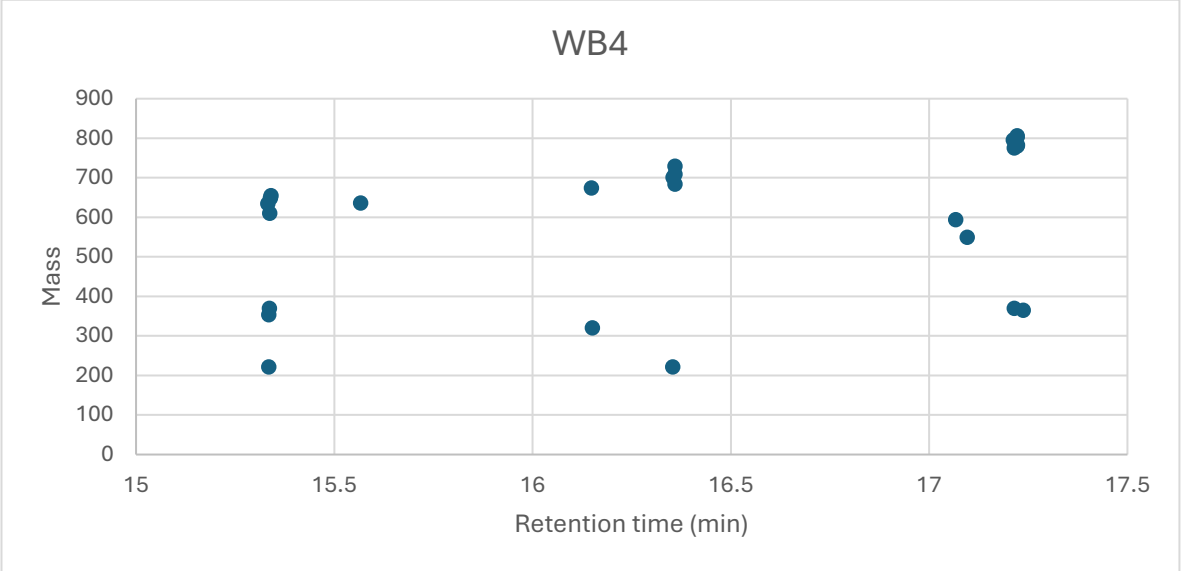

Figure 32 shows the scatter plot of the unknown ion peak in the WB4 fraction against retention time. The scatter plot indicates that all the compounds eluted are non-polar in nature and within the molecular weight range of 300-700 Da.

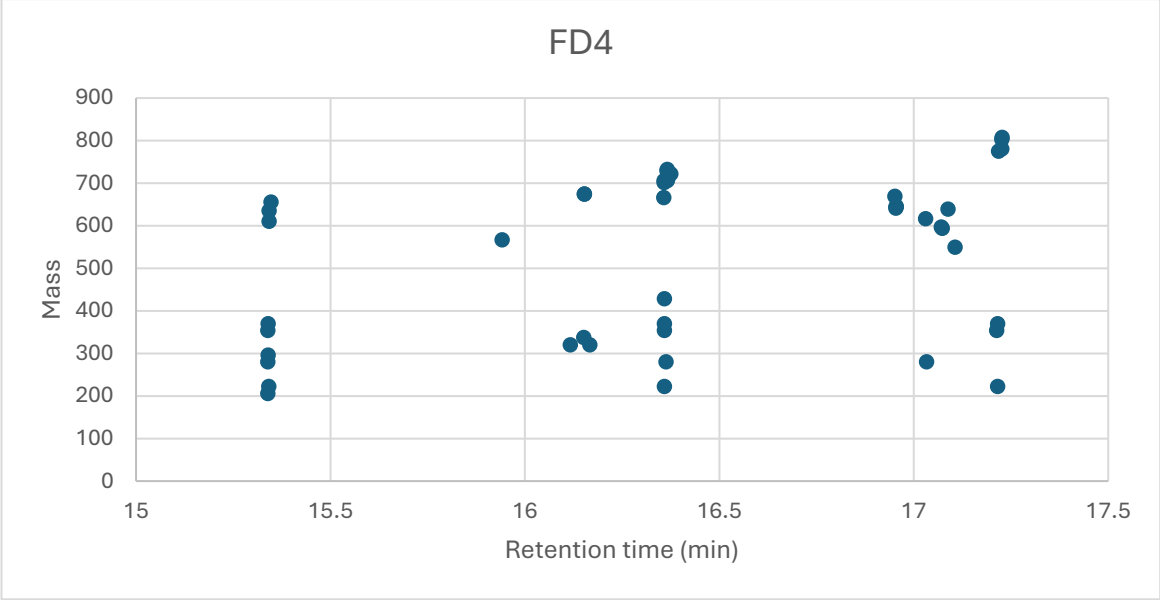

Figure 33 shows the scatter plot of the unknown ion peaks in the FD4 fraction against retention time. The scatter plot indicates that all the compounds eluted are non-polar in nature within the molecular weight range of 200-700 Da.

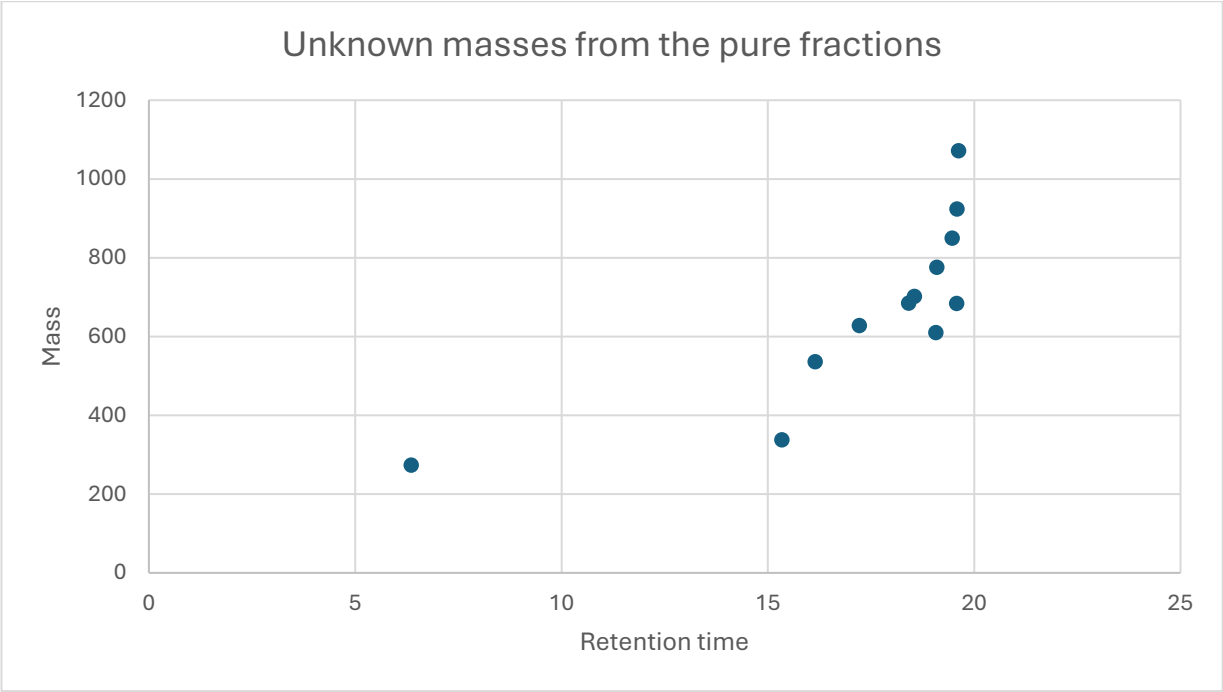

Figure 34 shows the scatter plot of the unknown ion peaks in all the purified fractions. The scatter plot indicates that majority of the compounds retained are non-polar in nature within the mass range of 400-900 Da. The data can be seen in the appendix sections on Table A5-A8.

4.3 Dereplication by NMR

Four compounds were selected for structural analysis based on their ^{1}H NMR spectral profile and these were FH4, FH5, FM7 and FM9, as shown in Figures 35, 36, 37 and 38, respectively, using the Bruker 300/400MHz spectrometer at the UCLan main campus in JB, Firth analytical suite. The 2D NMR data were measured at the School of Chemistry at the University of Edinburgh using the Bruker Avance III HD 800MHz spectrometer. The chemical shift values were referenced with the CD_3OD solvent with experiments such as COSY (10 min), HSQC-Edited (20 min), HSQC-TOCSY (40 min), ROESY (30 min), and HMBC (60 min) ran on each compound as explained in chapter 2.8.1.

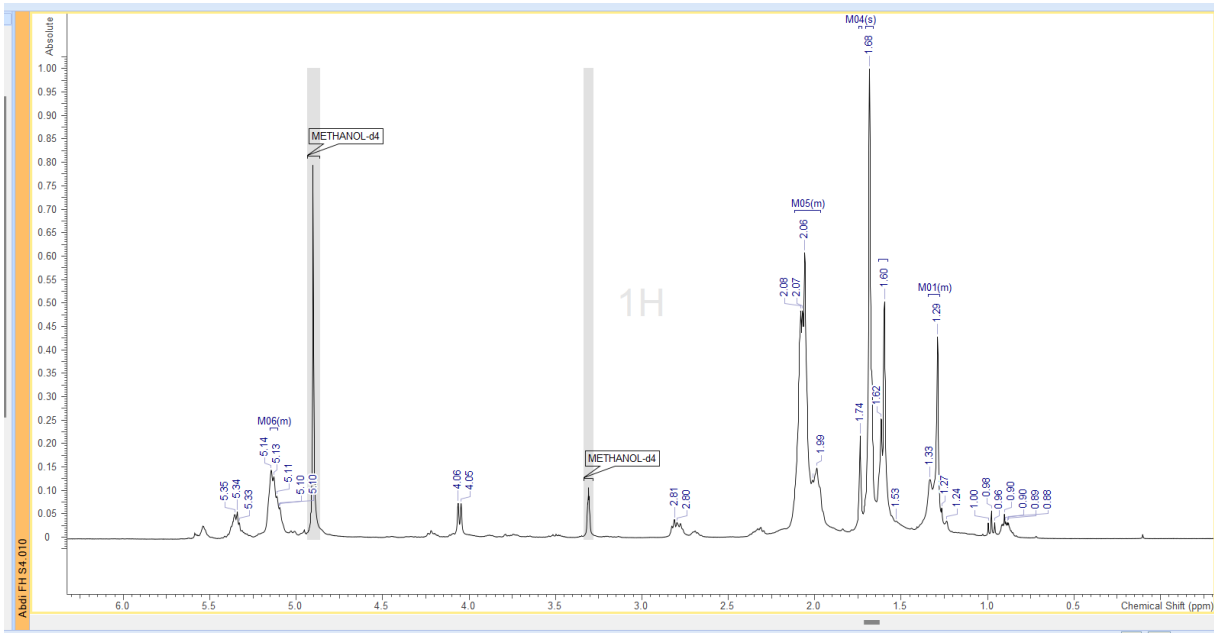

Figure 35 shows the ^{1}H NMR spectra of the FH4 fraction at 800 MHz in CD_3OD.

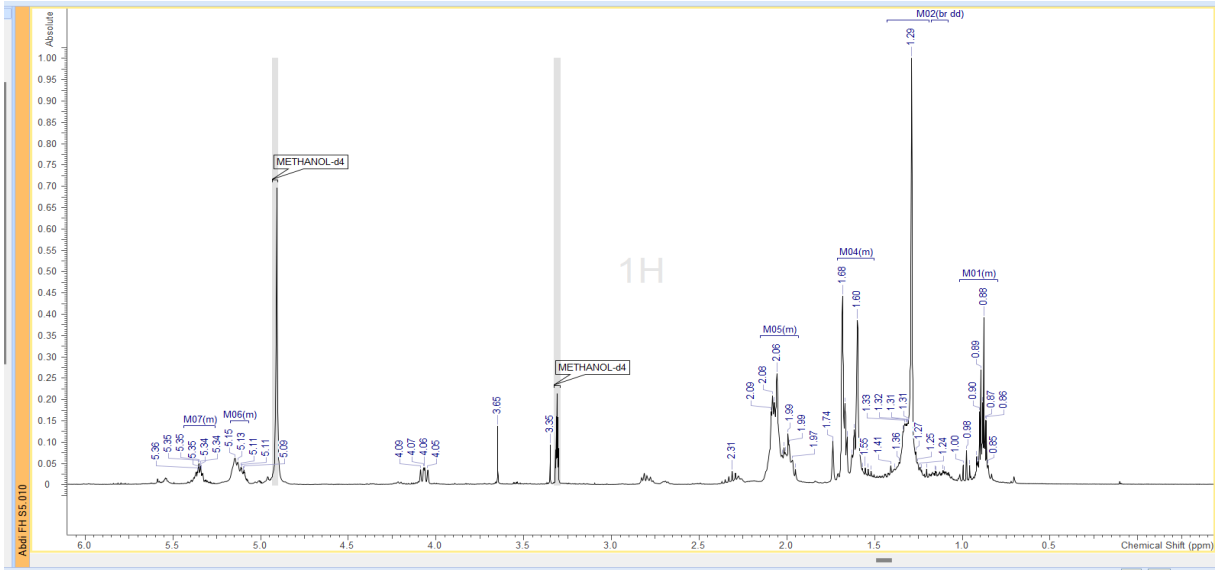

Figure 36 shows the ^{1}H NMR spectra of the FH5 fraction at 800 MHz in CD_3OD.

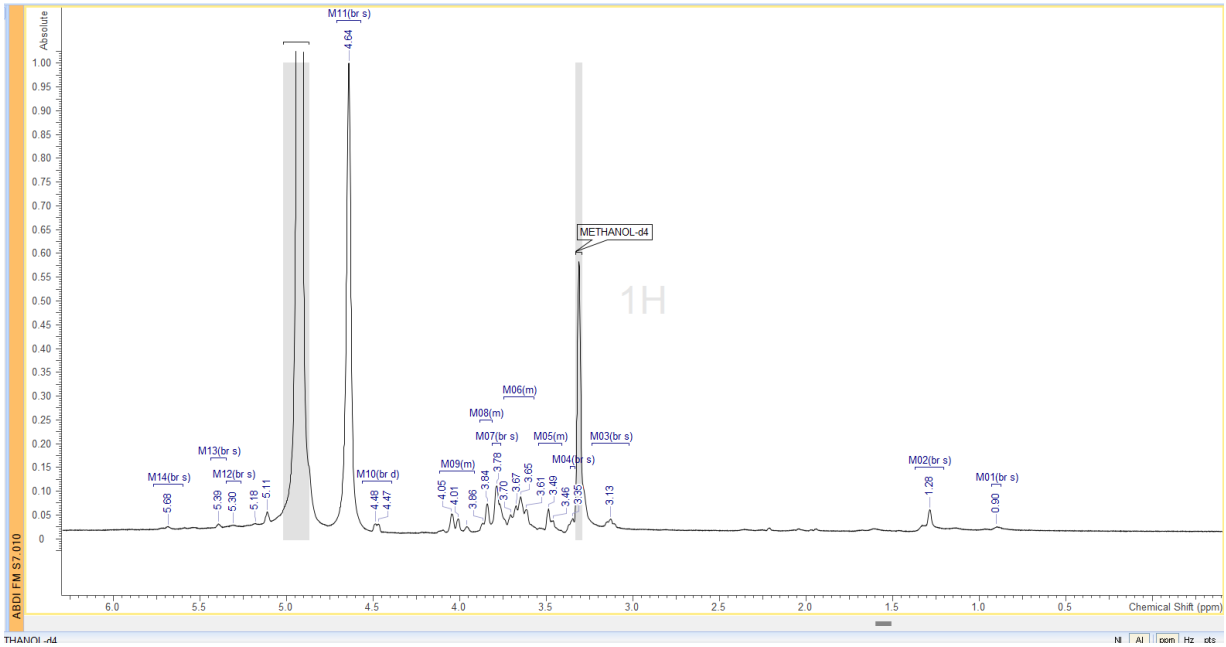

Figure 37 shows the ^{1}H NMR spectra of the FM7 fraction at 800 MHz in CD_3OD.

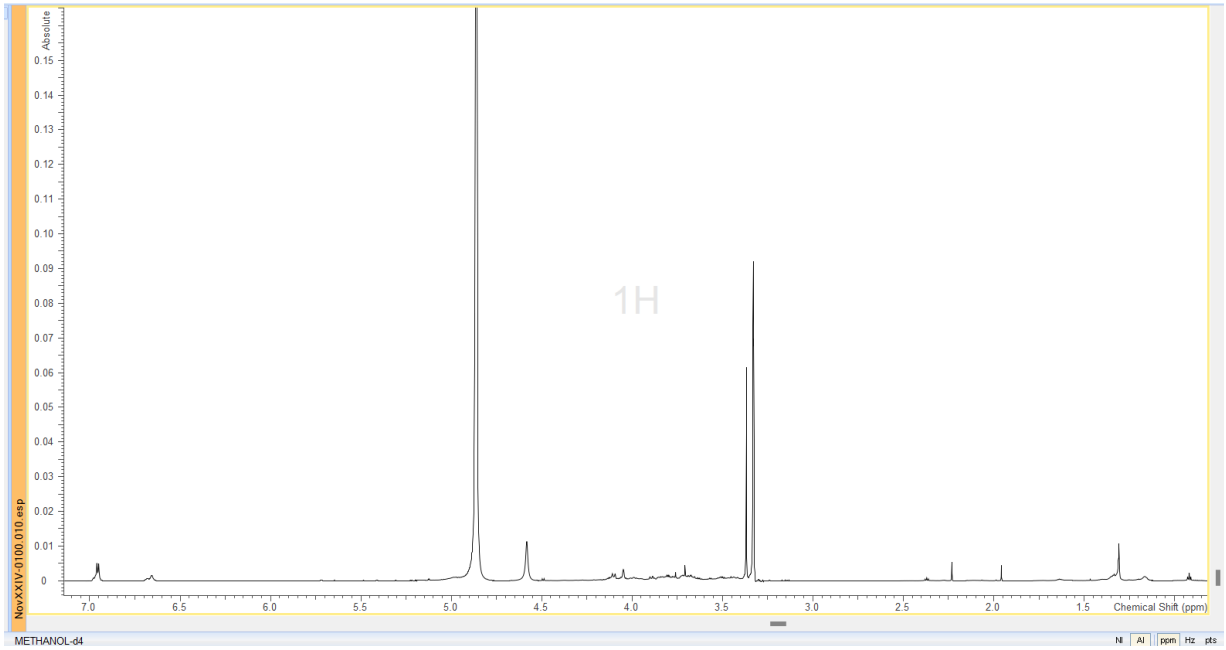

Figure 38 shows the ^{1}H NMR spectra of the FM9 fraction at 800 MHz in CD_3OD.

4.3.1 Dereplication through 1D-NMR and 2D-NMR for structural determination of compound FM7

HRMS analysis of the FM7 compound was showed a possible molecular formula of $C_{23}H_{30}O_{23}$ with the m/z value of 674.123 $[M+H]^+$. The full structure of this compound has not been derived yet, but glimpses of structural fragments could be derived from NMR spin systems (Figure 39). The ^{1}H and ^{13}C NMR spectra indicates signals characteristics of sugars and glycosylated structures with the presence of the anomeric carbons at δ_C 96.83 ppm and 92.56 ppm. Glycosylated compounds are known to exhibit therapeutic effects on diseases such as anti-cancer, antioxidant, and anti-inflammatory for bioactivity[72]. Glycosylated compounds such as vitexin and isovitexin which are derivatives of apigenin show activity against anti-diabetic, anti-Alzheimer's disease, and anti-inflammatory[73]. There are branched sugar moieties that is integrated into a larger structure based on the HMBC interactions and coupling constant. The cyclic regions from protons such as C (3.77 ppm), X (4.06 ppm), and Y (4.06 ppm) as shown in 23 (2A) indicates that they were interconnected based on the HSQC-TOCSY which indicates a cyclic saccharides or sugar-like molecules. The presence of the de-shielded carbon at carbon D (76.67 ppm) and carbon F (74.89 ppm) suggests that there are hydroxyl groups which indicates that the compound contains hydrophilic properties.

The 1D and 2D NMR were used to determine a partial structure (Figure 39) of the fraction FM7 of *Ficus barclayana* (Table A14 in the appendix section). The CH bond at 96.83 ppm(A) and 92.56 ppm (B) are anomeric carbons attached directly to some oxygen in a highly deshielded environment, which correlates to the characteristics of sugar linkages. The first anomeric carbon (A) at 96.83 ppm was a doublet and showed

coupling with proton F (3.15 ppm), which indicates they are part of the same structural unit. The carbon A (96.83 ppm) showed HMBC interactions with carbon D (76.67 ppm), which suggests that they are indirectly bonded in the same structural unit. Proton D (3.36 ppm) correlates with protons F (3.15 ppm) and L (3.30 ppm), which shows they are interconnected in the same region. Carbon F (74.89 ppm) interacts with Carbons A (96.83 ppm) and D (76.67 ppm) on the HMBC. Proton E (3.30 ppm) couples with Protons D (3.36 ppm), L (3.30 ppm), and Ta (3.87 ppm), further supporting the branched structure. This is also the case for the HMBC, as carbon E (76.61 ppm) correlates to carbon T (61.45 ppm), which suggests it's in the same environment in the cyclic region. The HSQC-TOCSY confirms that protons B (5.13 ppm), G (3.69 ppm), H (3.38 ppm), I (3.80 ppm), K (3.32 ppm) and T (3.87 ppm for t_A and 3.67 ppm for t_B) are all in the same cyclic environment as shown in figure 23 (A1) as the determined structure.

The other anomeric carbon B (92.56 ppm) correlates with Carbons H (72.40 ppm) and I (71.57 ppm), indicating these carbons are part of the same chain, according to the HMBC. The Proton B (5.13 ppm) correlates with Proton H (3.38 ppm), which means they are directly bonded together. The proton H (3.38 ppm) correlates to proton G (3.69 ppm), which shows they are directly bonded together, as shown in COSY. Proton G (3.69 ppm) correlates to proton K (3.32 ppm), confirming their direct bond. Proton K (3.32 ppm) is directly bonded to proton I (3.80 ppm), as proton I (3.80 ppm) is directly bonded to proton U (3.80 ppm for u_A and 3.71 ppm for u_B). Carbon I (71.57 ppm) shows interactions with Carbons U (61.36 ppm) on the HMBC as it confirms they are in the same environment of the cyclic region. The HSQC-TOCSY shows that protons B

(5.13 ppm), G (3.69), h (3.38 ppm), I (3.80 ppm), k (3.32 ppm) and U (3.80 ppm for u_A and 3.71 ppm for u_B) are all in the same cyclic environment as shown in figure 39 (1B).

Proton C (3.77 ppm) correlates with proton X (4.06 ppm), which confirms a direct bond between them. Proton X (4.06 ppm) correlates with proton Y (4.06 ppm), confirming a direct bond between the two positions. On the HMBC, Carbon C (81.87 ppm) exhibits correlations with Carbon Y (75.33 ppm), and carbon R (62.79 ppm) correlates with carbon C (81.87 ppm), confirming that it is within the same cyclic region within the structure. The HSQC-TOCSY confirms that protons C (3.77 ppm), X (4.06 ppm), Y (4.06 ppm) and R (3.73 ppm for r_A and 3.63 ppm for r_B) are all within the same environment in the same structure as shown in Figure 39 (2A).

On the COSY proton, N (3.80 ppm) correlates with protons M (3.86 ppm) and P (4.04 ppm for p_A and 3.65 ppm for p_B), which suggests that they are within the same structural environment. This is further confirmed by the HMBC as carbon P (63.15 ppm) shows interactions with carbon M (69.83 ppm), confirming the related arrangements between them. Furthermore, carbon N (67.99 ppm) shows a correlation with carbon M (69.83 ppm), which again confirms that they are in the same region in the cyclic environment. The HSQC-TOCSY shows that protons U (3.80 ppm for u_A and 3.71 ppm for u_B), M (3.86 ppm), N (3.80 ppm) and P (4.04 ppm for p_A and 3.65 ppm for p_B) are all in the same environment as shown in figure 39 (2B).

As for the final information of the last part to the partial structure of compound FM7, the COSY shows proton O (3.68 ppm for o_A and 3.50 for o_B) showing correlations with proton Q (3.64 ppm for q_A and 3.51 ppm for q_B) which shows that they are in the same environment or potentially share a direct bond. On the HMBC, it shows that carbon Q (63.06 ppm) correlates with carbon M (69.83 ppm), which confirms their direct

interactions with each other. A potential structure was determined based on the information from COSY and HMBC, as shown in Figure 39 (3).

Proton J (3.81 ppm) and proton S (3.78 ppm), with the peaks appearing at 70.43 ppm and 61.97 ppm, appear to show no correlation with any other peaks or protons on the COSY and HMBC, which may indicate impurities in the FM7 compound. The reason why a complete structure could not be elucidated for FM7, and partial structures is shown to be due to the impurities in this compound. Therefore, it is not easy to consider whether the elucidated structures are part of the structure of the active compound or not. Further purification using HPLC would increase the chances of fully elucidating the structure of the active compound as it removes the impurities that appear as peaks on the 2D NMR. The COSY, HSQC-Edited, HSQC-TOCSY, ROESY, and HMBC are shown in the appendix as Figures A21-A26.

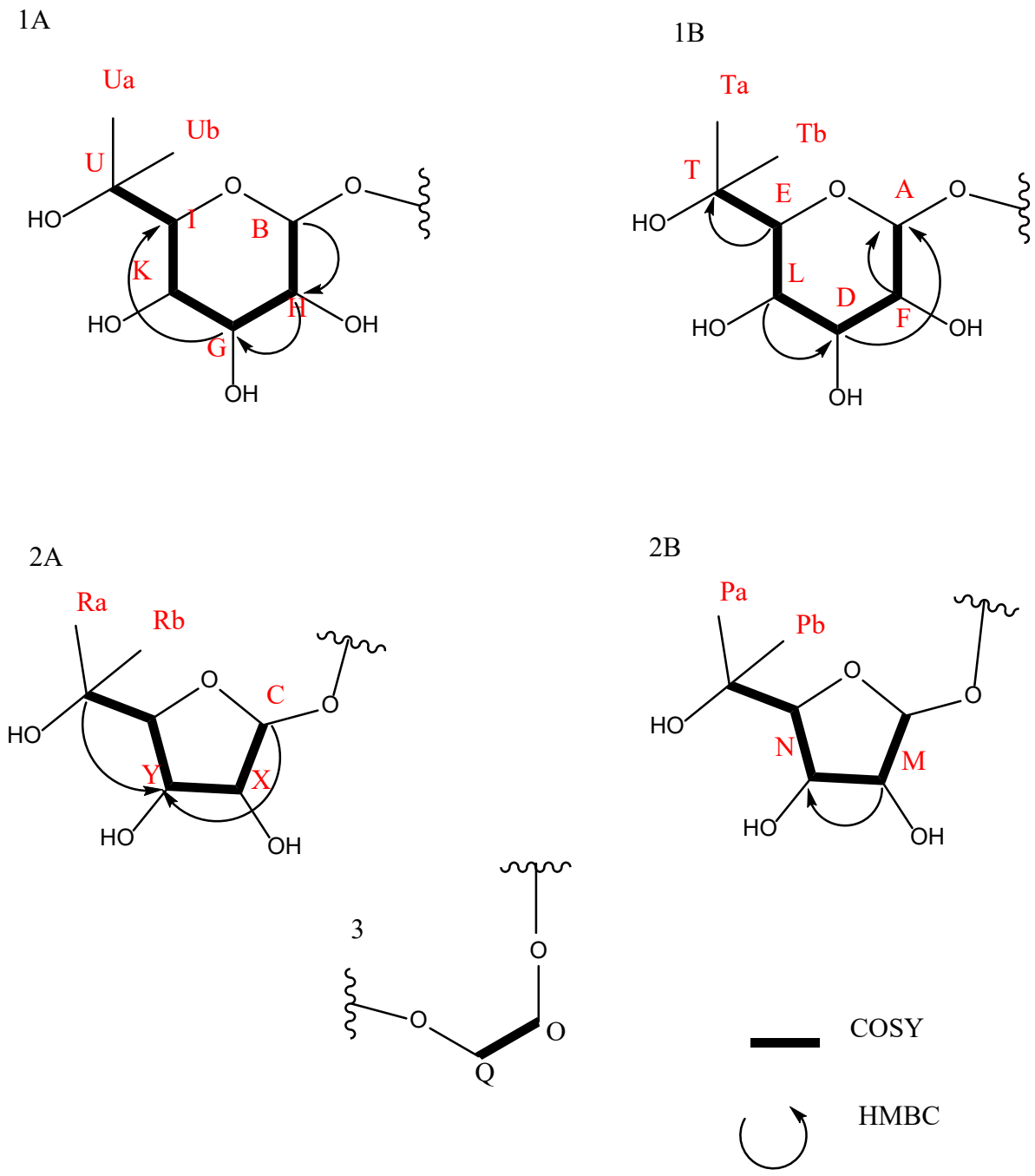

Figure 39 shows the partial structural fragments determined for compound FM7 from the 1D and 2D NMR.

4.3.2 Dereplication through 1D-NMR and 2D-NMR for structural determination of compound FH4

Analysis of NMR data indicates that FH4 is impure and possibly contains three compounds with one major and two minor components. NMR data (Table A13 in the appendix section) have been extracted from ^{1}H, HSQC and HMBC data. Interpretation of NMR data suggests that the compounds belong to a family of compounds called glycolipids based on ^{13}C chemical shifts of the sugars prominent at δ_C 104.08, 90.55, 80.44 ppm for anomeric carbons, δ_C 70-76 ppm for protonated carbons in the sugar framework and δ_C 60-68 ppm for hydroxylated methylenes. The table 6 is partially filled with the COSY and HMBC with what each proton and carbon correlate with.

Interesting chemical shifts can be observed at δ_C 42-52 ppm, suggesting protonated carbons adjacent to nitrogen-containing moieties, such as in amino lipids or peptides (Figure A18 in the appendix section). The fatty acid framework contains both saturated and unsaturated components. Some of these structural fragments are shown in Figure 40. It is difficult to elucidate structures like this as fatty acids and amino lipid share similar structures such as the position of doubles or chain length that makes it difficult to distinguish them. Furthermore, the proton NMR spectra can be crowded as evident in Table A13 in the appendix section because of the overlapping peaks from similar chemicals and they also produce weak spectroscopic signals. The COSY, HSQC and HMBC of the substructures are shown in the appendix as Figures A15-A20.

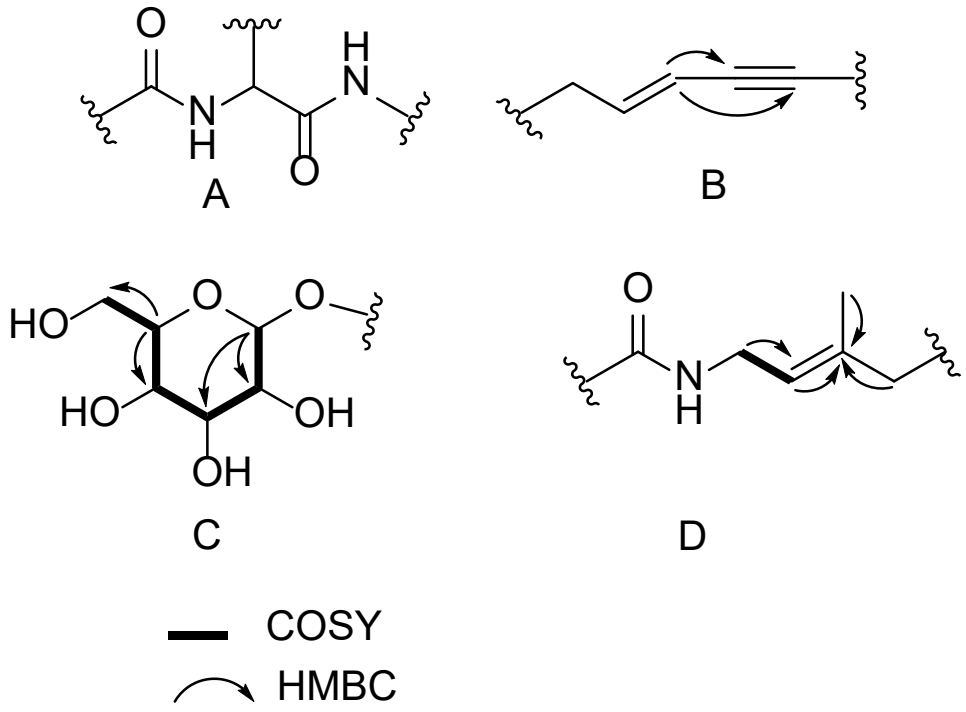

Figure 40 shows structural fragments (A-D) elucidated from FH-4 NMR data suggesting presence of glycolipids and/or amino lipids or potentially lipopeptides.

4.4 Bioassay results

The extracts obtained from the LH-20 Sephadex[62] with the most promising NMR spectra were sent for anticancer screening at Maribo, UiT, the Artic University of Norway, Tromsø[67]. Table A4 in the appendix section). Furthermore, the extracts were also sent for anti-Alzheimer screening for TauRx[39] assay at the University of Aberdeen by Dr David Horsley based on the NMR spectra obtained from the LH-20 Sephadex[62] of the fractions as shown in the appendix (Table A3 in the appendix section). Codes such as FD4 means that it is the fourth fraction from the size exclusion chromatography using the LH-20 Sephadex[62] of the FD fraction.

4.4.1 Anti-cancer screening

The fractions were assayed against three cell lines: A2058_MTT (human melanoma cell line), MRC5_MTT (human lung fibroblast cells), and MCF7_MTT (human breast cancer cell line) to see if they had inhibitory activities against these cancer cells. The results are shown below in Table 1.

The fraction with the most promising activity for the human melanoma cell line (A2058) is the FH5 fraction, with an activity of 1, followed by the fraction FD3, with an activity of 5. When a compound shows an activity of 1 it means that the compound exhibits full activity against the assay. The FH6 and FD 4 are still active for human melanoma, with activities of 27 and 48, respectively. The crude extract of *Ficus barclayana*, FM6, FD5, and WB3 were inactive for the human melanoma cell line, with activities of 104, 108, 101, and 103, respectively.

As for the human lung fibroblast cells assay (MRC5_MTT), it was the fraction FH5 that was the most active at 2, followed by the fraction FD3 with activity at 10. FD5 and FH6

were also active for the human lung fibroblast cells assay (MRC5_MTT), with activities of 39 and 47, respectively. The crude extract of *Ficus barclayana*, FM6, FD4, and WB3 were all inactive for the MRC5_MTT assay as they were all above 50 for activity.

Lastly, the fractions with the most activity for the human breast cell line assay (MCF7_MTT) were FH5, FD3, and FD4, with activities of 1,5 and 6, respectively. The fractions of FH6 and FD5 were also active, with activities of 12 and 22, respectively. The crude extract of *Ficus barclayana*, FM6, and WB3 were all inactive for the MCF7_MTT assay.

Table 1 shows the samples that were active for the anticancer screening.

MATERIAL_ID	MATERIAL_TYPE	ASSAY_CATEGORY	ASSAY_NAME	ACTIVITY	UNITS	ASSAY_QUAL_RESULT	ASSAY_DATE	CONCENTRATION
FH5	F	ANTI-CANCER	A2058_MTT	1	PCT_SURVIVAL	A	09/12/2024	200
FH6	F	ANTI-CANCER	A2058_MTT	27	PCT_SURVIVAL	A	09/12/2024	200
FD3	F	ANTI-CANCER	A2058_MTT	5	PCT_SURVIVAL	A	09/12/2024	200
FD4	F	ANTI-CANCER	A2058_MTT	48	PCT_SURVIVAL	A	09/12/2024	200
FH5	F	ANTI-CANCER	MRC5_MTT	2	PCT_SURVIVAL	A	09/12/2024	200
FH6	F	ANTI-CANCER	MRC5_MTT	47	PCT_SURVIVAL	A	09/12/2024	200
FD3	F	ANTI-CANCER	MRC5_MTT	10	PCT_SURVIVAL	A	09/12/2024	200
FD5	F	ANTI-CANCER	MRC5_MTT	39	PCT_SURVIVAL	A	09/12/2024	200
FH5	F	ANTI-CANCER	MCF7_MTT	1	PCT_SURVIVAL	A	13/12/2024	200
FH6	F	ANTI-CANCER	MCF7_MTT	12	PCT_SURVIVAL	A	13/12/2024	200
FD3	F	ANTI-CANCER	MCF7_MTT	5	PCT_SURVIVAL	A	13/12/2024	200
FD4	F	ANTI-CANCER	MCF7_MTT	6	PCT_SURVIVAL	A	13/12/2024	200
FD5	F	ANTI-CANCER	MCF7_MTT	22	PCT_SURVIVAL	A	13/12/2024	200

4.4.2 Anti-Alzheimer's screening

The fractions were sent for the B_{50} assay and run on the EC_{50} assay (cells), and the fractions showed some activity, as shown in the table below. The active samples were FD4, FD5, FH5, and FM6. The method for the anti-Alzheimer's screening in chapter 3.7 of the method section. The assay that the fractions were tested against is the EC_{50} and B_{50} which means that the results will show how much of the fractions is required to inhibit a given biological activity by half. These are compared with Methyl 3,4,5-trimethoxycinnamate (MTC) which was the reference and has an activity at 191uM as shown in table 5 and the FD4 showing activity of 69.2 ug/mL on 25/11/2024 and 30.8 ug/mL. The FD5, FH5 and FM6 showed activity for the anti-Alzheimer's screening as they had activity of 57.1 ug/mL, 104 ug/mL and 466 ug/mL respectively. FD3, WB3 and FH4 fraction showed no activity because the result obtained from the B_{50} to be more than 500 ug/mL. The results are shown below as Table 2.

Table 2 shows the results of the fractions for the B50 assay.

Name and structure	**Experiment**	**B_{50}**	**B_{50} (µg/mL) mean±SEM**	**Notes**
Sample 1 Crude	25Nov24 26Nov24	NE (500) NE (500)	NE (500µg/mL) n=2	1.5mg +150µL DMSO 10mg/mL
Sample 2 FD3	25Nov24 26Nov24	NE (500) >600µg/mL		12.3mg +123µL DMSO 100mg/mL
Sample 3 FD4	25Nov24 26Nov24	69.2 µg/mL 30.8µg/mL		1.4mg +140µL DMSO 10mg/mL
Sample 4 FD5	25Nov24 26Nov24	~600µg/mL 57.1µg/mL		3.6mg +360µL DMSO 10mg/mL
Sample 5 WB3	25Nov24 26Nov24	NE (500) NE (500)	NE (500µg/mL) n=2	45.6mg + 456µL DMSO 100mg/mL
Sample 6 FH4	25Nov24 26Nov24	NE (500) NE (500)	NE (500µg/mL) n=2	8mg +80µL DMSO 100mg/mL
Sample 7 FH5	25Nov24 26Nov24	138 µg/mL 104µg/mL		7mg +70µL DMSO 100mg/mL

Name and structure	**Experiment**	**B_{50}**	**B_{50} (µg/mL)** **mean±SEM**	**Notes**
Sample 8 FM6	25Nov24 26Nov24	>600µg/mL 466µg/mL		1mg +100µL DMSO 10mg/mL

Table 3 shows the reference compounds used for the B50 assay.

Name and structure	**Experiment**	**B_{50}**
MTC 6599SC177 WL0014.062 (Reference) 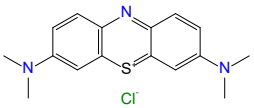		
MTC 8865SR57 WL0014.063 (Reference) 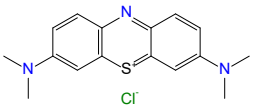	25Nov24 26Nov24	191µM 190µM
DMMTC WL007.004 Serva 14535	25Nov24 26Nov24	7.35µM 3.23µM

Name and structure	Experiment	B_{50}
(Reference) 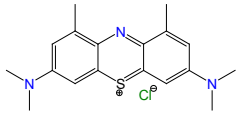		

CHAPTER FIVE

5.0 Conclusion

This research aimed to isolate the tau aggregation inhibitor from the Fijian plant, *Ficus barclayana,* using advanced chromatography, mass spectrometry and NMR techniques against the backdrop that there was no available information or chemical profiling of this plant. Eight compounds were generally isolated, of which six showed activity in the bioassay analysis for anti-cancer and anti-Alzheimer's screening. However, none of them were deemed pure enough for full confirmation of structures.

This project's aim and objectives were met as four active compounds were isolated for the B_{50} anti-Alzheimer's bioassay screening, which showed activity. The four active compounds were FD4, FD5, FH5 and FM6, whereas FD3, WB3 and FH4, showed no activity for the anti-Alzheimer's screening. The extracts were also screened for three different cancer lines: A2058_MTT (human melanoma cell line), MRC5_MTT (human lung fibroblast cells), and MCF7_MTT (human breast cancer cell line. The extracts that showed the most activity for the three cancer lines were FH5, FH6 and FD3. The FD4 and FD3 extracts were active against two cancer lines, whereas the rest were inactive for any of the three cancer lines.

The FH5 extract showed very interesting activities as it showed activities in all three anti-cancer cell lines and for the anti-Alzheimer's B_{50} assay. 1D and 2D NMR analysis was done on the FH5 fraction, but structural elucidation was not possible for this compound because the compound was not fully pure. To successfully determine the structure of the FH5 fraction, HPLC will be used to purify the compound, allowing the structure to be determined through 1D and 2D NMR analysis. Data from high-resolution mass spectrometry including the identification of the correct molecular

formula will be used to support the structure proposed by NMR techniques. The exact process will be performed with the FD3 and FD4 fractions as they showed activity against two of the three cancer line screenings and activity for the anti-Alzheimer's screening. Furthermore, the remaining three active compounds will need their potential structures determined by 2D NMR and confirmed using high-resolution mass spectrometry. All this needs to be completed so that this research can be published as a peer-reviewed journal article and a review written for the compounds in *Ficus barclayana*, as limited research have been performed on this plant.

Since *Ficus barclayana* has not been studied before, the findings of this research hold great potential for developing an anti-cancer and anti-Alzheimer drug in the future for the cosmetic and pharmaceutical industries. Overall, the aims and objectives of this research have been accomplished.

5.1 Limitations

The purity of the compounds such as Glycolipids, amino lipids, or Glycosylated within the FM7 and FH4 fractions make it difficult for the structures to be determined due to their structural variants. This makes it difficult to assign the NMR peaks as they overlap. The glycosylated and sugar compounds have multiple stereoisomers and anomers, making it difficult to distinguish them because the distinct signals are too close apart. These are the reasons why a partial structure was proposed for the FM7 and FH4 compounds.

Small quantities of the compounds yielded during the isolation process restricted the analysis that could be done, such as repeated screening for biological activities. The compound’s biological activity showed promising anti-cancer and anti-Alzheimer's activity with six active compounds. However, it did not specify if the active compounds

were ready for therapeutic potential as more testing was needed, and the yield and time were insufficient. Furthermore, the isolated compounds needed to be analysed using NMR spectroscopy techniques and LCMS as that was the only quantity available that was extracted from the crude.

Lastly, since there was minimal information on the *Ficus barclayana* plant, there was a lack of comparative standards for the compound classes that could have helped in the biological activities of the compounds and the structural determination. Furthermore, there is also a lack of literature review on the *Ficus barclayana* as there is no industrial use for this plant that could have helped in solving the structures of the active compounds. The results and data generated for this thesis should help in future work on this plant. They allow for comparisons and the complete structure determination of the active compounds.

5.2 Future wok

Since there's a lack of available literature review for the *Ficus barclayana* plant, one of the objectives of this research aimed at creating a review of the compounds found in *Ficus barclayana* as these compounds have an excellent potential for developing an anti-cancer and anti-Alzheimer's drug. Based on the bioassay results, six active compounds were managed to be isolated (FH5, FH6, FM6, FD3, FD4 and FD5) for the anti-cancer and anti-Alzheimer's screening, as shown in the results section. These active compounds need their whole structure to be determined and confirmed using high-resolution mass spectrometry, which was impossible in this research as only one structure was partially determined. A complete chemical profile needs to be done for these active compounds for this research to be published, which is the next step after the submission of this thesis. The active compounds would need to be purified using

HPLC to remove the impurities and then sent for 1D and 2D analysis to fully determine the structure. LCMS would need to be performed on these active compounds to confirm the chemical formula; this way, you must analyse both NMR and LCMS to propose these active compounds' structure and chemical profile.

This research provides a promising foundation of the isolated compounds for exploration into their anti-cancer and anti-Alzheimer potential by scaling up the isolation process and producing higher yields of the active compounds. The limited yield of the active compounds massively restricts the extent of the analysis that can be done, such as repeated bioassay tests, to understand these compounds fully. For instance, future research should look at expanding the scope of bioassays to include cytotoxicity, which will provide necessary information on the therapeutic potential of these compounds. More active compounds can be obtained by scaling up the isolation and extraction processes, providing materials for comprehensive structural studies that were unavailable during this research. This should establish a standardised protocol for compound isolation, purification, and analysis to maximise the ability for comparative studies to be done and the yield produced for the active compounds.

After this research is published and the structures of the active compounds are confirmed, the following steps should be taken: Pharmacological studies to understand the active compounds' bioavailability, metabolism, and potent toxicity, which would be crucial for their therapeutic applications. Also, to find viable therapeutic agents, collaborations with academic and pharmaceutical industries that specialise in drug development and can facilitate these findings if needed, as they are expensive.

References

(1) Houssen, W. E.; Jaspars, M. Isolation of Marine Natural Products. In *Natural Products Isolation*; Sarker, S. D., Nahar, L., Eds.; Humana Press: Totowa, NJ, 2012; pp 367–392. https://doi.org/10.1007/978-1-61779-624-1_14.

(2) *Alzheimer's disease - Symptoms and causes*. Mayo Clinic. https://www.mayoclinic.org/diseases-conditions/alzheimers-disease/symptoms-causes/syc-20350447 (accessed 2024-12-03).

(3) Crowther, R. A.; Wischik, C. M. Image Reconstruction of the Alzheimer Paired Helical Filament. *EMBO J* **1985**, *4* (13B), 3661–3665.

(4) Grundke-Iqbal, I.; Iqbal, K.; Tung, Y. C.; Quinlan, M.; Wisniewski, H. M.; Binder, L. I. Abnormal Phosphorylation of the Microtubule-Associated Protein Tau (Tau) in Alzheimer Cytoskeletal Pathology. *Proc Natl Acad Sci U S A* **1986**, *83* (13), 4913–4917. https://doi.org/10.1073/pnas.83.13.4913.

(5) Breijyeh, Z.; Karaman, R. Comprehensive Review on Alzheimer's Disease: Causes and Treatment. *Molecules* **2020**, *25* (24), 5789. https://doi.org/10.3390/molecules25245789.

(6) Schachter, A. S.; Davis, K. L. <no Title>. **2000**.

(7) Spires-Jones, T. L.; Hyman, B. T. The Intersection of Amyloid Beta and Tau at Synapses in Alzheimer's Disease. *Neuron* **2014**, *82* (4), 756–771. https://doi.org/10.1016/j.neuron.2014.05.004.

(8) Overk, C. R.; Masliah, E. Pathogenesis of Synaptic Degeneration in Alzheimer's Disease and Lewy Body Disease. *Biochemical Pharmacology* **2014**, *88* (4), 508–516. https://doi.org/10.1016/j.bcp.2014.01.015.

(9) Anand, P.; Singh, B. A Review on Cholinesterase Inhibitors for Alzheimer's Disease. *Arch. Pharm. Res.* **2013**, *36* (4), 375–399. https://doi.org/10.1007/s12272-013-0036-3.

(10) Sharma, K. Cholinesterase Inhibitors as Alzheimer's Therapeutics (Review). *Molecular Medicine Reports* **2019**, *20* (2), 1479–1487. https://doi.org/10.3892/mmr.2019.10374.

(11) Tweedie, D.; Fukui, K.; Li, Y.; Yu, Q.; Barak, S.; Tamargo, I. A.; Rubovitch, V.; Holloway, H. W.; Lehrmann, E.; Iii, W. H. W.; Zhang, Y.; Becker, K. G.; Perez, E.; Praag, H. V.; Luo, Y.; Hoffer, B. J.; Becker, R. E.; Pick, C. G.; Greig, N. H. Cognitive Impairments Induced by Concussive Mild Traumatic Brain Injury in Mouse Are Ameliorated by Treatment with Phenserine via Multiple Non-Cholinergic and Cholinergic Mechanisms. *PLOS ONE* **2016**, *11* (6), e0156493. https://doi.org/10.1371/journal.pone.0156493.

(12) Kamal, M. A.; Greig, N. H.; Alhomida, A. S.; Al-Jafari, A. A. Kinetics of Human Acetylcholinesterase Inhibition by the Novel Experimental Alzheimer Therapeutic Agent, Tolserine. *Biochemical Pharmacology* **2000**, *60* (4), 561–570. https://doi.org/10.1016/S0006-2952(00)00330-0.

(13) Zhan, Z.-J.; Bian, H.-L.; Wang, J.-W.; Shan, W.-G. Synthesis of Physostigmine Analogues and Evaluation of Their Anticholinesterase Activities. *Bioorganic & Medicinal Chemistry Letters* **2010**, *20* (5), 1532–1534. https://doi.org/10.1016/j.bmcl.2010.01.097.

(14) Liu, J.; Chang, L.; Song, Y.; Li, H.; Wu, Y. The Role of NMDA Receptors in Alzheimer's Disease. *Front. Neurosci.* **2019**, *13*. https://doi.org/10.3389/fnins.2019.00043.

(15) Delacourte, A.; Flament, S.; Dibe, E. M.; Hublau, P.; Sablonnière, B.; Hémon, B.; Shérrer, V.; Défossez, A. Pathological Proteins Tau 64 and 69 Are Specifically Expressed in the Somatodendritic Domain of the Degenerating Cortical Neurons during Alzheimer's Disease. Demonstration with a Panel of Antibodies against Tau Proteins. *Acta Neuropathol* **1990**, *80* (2), 111–117. https://doi.org/10.1007/BF00308912.
(16) Indrayanto, G. The Importance of Method Validation in Herbal Drug Research. *Journal of Pharmaceutical and Biomedical Analysis* **2022**, *214*, 114735. https://doi.org/10.1016/j.jpba.2022.114735.
(17) In Vivo *vs* In Vitro*: Definition, Pros and Cons*. Drug Discovery from Technology Networks. http://www.technologynetworks.com/drug-discovery/articles/in-vivo-vs-in-vitro-definition-pros-and-cons-350415 (accessed 2025-01-10).
(18) *Definition of ex vivo - NCI Dictionary of Cancer Terms - NCI*. https://www.cancer.gov/publications/dictionaries/cancer-terms/def/ex-vivo (accessed 2025-01-10).
(19) Lei, Y.; Yong, Z.; Junzhi, W. Development and Application of Potency Assays Based on Genetically Modified Cells for Biological Products. *Journal of Pharmaceutical and Biomedical Analysis* **2023**, *230*, 115397. https://doi.org/10.1016/j.jpba.2023.115397.
(20) Aykul, S.; Martinez-Hackert, E. Determination of Half-Maximal Inhibitory Concentration Using Biosensor-Based Protein Interaction Analysis. *Analytical Biochemistry* **2016**, *508*, 97–103. https://doi.org/10.1016/j.ab.2016.06.025.
(21) Ji, H.-F.; Li, X.-J.; Zhang, H.-Y. Natural Products and Drug Discovery. Can Thousands of Years of Ancient Medical Knowledge Lead Us to New and Powerful Drug Combinations in the Fight against Cancer and Dementia? *EMBO Rep* **2009**, *10* (3), 194–200. https://doi.org/10.1038/embor.2009.12.
(22) Katiyar, C.; Gupta, A.; Kanjilal, S.; Katiyar, S. Drug Discovery from Plant Sources: An Integrated Approach. *Ayu* **2012**, *33* (1), 10–19. https://doi.org/10.4103/0974-8520.100295.
(23) Norn, S.; Permin, H.; Kruse, P. R.; Kruse, E. [From willow bark to acetylsalicylic acid]. *Dan Medicinhist Arbog* **2009**, *37*, 79–98.
(24) *The Chemistry of Aspirin | The International Aspirin Foundation*. Aspirin Foundation. https://www.aspirin-foundation.com/history/chemistry/ (accessed 2024-04-24).
(25) Dias, D. A.; Urban, S.; Roessner, U. A Historical Overview of Natural Products in Drug Discovery. *Metabolites* **2012**, *2* (2), 303–336. https://doi.org/10.3390/metabo2020303.
(26) Newman, D. J.; Cragg, G. M.; Snader, K. M. The Influence of Natural Products upon Drugdiscovery. *Nat. Prod. Rep.* **2000**, *17* (3), 215–234. https://doi.org/10.1039/A902202C.
(27) Briskin, D. P. Medicinal Plants and Phytomedicines. Linking Plant Biochemistry and Physiology to Human Health. *Plant Physiology* **2000**, *124* (2), 507–514.
(28) Press, N. J.; Joly, E.; Ertl, P. Chapter Four - Natural Product Drug Delivery: A Special Challenge? In *Progress in Medicinal Chemistry*; Witty, D. R., Cox, B., Eds.; Elsevier, 2019; Vol. 58, pp 157–187. https://doi.org/10.1016/bs.pmch.2019.01.001.
(29) Shaivi, L.; Turabi, K. S.; Aich, J.; Devarajan, S.; Unni, D.; Garse, S. Chapter 6 - In Silico Approaches in the Repurposing of Bioactive Natural Products for Drug

Discovery. In *Phytochemistry, Computational Tools and Databases in Drug Discovery*; Egbuna, C., Rudrapal, M., Tijjani, H., Eds.; Drug Discovery Update; Elsevier, 2023; pp 125–147. https://doi.org/10.1016/B978-0-323-90593-0.00010-1.
(30) Lam, K. S. New Aspects of Natural Products in Drug Discovery. *Trends in Microbiology* **2007**, *15* (6), 279–289. https://doi.org/10.1016/j.tim.2007.04.001.
(31) *Anticancer Screening - an overview | ScienceDirect Topics*. https://www.sciencedirect.com/topics/pharmacology-toxicology-and-pharmaceutical-science/anticancer-screening (accessed 2025-07-06).
(32) Ganot, N.; Meker, S.; Reytman, L.; Tzubery, A.; Tshuva, E. Y. Anticancer Metal Complexes: Synthesis and Cytotoxicity Evaluation by the MTT Assay. *J Vis Exp* **2013**, No. 81, 50767. https://doi.org/10.3791/50767.
(33) *Ficus | Description, Pollination, & Major Species | Britannica*. https://www.britannica.com/plant/Ficus (accessed 2024-04-18).
(34) Badgujar, S. B.; Patel, V. V.; Bandivdekar, A. H.; Mahajan, R. T. Traditional Uses, Phytochemistry and Pharmacology of Ficus Carica: A Review. *Pharmaceutical Biology* **2014**, *52* (11), 1487–1503. https://doi.org/10.3109/13880209.2014.892515.
(35) Chawla, A.; Kaur, R.; Sharma, A. K. Ficus Carica Linn.: A Review on Its Pharmacognostic, Phytochemical and Pharmacological Aspects. *Int J Pharmacol Res* **2012**, *2012*, 215–232.
(36) Rubnov, S.; Kashman, Y.; Rabinowitz, R.; Schlesinger, M.; Mechoulam, R. Suppressors of Cancer Cell Proliferation from Fig (Ficus Carica) Resin: Isolation and Structure Elucidation. *J. Nat. Prod.* **2001**, *64* (7), 993–996. https://doi.org/10.1021/np000592z.
(37) Yang, J. The SNP-Based Heritability — A Commentary on Yang et al. (2010). *Twin Res Hum Genet* **2020**, *23* (2), 118–119. https://doi.org/10.1017/thg.2020.25.
(38) Patil, V.; Patil, V. Evaluation of Anti-Inflammatory Activity of Ficus Carica Linn. Leaves. *Indian Jouranl of Natural Products and Resources* **2011**, *2*.
(39) *Investors*. TauRx. https://taurx.com/ (accessed 2025-01-13).
(40) Zhang, L.; Song, J.; Kong, L.; Yuan, T.; Li, W.; Zhang, W.; Hou, B.; Lu, Y.; Du, G. The Strategies and Techniques of Drug Discovery from Natural Products. *Pharmacology & Therapeutics* **2020**, *216*, 107686. https://doi.org/10.1016/j.pharmthera.2020.107686.
(41) Atanasov, A. G.; Zotchev, S. B.; Dirsch, V. M.; Supuran, C. T. Natural Products in Drug Discovery: Advances and Opportunities. *Nat Rev Drug Discov* **2021**, *20* (3), 200–216. https://doi.org/10.1038/s41573-020-00114-z.
(42) Seeman, J. I. R. B. Woodward: A Larger-than-Life Chemistry Rock Star. *Angewandte Chemie* **2017**, *129* (34), 10362–10379. https://doi.org/10.1002/ange.201702635.
(43) Nicolaou, K. C.; Vourloumis, D.; Winssinger, N.; Baran, P. S. The Art and Science of Total Synthesis at the Dawn of the Twenty-First Century. *Angewandte Chemie International Edition* **2000**, *39* (1), 44–122. https://doi.org/10.1002/(SICI)1521-3773(20000103)39:1<44::AID-ANIE44>3.0.CO;2-L.
(44) Birdsall, T. C. Berberine: Therapeutic Potential of an Alkaloid Found in Several Medicinal Plants. *Alternative Medicine Review* **1997**, *2* (2), 94–103.

(45) Ilyas, Z.; Perna, S.; Al-thawadi, S.; Alalwan, T. A.; Riva, A.; Petrangolini, G.; Gasparri, C.; Infantino, V.; Peroni, G.; Rondanelli, M. The Effect of Berberine on Weight Loss in Order to Prevent Obesity: A Systematic Review. *Biomedicine & Pharmacotherapy* **2020**, *127*, 110137. https://doi.org/10.1016/j.biopha.2020.110137.
(46) Sun, C.; Dong, S.; Chen, W.; Li, J.; Luo, E.; Ji, J. Berberine Alleviates Alzheimer's Disease by Regulating the Gut Microenvironment, Restoring the Gut Barrier and Brain-Gut Axis Balance. *Phytomedicine* **2024**, *129*, 155624. https://doi.org/10.1016/j.phymed.2024.155624.
(47) Hertzberg, R. P.; Pope, A. J. High-Throughput Screening: New Technology for the 21st Century. *Current Opinion in Chemical Biology* **2000**, *4* (4), 445–451. https://doi.org/10.1016/S1367-5931(00)00110-1.
(48) Boutros, M.; Heigwer, F.; Laufer, C. Microscopy-Based High-Content Screening. *Cell* **2015**, *163* (6), 1314–1325. https://doi.org/10.1016/j.cell.2015.11.007.
(49) Young, D. W.; Bender, A.; Hoyt, J.; McWhinnie, E.; Chirn, G.-W.; Tao, C. Y.; Tallarico, J. A.; Labow, M.; Jenkins, J. L.; Mitchison, T. J.; Feng, Y. Integrating High-Content Screening and Ligand-Target Prediction to Identify Mechanism of Action. *Nat Chem Biol* **2008**, *4* (1), 59–68. https://doi.org/10.1038/nchembio.2007.53.
(50) Shoichet, B. K. Virtual Screening of Chemical Libraries. *Nature* **2004**, *432* (7019), 862–865. https://doi.org/10.1038/nature03197.
(51) *Structure Elucidation - an overview | ScienceDirect Topics*. https://www.sciencedirect.com/topics/pharmacology-toxicology-and-pharmaceutical-science/structure-elucidation (accessed 2024-12-10).
(52) *2D NMR Introduction*. Chemistry LibreTexts. https://chem.libretexts.org/Bookshelves/Physical_and_Theoretical_Chemistry_Textbook_Maps/Supplemental_Modules_(Physical_and_Theoretical_Chemistry)/Spectroscopy/Magnetic_Resonance_Spectroscopies/Nuclear_Magnetic_Resonance/2D_NMR/2D_NMR_Introduction (accessed 2024-12-10).
(53) Elyashberg, M. Identification and Structure Elucidation by NMR Spectroscopy. *TrAC Trends in Analytical Chemistry* **2015**, *69*, 88–97. https://doi.org/10.1016/j.trac.2015.02.014.
(54) *Handbook of Marine Natural Products*; Fattorusso, E., Gerwick, W. H., Taglialatela-Scafati, O., Eds.; Springer Netherlands: Dordrecht, 2012. https://doi.org/10.1007/978-90-481-3834-0.
(55) Xie, T.; Song, S.; Li, S.; Ouyang, L.; Xia, L.; Huang, J. Review of Natural Product Databases. *Cell Prolif* **2015**, *48* (4), 398–404. https://doi.org/10.1111/cpr.12190.
(56) Gallo, K.; Kemmler, E.; Goede, A.; Becker, F.; Dunkel, M.; Preissner, R.; Banerjee, P. SuperNatural 3.0—a Database of Natural Products and Natural Product-Based Derivatives. *Nucleic Acids Research* **2023**, *51* (D1), D654–D659. https://doi.org/10.1093/nar/gkac1008.
(57) Kim, S.; Thiessen, P. A.; Bolton, E. E.; Chen, J.; Fu, G.; Gindulyte, A.; Han, L.; He, J.; He, S.; Shoemaker, B. A.; Wang, J.; Yu, B.; Zhang, J.; Bryant, S. H. PubChem Substance and Compound Databases. *Nucleic Acids Res* **2016**, *44* (Database issue), D1202–D1213. https://doi.org/10.1093/nar/gkv951.

(58) Appendino, G.; Fontana, G.; Pollastro, F. Natural Products Drug Discovery. In *Comprehensive Natural Products II*; Elsevier, 2010; pp 205–236. https://doi.org/10.1016/B978-008045382-8.00064-2.
(59) Lianza, M.; Leroy, R.; Machado Rodrigues, C.; Borie, N.; Sayagh, C.; Remy, S.; Kuhn, S.; Renault, J.-H.; Nuzillard, J.-M. The Three Pillars of Natural Product Dereplication. Alkaloids from the Bulbs of Urceolina Peruviana (C. Presl) J.F. Macbr. as a Preliminary Test Case. *Molecules* **2021**, *26* (3), 637. https://doi.org/10.3390/molecules26030637.
(60) Bakiri, A.; Plainchont, B.; de Paulo Emerenciano, V.; Reynaud, R.; Hubert, J.; Renault, J.-H.; Nuzillard, J.-M. Computer-Aided Dereplication and Structure Elucidation of Natural Products at the University of Reims. *Molecular Informatics* **2017**, *36* (10), 1700027. https://doi.org/10.1002/minf.201700027.
(61) Zani, C. L.; Carroll, A. R. Database for Rapid Dereplication of Known Natural Products Using Data from MS and Fast NMR Experiments. *J. Nat. Prod.* **2017**, *80* (6), 1758–1766. https://doi.org/10.1021/acs.jnatprod.6b01093.
(62) Mottaghipisheh, J.; Iriti, M. Sephadex® LH-20, Isolation, and Purification of Flavonoids from Plant Species: A Comprehensive Review. *Molecules* **2020**, *25* (18), 4146. https://doi.org/10.3390/molecules25184146.
(63) *Lab Software | Software for R&D | Chemistry Applications | ACD/Labs*. https://www.acdlabs.com/products/ (accessed 2025-01-09).
(64) *Mnova Software Suite - Mestrelab*. https://mestrelab.com/main-product/mnova (accessed 2025-01-13).
(65) *Mass spec screening software, MassHunter Qualitative Analysis | Agilent*. https://www.agilent.com/en/product/software-informatics/mass-spectrometry-software/data-analysis/qualitative-analysis (accessed 2025-01-10).
(66) Horsley, D.; Rickard, J. E.; Vorley, T.; Leeper, M. F.; Wischik, C. M.; Harrington, C. R. Assays for the Screening and Characterization of Tau Aggregation Inhibitors. In *Tau Protein: Methods and Protocols*; Smet-Nocca, C., Ed.; Springer US: New York, NY, 2024; pp 93–104. https://doi.org/10.1007/978-1-0716-3629-9_5.
(67) *Marbio – an analytical platform for natural products | UiT*. https://en.uit.no/forskning/forskningsgrupper/gruppe?p_document_id=380005 (accessed 2025-01-09).
(68) Lauritano, C.; Andersen, J. H.; Hansen, E.; Albrigtsen, M.; Escalera, L.; Esposito, F.; Helland, K.; Hanssen, K. Ø.; Romano, G.; Ianora, A. Bioactivity Screening of Microalgae for Antioxidant, Anti-Inflammatory, Anticancer, Anti-Diabetes, and Antibacterial Activities. *Front. Mar. Sci.* **2016**, *3*. https://doi.org/10.3389/fmars.2016.00068.
(69) PubChem. *Rutin*. https://pubchem.ncbi.nlm.nih.gov/compound/5280805 (accessed 2025-01-10).
(70) PubChem. *Myricetin*. https://pubchem.ncbi.nlm.nih.gov/compound/5281672 (accessed 2025-01-10).
(71) PubChem. *24-Ethylcholest-6-ene-3,5-diol*. https://pubchem.ncbi.nlm.nih.gov/compound/44407138 (accessed 2025-01-10).
(72) Pourakbari, R.; Taher, S. M.; Mosayyebi, B.; Ayoubi-Joshaghani, M. H.; Ahmadi, H.; Aghebati-Maleki, L. Implications for Glycosylated Compounds and Their

Anti-Cancer Effects. *International Journal of Biological Macromolecules* **2020**, *163*, 1323–1332. https://doi.org/10.1016/j.ijbiomac.2020.06.281.

(73) Choi, J. S.; Nurul Islam, Md.; Yousof Ali, Md.; Kim, E. J.; Kim, Y. M.; Jung, H. A. Effects of *C*-Glycosylation on Anti-Diabetic, Anti-Alzheimer's Disease and Anti-Inflammatory Potential of Apigenin. *Food and Chemical Toxicology* **2014**, *64*, 27–33. https://doi.org/10.1016/j.fct.2013.11.020.

Appendix

1.0 In-house library of known compounds of Ficus.

Table A 1 shows the self-made database of the known compounds of Ficus.

Compound	**Mass**	**Formula**	**$[M+H]^+$**	**$[M-H]^-$**	**structure**
Psoralen	186.03	$C_{11}H_6O_3$	187.04	185.02	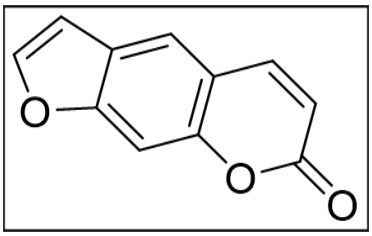
Rutin	610.15	$C_{27}H_{30}O_{16}$	611.16	609.14	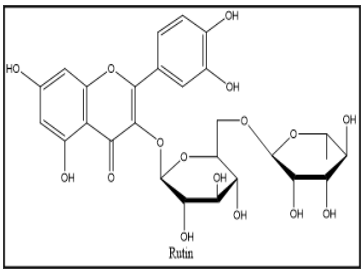
Luteolin	286.05	$C_{15}H_{10}O_6$	287.06	285.04	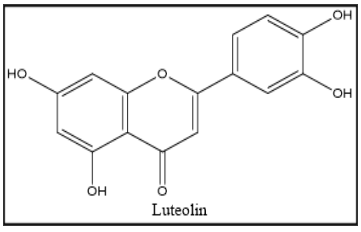
Genistein	270.05	$C_{15}H_{10}O_5$	271.06	269.04	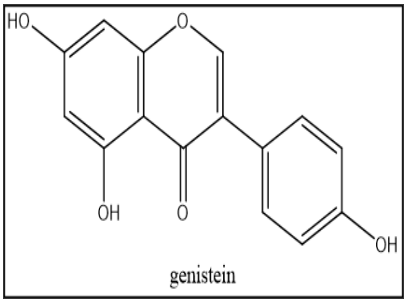
Kaempferol	286.05	$C_{15}H_{10}O_6$	287.05	285.04	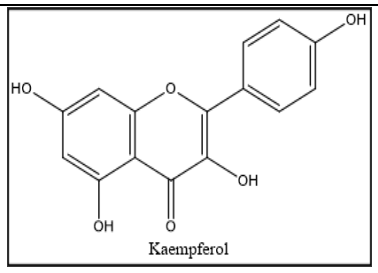

Myricetin	318.04	$C_{15}H_{10}O_8$	319.04	317.04	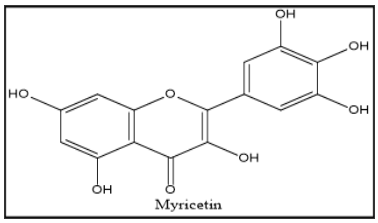
Apigenin	270.05	$C_{15}H_{10}O_5$	271.06	269.04	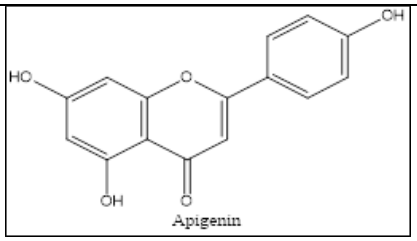
2′-hydroxygenistein	286.05	$C_{15}H_{10}O_6$	287.05	285.05	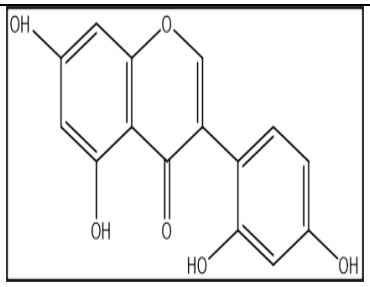
euphol-3-O-cinnamate	570.44	$C_{40}H_{58}O_2$	571.44	569.44	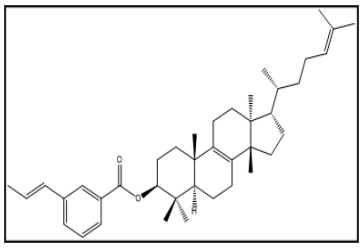
Lupeol	426.39	$C_{30}H_{50}O$	427.39	425.39	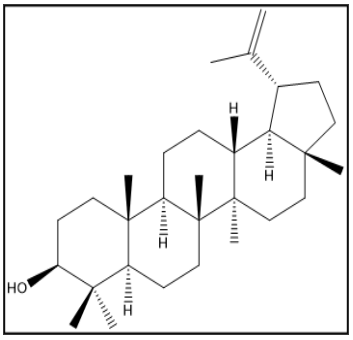
taraxer-14-ene	410.39	$C_{30}H_{50}O$	411.39	409.39	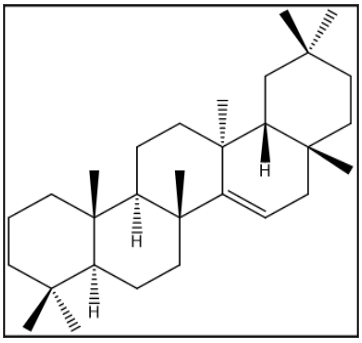

Ursolic acid	456.36	$C_{30}H_{48}O_3$	457.36	455.36	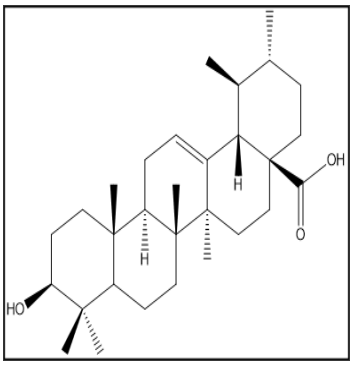
Betulinic acid	506.49	$C_{37}H_{62}$	507.49	505.49	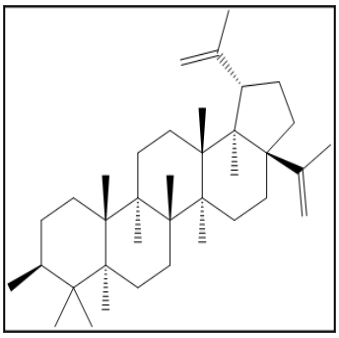
4,14,24-trimethyl-cholestane-3,11-diol	446.41	$C_{30}H_{54}O_2$	447.41	445.41	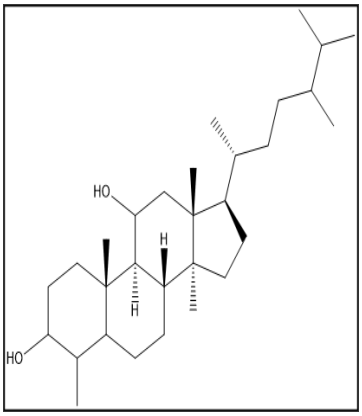
(24R)-ethylcholest-4-ene-3,6-diol	430.38	$C_{29}H_{50}O_2$	431.38	429.38	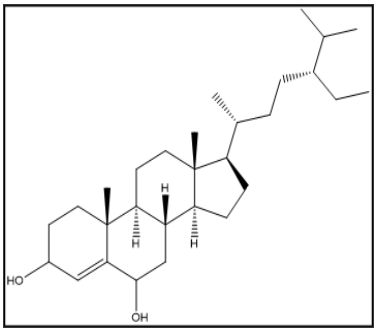

-amyrin	426.39	$C_{30}H_{50}O$	427.39	425.39	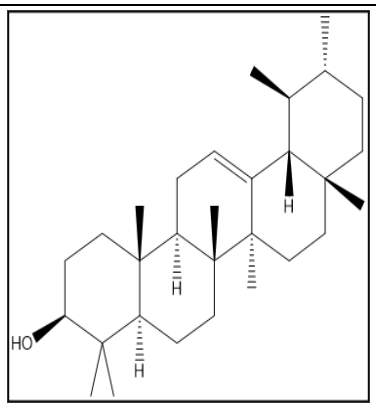
-sitosterol	414.39	$C_{29}H_{50}0$	415.39	413.39	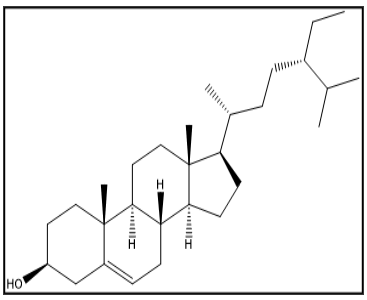
Quercetin	302.04	$C_{15}H_{10}O_7$	303.05	301.04	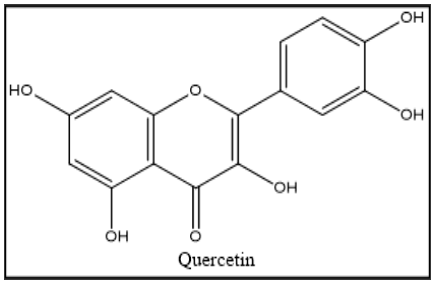

2.0 Bioassay

2.1 Anti-Alzheimer's bioassay

Table A 2 shows the activity of the samples (highlighted in yellow) for anti-Alzheimer 's screening.

Name and Structure	Experiment	Active at (μM) EC_{50} full assay	EC_{50} (μM) mean±SEM	Experiment	B_{50}	B_{50} (μg/mL) mean±SEM	Experiment	LD_{50} (μM)	LD_{50} (μM) mean±SEM	Notes
Sample 1 Crude				25Nov24 26Nov24	NE (500) NE (500)	NE (500μg/mL) n=2				1.5mg +150μL DMSO 10mg/mL
Sample 2 FD3				25Nov24 26Nov24	NE (500) >600μg/mL					12.3mg +123μL DMSO 100mg/mL
Sample 3 FD4				25Nov24 26Nov24	69.2 μg/mL 30.8μg/mL					1.4mg +140μL DMSO 10mg/mL
Sample 4 FD5				25Nov24 26Nov24	~600μg/mL 57.1μg/mL					3.6mg +360μL DMSO 10mg/mL

Name and Structure	Experiment	Active at (μM) EC_{50} full assay	EC_{50} (μM) mean±SEM	Experiment	B_{50}	B_{50} (μg/mL) mean±SEM	Experiment	LD_{50} (μM)	LD_{50} (μM) mean±SEM	Notes
Sample 5 WB3				25Nov24 26Nov24	NE (500) NE (500)	NE (500μg/mL) n=2				45.6mg + 456μL DMSO 100mg/mL
Sample 6 FH4				25Nov24 26Nov24	NE (500) NE (500)	NE (500μg/mL) n=2				8mg +80μL DMSO 100mg/mL
Sample 7 FH5				25Nov24 26Nov24	138 μg/mL 104μg/mL					7mg +70μL DMSO 100mg/mL
Sample 8 FM6				25Nov24 26Nov24	>600μg/mL 466μg/mL					1mg +100μL DMSO 10mg/mL

Table A 3shows the samples and their weight which was sent for anti-Alzheimer screening.

Sample code	**Weight (g)**
(1) Crude	0.0015g
(2) FD3	0.0123g
(3) FD4	0.0014g
(4) FD5	0.0036g
(5) WB3	0.0456g
(6) FH4	0.008g
(7) FH5	0.007g
(8) FM6	0.001g

2.2 Anti-cancer screening

Table A 4 shows the samples and their weight that was sent for anti-cancer screening.

Sample codes	**Weight (g)**
FM6	0.0002g
FH5	0.0004g
FH6	0.0008g
FD3	0.0007g
FD4	0.0010g
FD5	0.0011g
WB3	0.0010g
Crude	0.0008g

3.0 LCMS

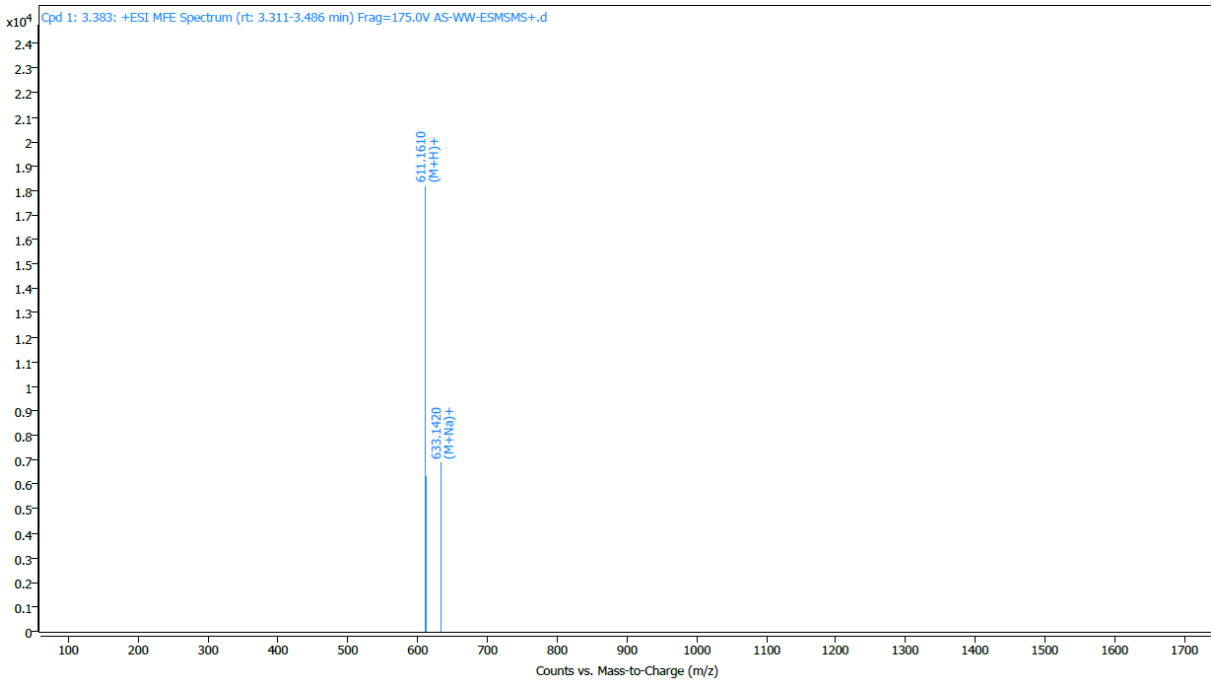

Figure A 1 shows the MS spectrum of the WW fraction of the identified known compound of Ficus.

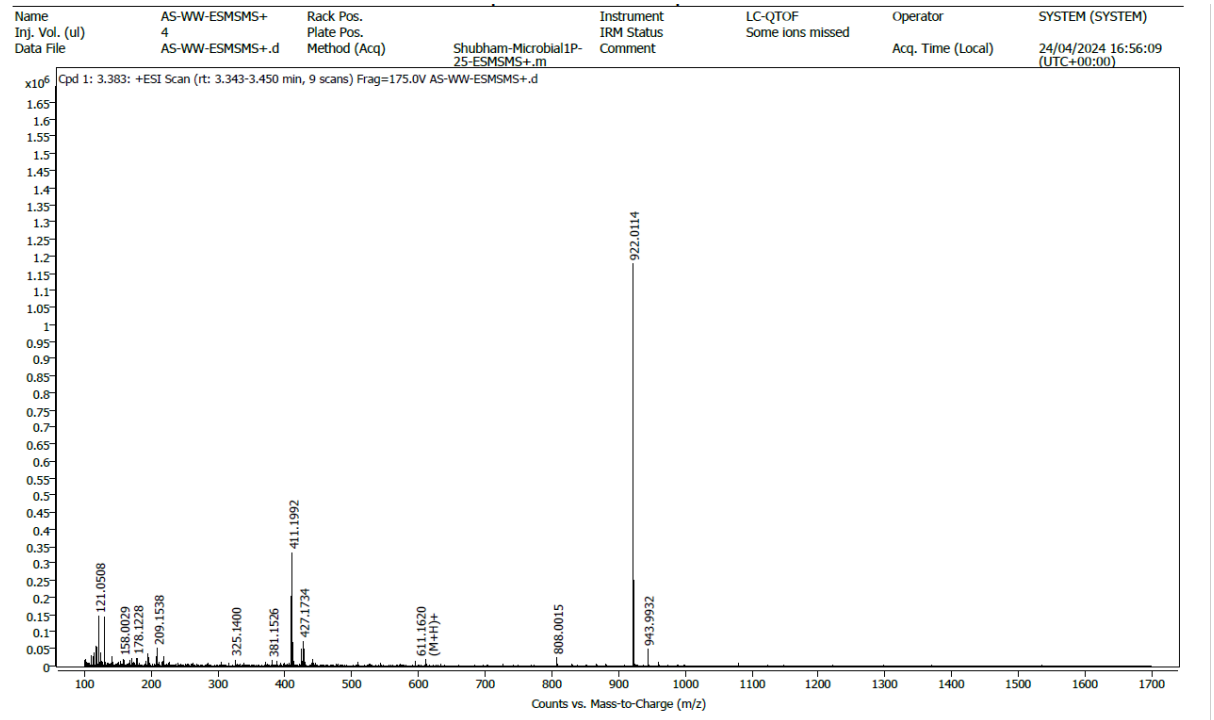

Figure A1. 1 shows the MS spectrum of WW fraction.

Figure A1. 2 shows the MS $(M+H)^+$ of the known compound that was identified in the WW fraction.

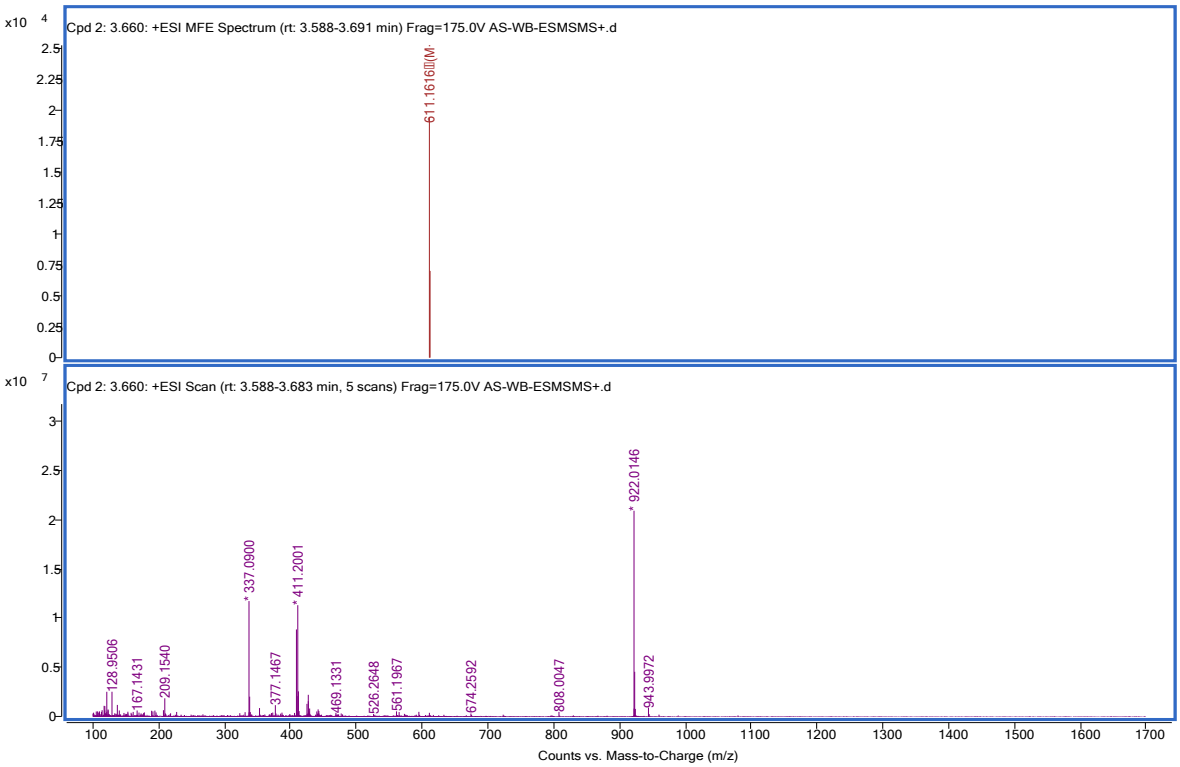

Figure A 2 shows the mass spectrum $(M+H)^+$ peak of the identified compound (Rutin) in the WB fraction.

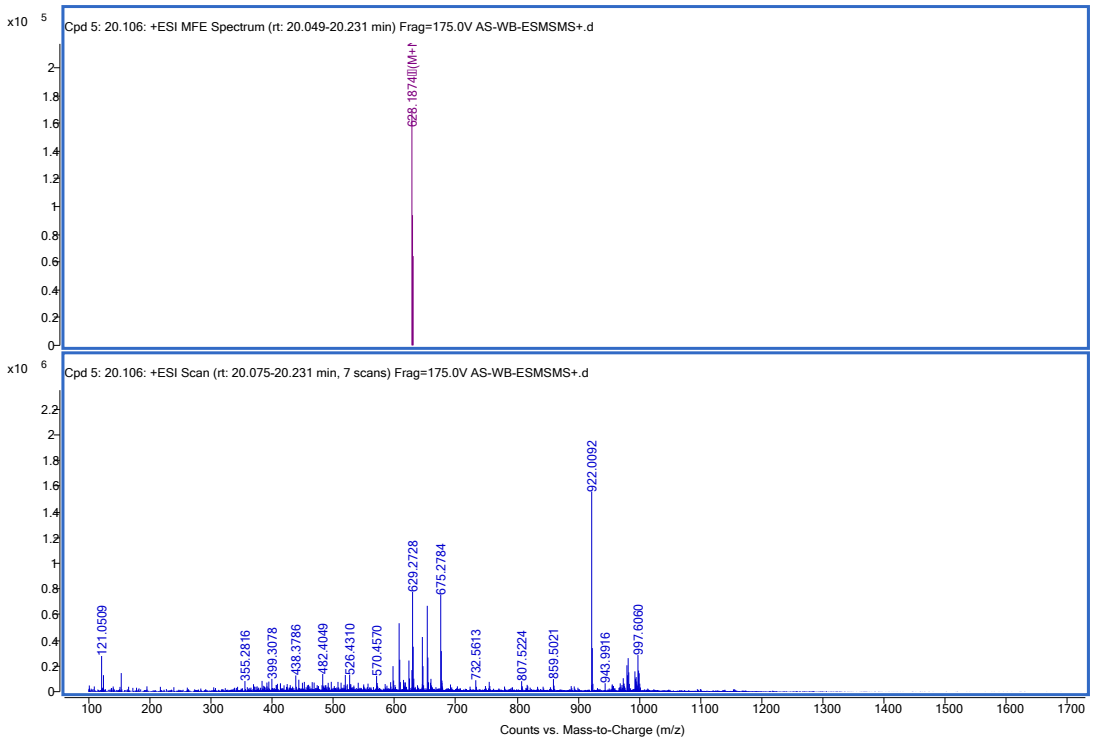

Figure A2. 1 shows the mass spectrum $(M+NH_4)^+$ peak of the identified compound (Rutin) in the WB fraction.

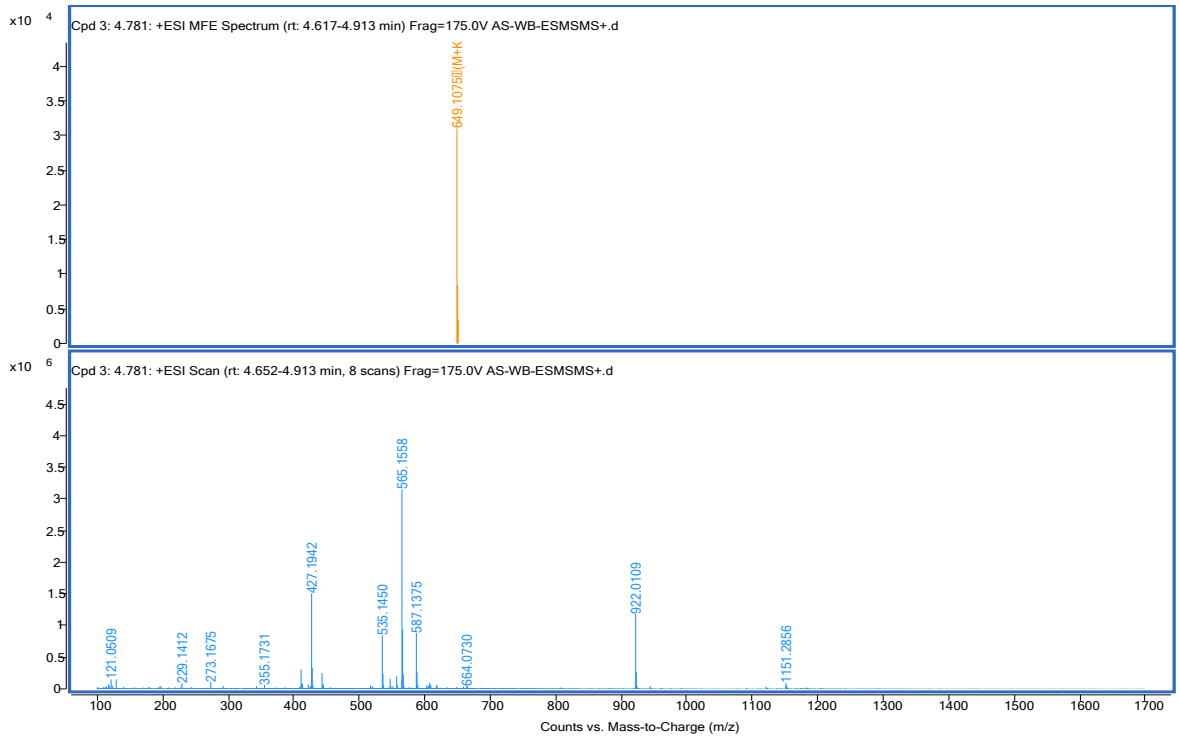

Figure A2. 2 shows the $(M+K)^+$ peak of the identified compound (Rutin) in the WB fraction.

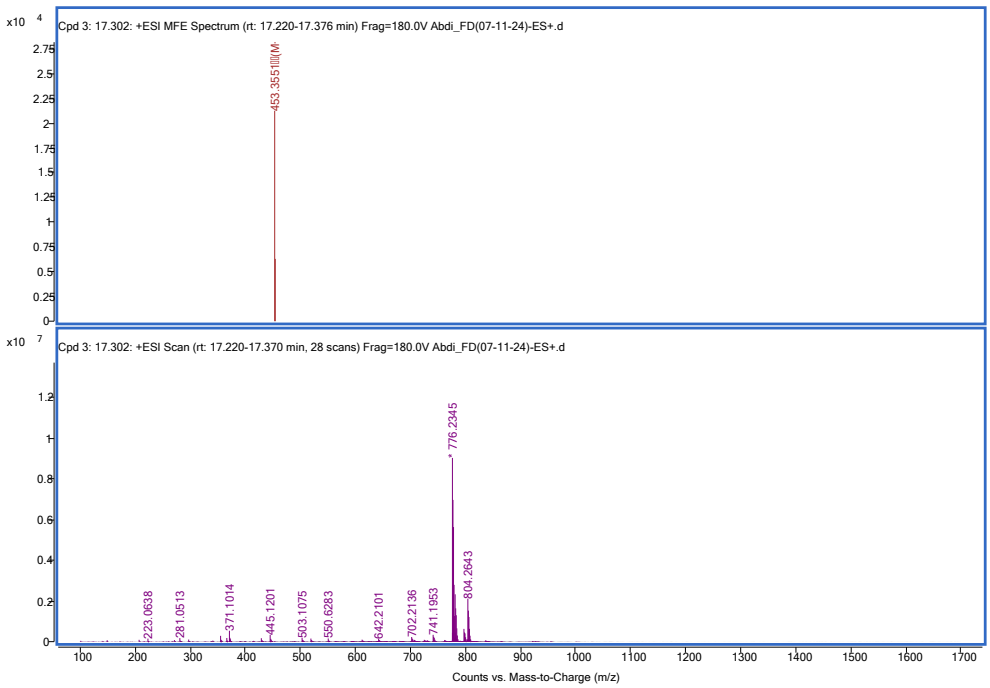

Figure A 3 shows the MS identified compound of the -sitosterol that was identified in the FD4 fraction.

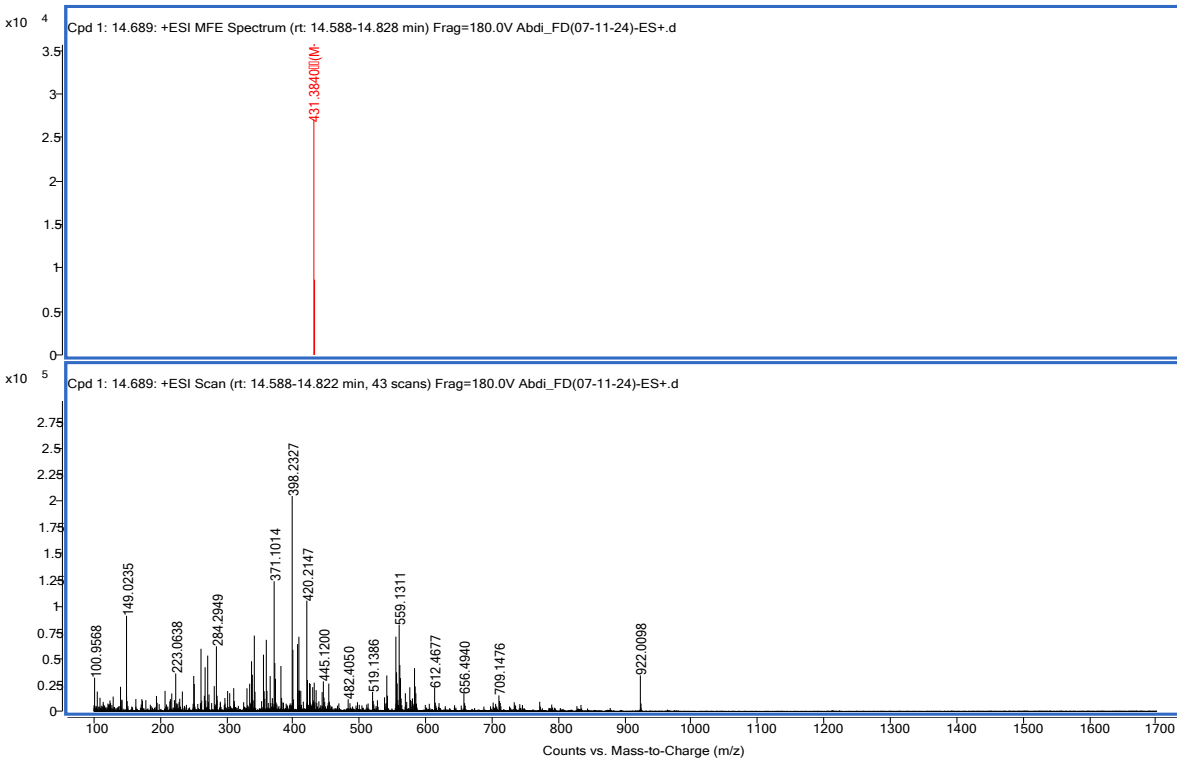

Figure A3. 1shows the mass spectrum $(M+H)^+$ of (24R)-ethylcholest-4-ene-3,6-diol that was identified in the FD4 fraction.

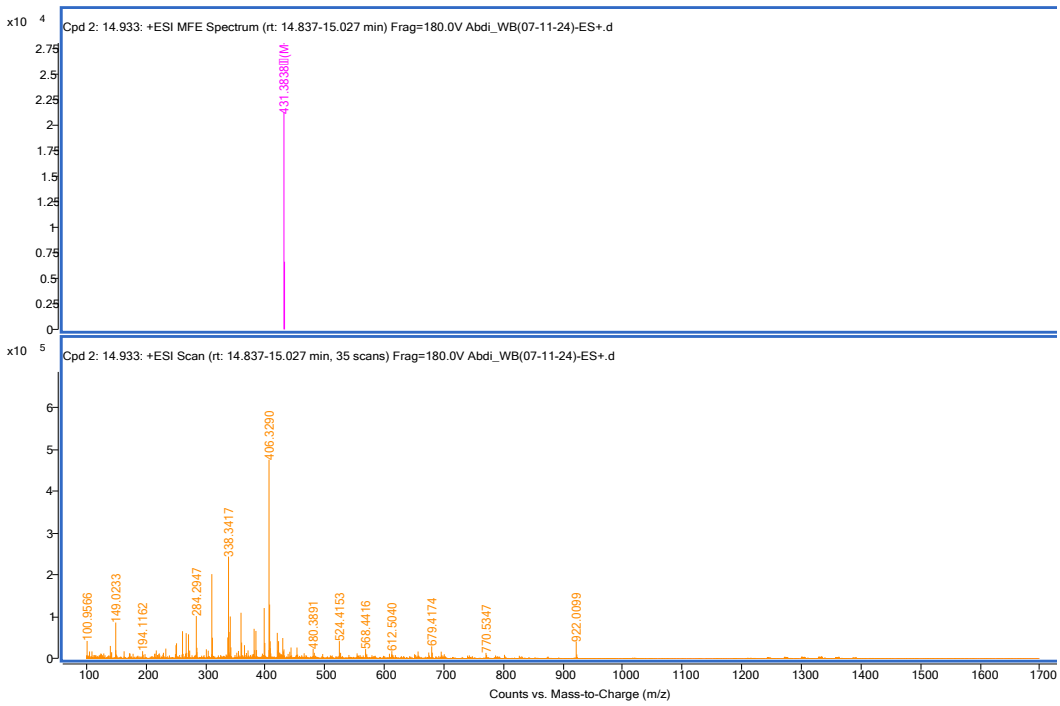

Figure A 4 shows the mass spectrum $(M+H)^+$ peak of the compound (24R)-ethylcholest-4-ene-3,6-diol that was identified in the WB4 fraction.

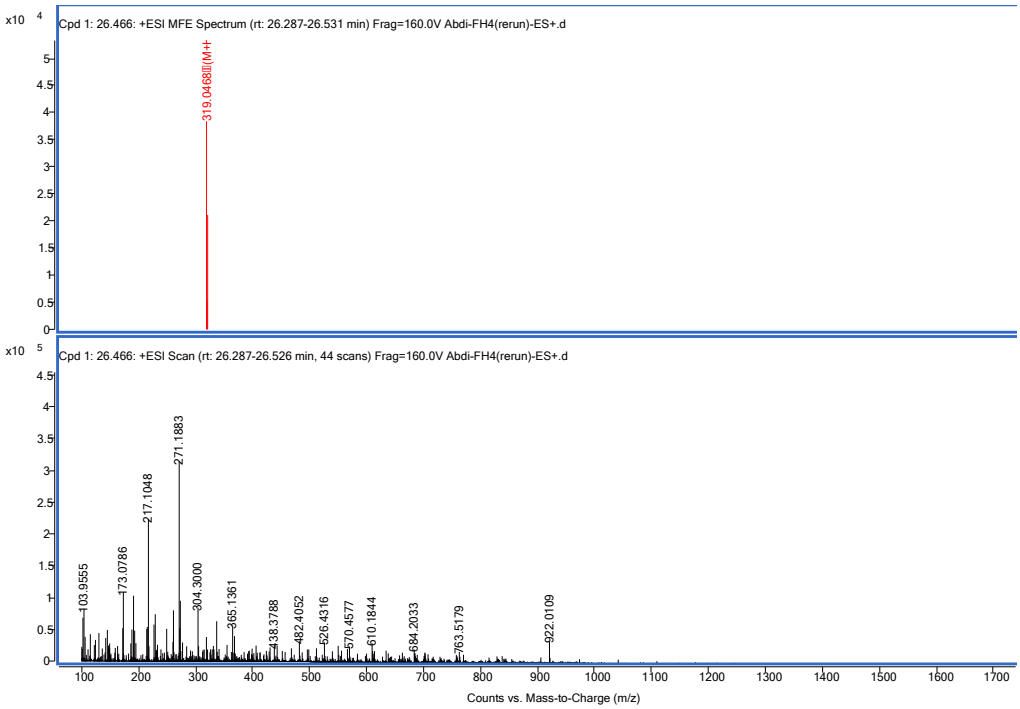

Figure A 5 shows the mass spectrum $(M+H)^+$ peak of the compound Myricetin that was identified in the FH4 fraction.

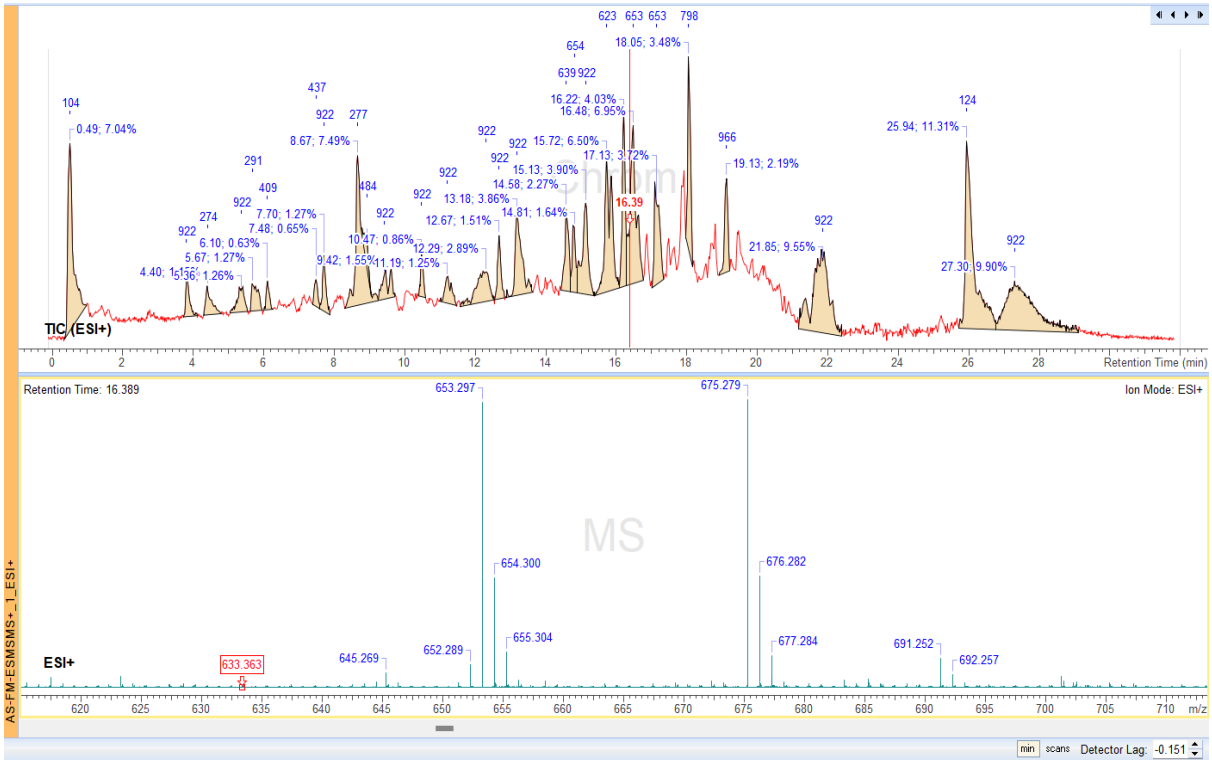

Figure A 6 shows the retention time and the mass spec of the unknown compound in the FM fraction.

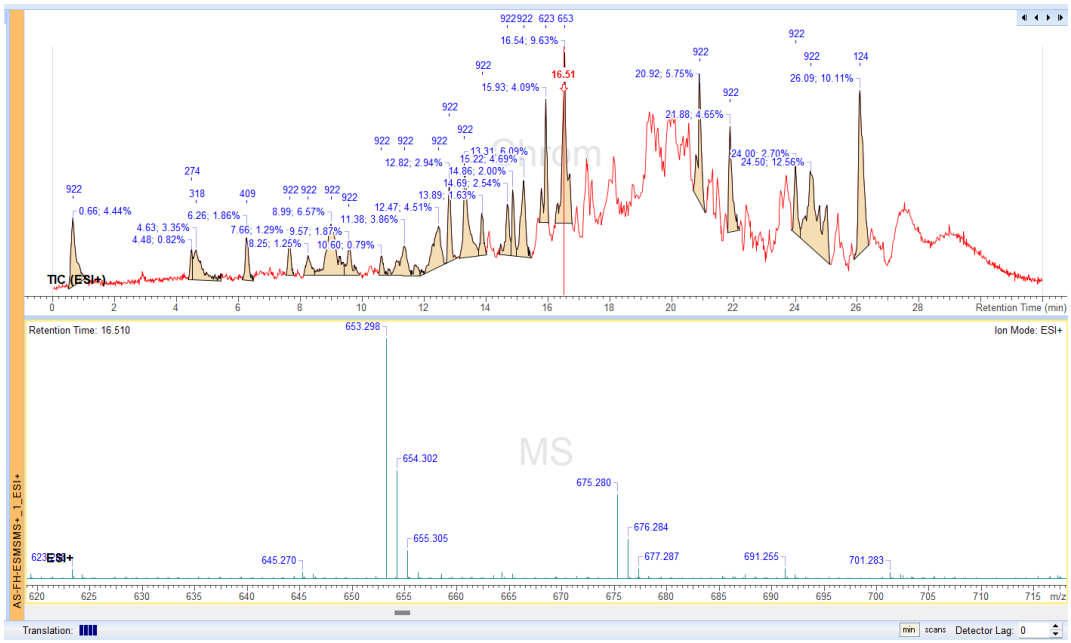

Figure A6. 1 shows the retention time and the mass spec of the unknown compound in the FH fraction.

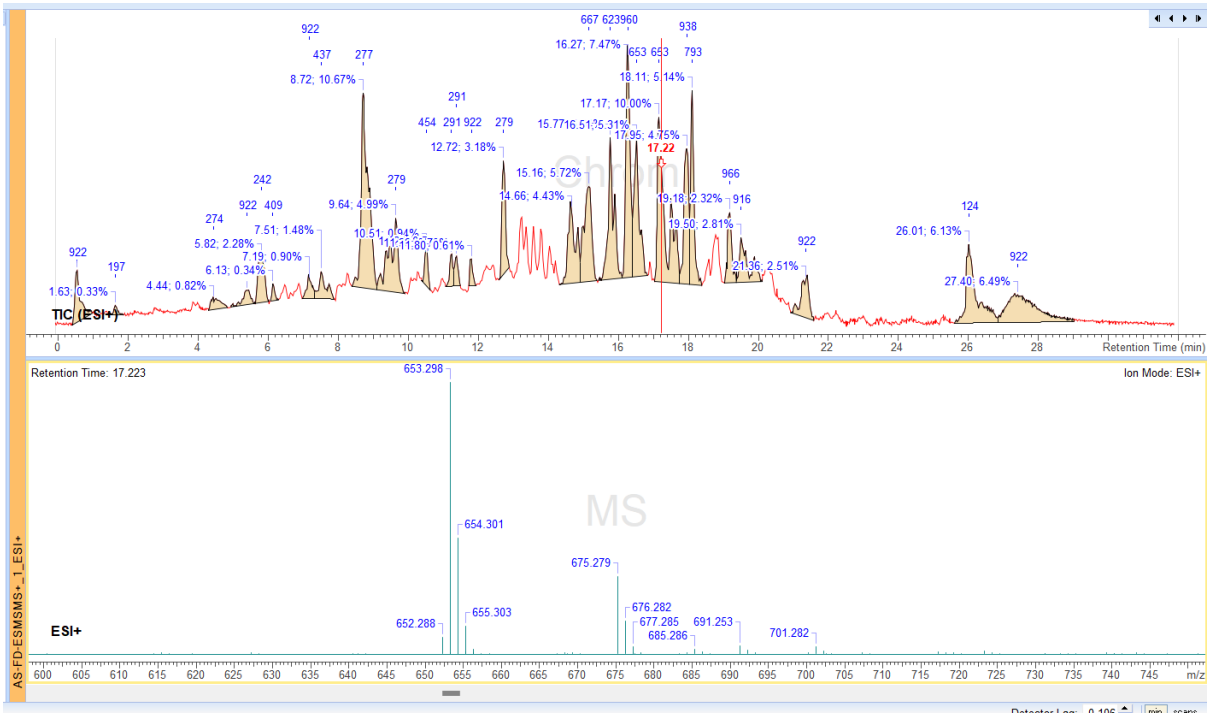

Figure A6. 2 shows the retention time and the mass spec of the unknown compound in the FD fraction.

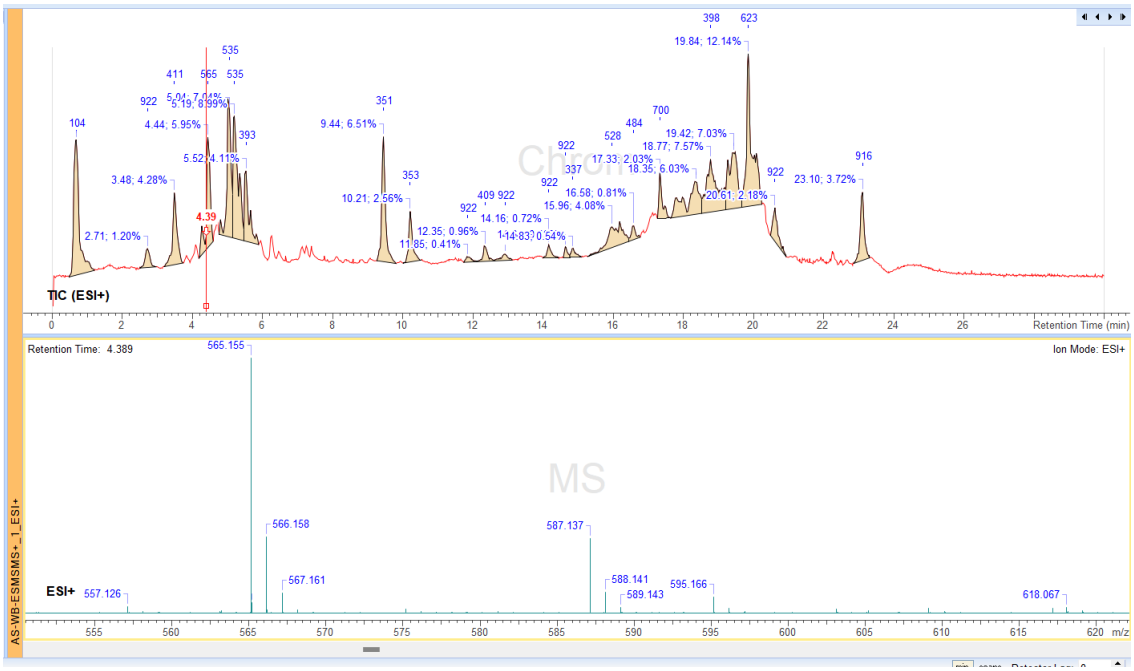

Figure A 7 shows the retention time and the mass spec of the unknown compound in the WB fraction.

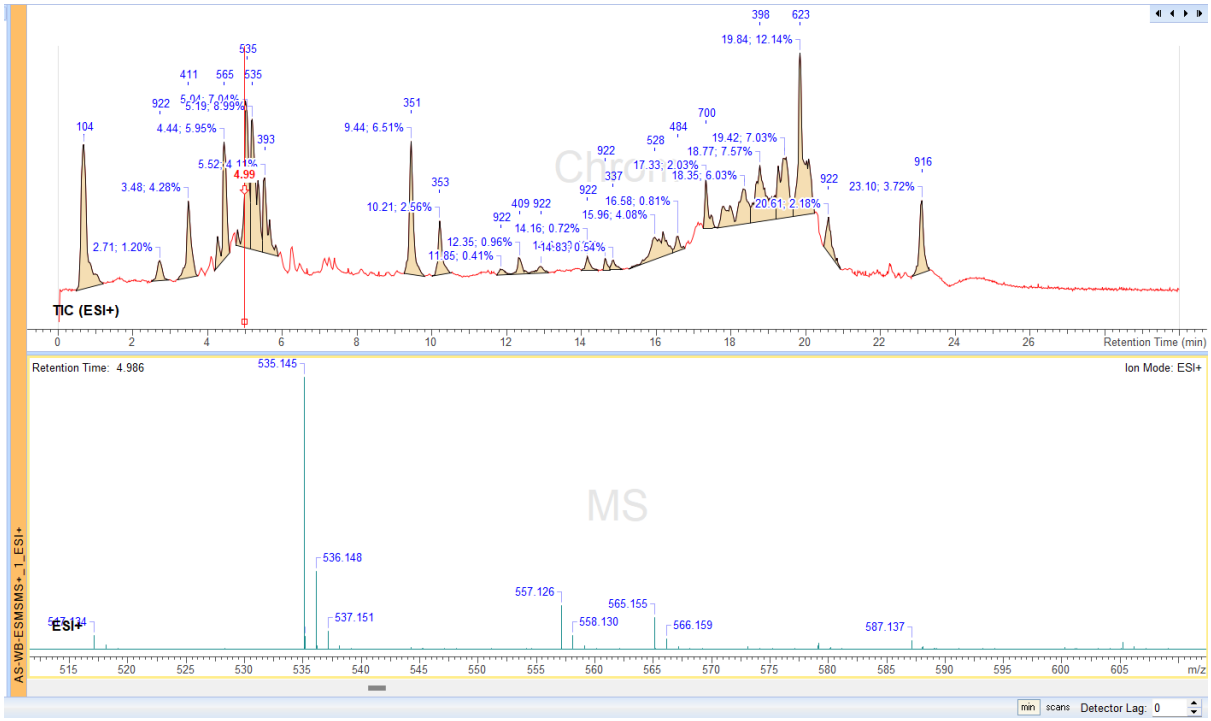

Figure A 8 shows the retention time and the mass spec of the unknown compound in the WB fraction.

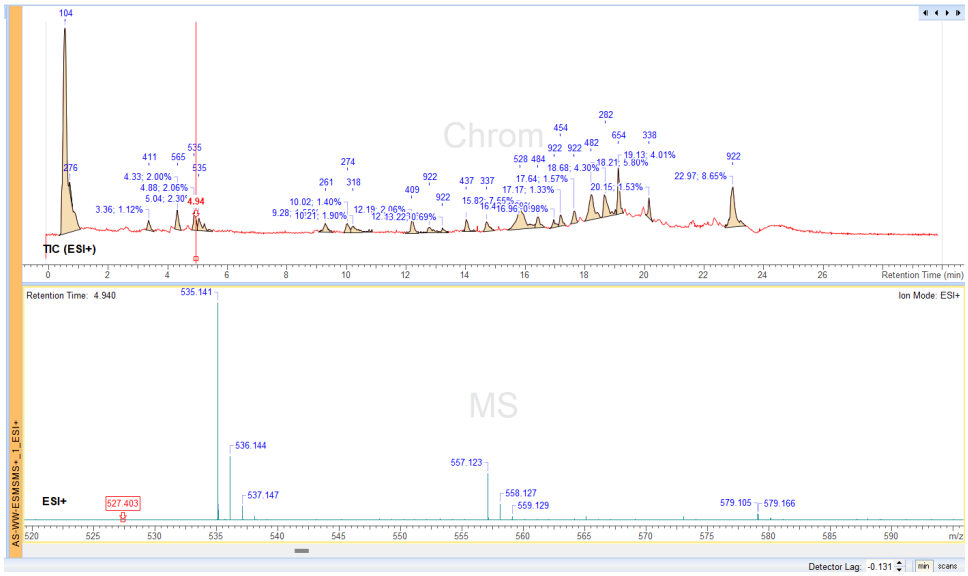

Figure A 9 shows the retention time and the mass spec of the unknown compound in the WW fraction.

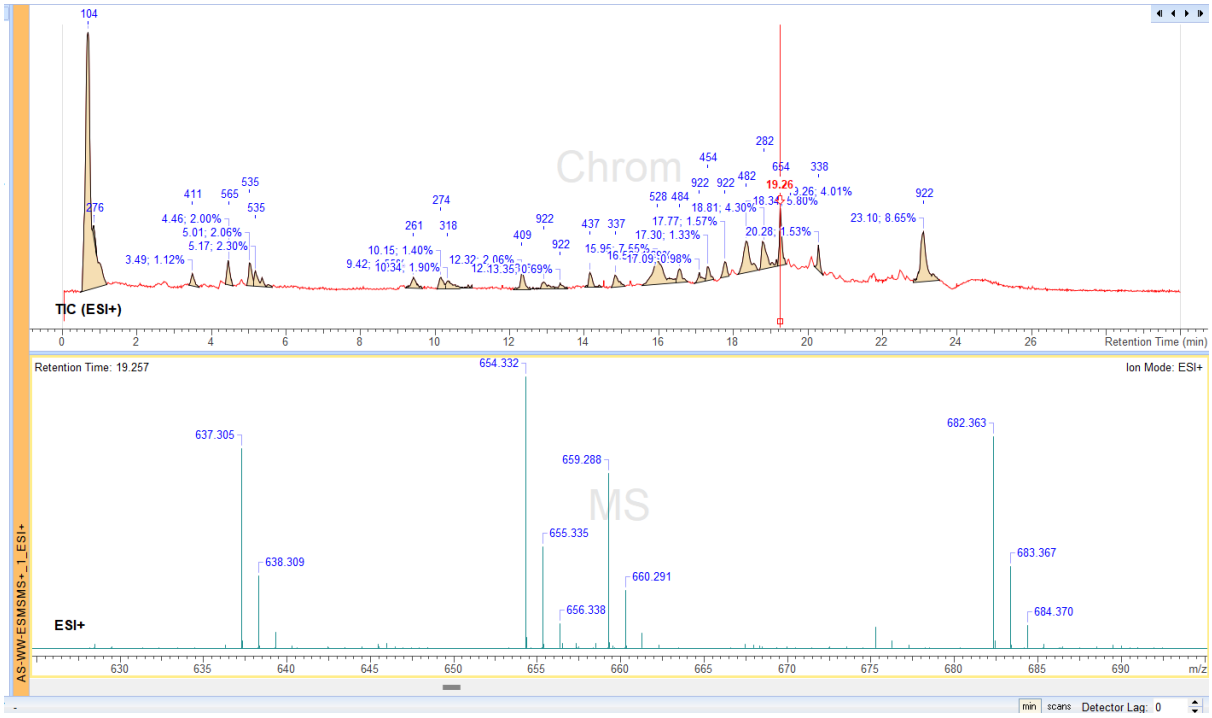

Figure A 10 shows the retention time and the mass spec of the unknown compound in the WW fraction.

Table A 5 shows the unknown compounds with their masses and retention time in FM7 fraction.

Compound Summary

Cpd	Name	Formula	RT	Mass	CAS	ID Source	Score	Score (Lib)	Score (DB)	Score (MFG)	Algorithm
1			15.247	636.2580							MFE
2			16.419	1266.5401							MFE
3			16.420	623.3354							MFE
4			16.421	622.2786							MFE
5			16.428	620.2632							MFE
6			16.437	637.6005							MFE
7			16.527	521.5894							MFE
8			16.842	415.3661							MFE
9			16.846	652.2895							MFE
10			17.062	435.3346							MFE
11			17.097	549.6209							MFE
12			17.098	606.2827							MFE

MassHunter Qual 10.0
(End of Report)

Table A 6 shows the unknown compounds with their masses and retention time of the FD4 fraction.

Cpd	Name	Formula	RT	Mass	CAS	ID Source	Score	Score (Lib)	Score (DB)	Score (MFG)	Algorithm
1			15.339	354.0624							MFE
2			15.339	206.0246							MFE
3			15.339	280.0434							MFE
4			15.340	296.0749							MFE
5			15.340	370.0941							MFE
6			15.341	222.0561							MFE
7			15.342	635.1418							MFE
8			15.342	610.1615							MFE
9			15.347	655.2189							MFE
10			15.941	567.1842							MFE
11			16.117	320.3075							MFE
12			16.151	337.3064							MFE
13			16.153	674.7489							MFE
14			16.153	674.6693							MFE
15			16.167	320.3100							MFE
16			16.357	666.1695							MFE
17			16.358	706.2064							MFE
18			16.358	701.2066							MFE
19			16.359	428.0817							MFE
20			16.359	370.0944							MFE
21			16.359	354.0629							MFE
22			16.359	222.0566							MFE
23			16.363	280.0441							MFE
24			16.365	729.2379							MFE
25			16.366	732.2369							MFE
26			16.366	706.1622							MFE
27			16.367	709.1610							MFE
28			16.375	722.1358							MFE
29			16.951	669.2343							MFE
30			16.954	641.2031							MFE
31			16.955	646.1584							MFE

Compound Summary

Cpd	Name	Formula	RT	Mass	CAS	ID Source	Score	Score (Lib)	Score (DB)	Score (MFG)	Algorithm
32			16.955	644.2020							MFE
33			17.030	616.1115							MFE
34			17.033	280.0433							MFE
35			17.071	597.1284							MFE
36			17.073	594.1300							MFE
37			17.088	639.1875							MFE
38			17.106	549.6211							MFE
39			17.213	354.0623							MFE
40			17.216	222.0562							MFE
41			17.216	370.0938							MFE
42			17.218	775.2256							MFE
43			17.226	803.2566							MFE
44			17.226	780.1809							MFE
45			17.227	807.2545							MFE

Table A 7 shows the unknown masses and retention of the FH4 fraction.

Compound Summary

Cpd	Name	Formula	RT	Mass	CAS	ID Source	Score	Score (Lib)	Score (DB)	Score (MFG)	Algorithm
1			15.347	627.1876							MFE
2			15.352	632.1428							MFE
3			15.353	655.2189							MFE
4			15.644	639.5799							MFE
5			15.838	665.5951							MFE
6			15.840	545.3926							MFE
7			15.955	575.3239							MFE
8			15.959	493.5582							MFE
9			16.021	443.3164							MFE
10			16.169	227.1885							MFE
11			16.326	311.3187							MFE
12			16.363	706.1604							MFE
13			16.364	701.2053							MFE
14			16.364	722.1343							MFE
15			16.366	729.2366							MFE
16			16.477	323.3189							MFE
17			16.502	649.4893							MFE
18			16.577	521.5898							MFE
19			16.857	415.3657							MFE
20			17.019	666.6347							MFE
21			17.058	665.6319							MFE

Compound Summary

Cpd	Name	Formula	RT	Mass	CAS	ID Source	Score	Score (Lib)	Score (DB)	Score (MFG)	Algorithm
22			17.075	435.3349							MFE
23			17.075	278.1515							MFE
24			17.107	550.6241							MFE
25			17.126	611.1548							MFE
26			17.165	550.6234							MFE
27			17.223	803.2556							MFE
28			17.225	775.2249							MFE
29			17.225	778.2229							MFE
30			17.225	780.1803							MFE

Table A 8 shows the unknown mass and their retention time of the WB4 fraction.

Compound Summary

Cpd	Name	Formula	RT	Mass	CAS	ID Source	Score	Score (Lib)	Score (DB)	Score (MFG)	Algorithm
1			15.332	635.1420							MFE
2			15.335	354.0626							MFE
3			15.335	222.0563							MFE
4			15.336	370.0940							MFE
5			15.337	610.1614							MFE
6			15.339	648.1168							MFE
7			15.340	655.2188							MFE
8			15.566	636.2975							MFE
9			16.148	674.6688							MFE
10			16.151	320.3069							MFE
11			16.353	222.0566							MFE
12			16.353	370.0942							MFE
13			16.354	701.2069							MFE
14			16.359	729.2383							MFE
15			16.359	709.1613							MFE
16			16.359	684.1800							MFE
17			17.067	594.1296							MFE
18			17.096	549.6210							MFE
19			17.212	796.1548							MFE
20			17.215	370.0941							MFE
21			17.215	775.2253							MFE
22			17.222	803.2565							MFE
23			17.222	806.2557							MFE
24			17.222	780.1808							MFE
25			17.223	783.1798							MFE
26			17.237	365.3658							MFE

Table A 9 shows the masses, retention time and quality score for the FH4 fraction using the ACD lab software.

	A	B	C	D	E	F	G
1	**No.**	**m/z**	**tR (min)**	**Height (co**	**Notation**	**PQI**	
2	4	610.2	19.076	1494924	[M+H]+	92.196	
3	2	261.2	5.746	270888	[M+H]+	83.589	
4	5	758.2	20.067	797817	[M+H]+	77.666	
5	7	337.2	10.125	510197	[M+H]+	72.932	
6	8	712.2	19.577	431555	[M+H]+	68.848	
7	15	393.2	16.862	366824	[M+H]+	67.234	
8	16	536.2	18.437	329719	[M+H]+	65.873	
9	9	406.2	14.887	189985	[M+H]+	64.226	
10	20	550.2	17.151	192002	[M+H]+	63.681	
11	19	436.2	17.074	144472	[M+H]+	61.917	
12	11	845.2	20.1	94722	[M+H]+	61.641	
13	18	587.2	19.761	96055	[M+H]+	61.484	
14	1	453.2	9.123	54887	[M+H]+	61.404	
15	13	906.2	20.812	77305	[M+H]+	61.272	
16	22	668.2	16.284	49538	[M+H]+	61.021	
17	3	496.2	13.48	65280	[M+H]+	60.994	
18	21	540.2	13.424	62223	[M+H]+	60.963	
19	10	763.2	20.195	714984	[M+H]+	53.935	
20	12	786.2	20.061	319452	[M+H]+	46.053	
21	17	832.2	20.467	318081	[M+H]+	45.667	
22	14	860.2	20.473	102219	[M+H]+	42.027	
23	6	666.2	17.057	74714	[M+H]+	41.339	
24							

Table A 10 shows the masses, retention time and quality score for the FD4 fraction using the ACD lab software.

	A	B	C	D	E	F	G	H
1	No.	m/z	tR (min)	Height (co	Componer	Notation	Carbon	PQI
2	4	610.2	19.076	1492006	50	[M+H]+	12C	92.107
3	20	261.2	5.674	265977	2	[M+H]+	12C	83.527
4	16	337.2	10.119	523767	12	[M+H]+	12C	73.188
5	10	149.2	12.088	327582	16	[M+H]+	12C	72.142
6	13	365.2	11.832	286769	14	[M+H]+	12C	69.587
7	7	712.2	19.577	420580	52	[M+H]+	12C	68.765
8	18	301.2	12.066	186899	15	[M+H]+	12C	67.317
9	19	393.2	16.856	369035	40	[M+H]+	12C	67.015
10	1	413.2	17.073	321794	42	[M+Na]+	12C	65.801
11	12	536.2	18.436	320685	47	[M+H]+	12C	65.77
12	17	391.2	17.073	239772	42	[M+H]+	12C	64.111
13	23	550.2	17.145	188023	43	[M+H]+	12C	63.69
14	5	327.2	8.672	95955	6	[M+H]+	12C	63.233
15	24	251.2	13.885	129188	27	[M+H]+	12C	62.803
16	14	522.2	16.572	84396	39	[M+H]+	12C	61.367
17	15	666.2	17.051	77279	41	[M+H]+	12C	61.212
18	2	453.2	9.123	48803	9	[M+H]+	12C	60.943
19	22	269.2	6.141	40133	3	[M+H]+	12C	60.716
20	9	559.2	14.152	32830	29	[M+H]+	12C	60.642
21	6	485.2	12.767	35622	22	[M+H]+	12C	60.57
22	11	776.2	17.229	36577	44	[M+H]+	12C	60.505
23	3	929.2	18.564	32001	48	[M+H]+	12C	59.797
24	21	707.2	16.367	33053	37	[M+H]+	12C	59.684

Table A 11 shows the masses, retention time and quality score for the WB4 fraction using the ACD lab software.

C	D	E	F	G	H	I	J
.	m/z	tR (min)	Height (co	Componer	Notation	Carbon	PQI
6	610.2	19.077	1532821	67	[M+H]+	12C	92.06
8	274.2	6.376	568209	2	[M+H]+	12C	72.543
21	337.2	10.12	494372	21	[M+H]+	12C	72.534
15	365.2	11.834	291345	24	[M+H]+	12C	69.451
4	318.2	6.521	432297	3	[M+H]+	12C	69.404
7	712.2	19.578	408843	69	[M+H]+	12C	68.494
20	393.2	16.863	366809	57	[M+H]+	12C	66.939
13	536.2	18.443	331595	64	[M+H]+	12C	66.057
2	413.2	17.08	319137	59	[M+Na]+	12C	65.787
3	406.2	14.877	241842	48	[M+H]+	12C	64.488
24	391.2	17.075	241494	59	[M+H]+	12C	64.075
25	453.2	9.497	135005	16	[M+H]+	12C	62.906
14	149.2	10.115	121790	20	[M+H]+	12C	62.601
19	362.2	6.632	104153	4	[M+H]+	12C	62.488
10	368.2	13.069	113431	35	[M+H]+	12C	61.982
5	387.2	8.218	52961	8	[M+H]+	12C	61.194
1	409.2	8.218	79786	8	[M+Na]+	12C	61.071
16	702.2	16.368	43102	54	[M+H]+	12C	60.867
17	341.2	14.838	61686	46	[M+H]+	12C	60.762
11	460.2	9.503	55240	17	[M+H]+	12C	60.752
12	781.2	17.23	31203	61	[M+H]+	12C	59.949
9	1003.2	19.1	27139	68	[M+H]+	12C	59.843
23	929.2	18.566	33726	66	[M+H]+	12C	59.739
18	550.2	17.125	193859	60	[M+H]+	12C	43.314
22	666.2	17.036	78476	58	[M+H]+	12C	41.303

Table A 12 shows the masses, retention time and quality score for the FM7 fraction using the ACD lab software.

C	D	E	F	G	H	I	J
No.	m/z	tR (min)	Height (co	Componer	Notation	Carbon	PQI
13	623.2	16.419	3313004	59	[M+H]+	12C	99.067
38	623.27	16.419	3254631	60	[M+H]+	12C	96.905
7	610.2	19.062	1555103	73	[M+H]+	12C	78.289
17	274.2	6.361	593377	10	[M+H]+	12C	67.553
22	337.2	10.11	517850	24	[M+H]+	12C	67.529
34	365.2	11.824	264928	27	[M+H]+	12C	65.476
14	318.2	6.505	445223	11	[M+H]+	12C	65.295
27	301.2	12.063	207767	30	[M+H]+	12C	65.171
31	233.2	3.879	370915	5	[M+H]+	12C	64.217
23	712.2	19.568	403654	74	[M+H]+	12C	64.174
15	327.2	8.658	204896	17	[M+H]+	12C	63.47
20	536.2	18.428	331674	70	[M+H]+	12C	63.187
2	413.2	17.065	308949	66	[M+Na]+	12C	62.887
16	271.2	6.266	193229	9	[M+H]+	12C	62.426
29	391.2	17.065	299217	66	[M+H]+	12C	62.421
3	406.2	14.873	208016	52	[M+Na]+	12C	62.353
30	659.2	15.245	198549	53	[M+H]+	12C	61.894
32	362.2	6.617	107464	13	[M+H]+	12C	61.498
18	352.2	12.28	132721	34	[M+H]+	12C	61.328
28	437.2	9.493	160244	21	[M+H]+	12C	61.298
33	453.2	9.487	110575	20	[M+H]+	12C	61.245
25	667.2	15.941	76626	55	[M+H]+	12C	61.133
26	438.2	12.736	80943	40	[M+H]+	12C	60.949
36	526.2	12.664	75591	38	[M+H]+	12C	60.861
4	409.2	8.202	85933	16	[M+Na]+	12C	60.852
35	185.2	2.939	96775	2	[M+H]+	12C	60.802
24	666.2	17.003	80932	65	[M+H]+	12C	60.575
9	387.2	8.202	59322	16	[M+H]+	12C	60.442
6	425.2	8.202	63529	16	[M+K]+	12C	60.441
40	689.2	15.946	81081	56	[M+H]+	12C	60.42
39	385.2	13.871	60560	49	[M+H]+	12C	60.403
12	496.2	13.471	64613	46	[M+H]+	12C	60.343
37	384.2	14.873	80143	52	[M+H]+	12C	60.219
10	142.2	3.356	84723	4	[M+H]+	12C	59.996
19	629.2	19.924	61875	76	[M+H]+	12C	59.81
11	929.2	18.556	26545	71	[M+H]+	12C	59.423
1	645.2	16.419	760054	59	[M+Na]+	12C	47.754
8	652.2	17.426	497336	68	[M+H]+	12C	45.681

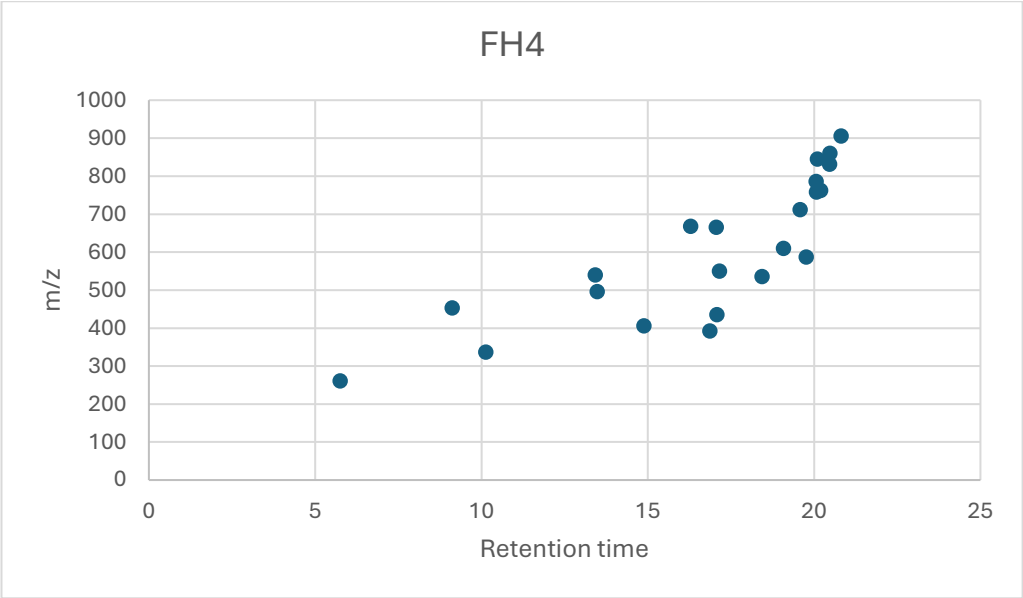

Figure A 11 shows the scatter plot of ion peaks in the FH4 fraction of retention time against m/z using the ACD lab software.

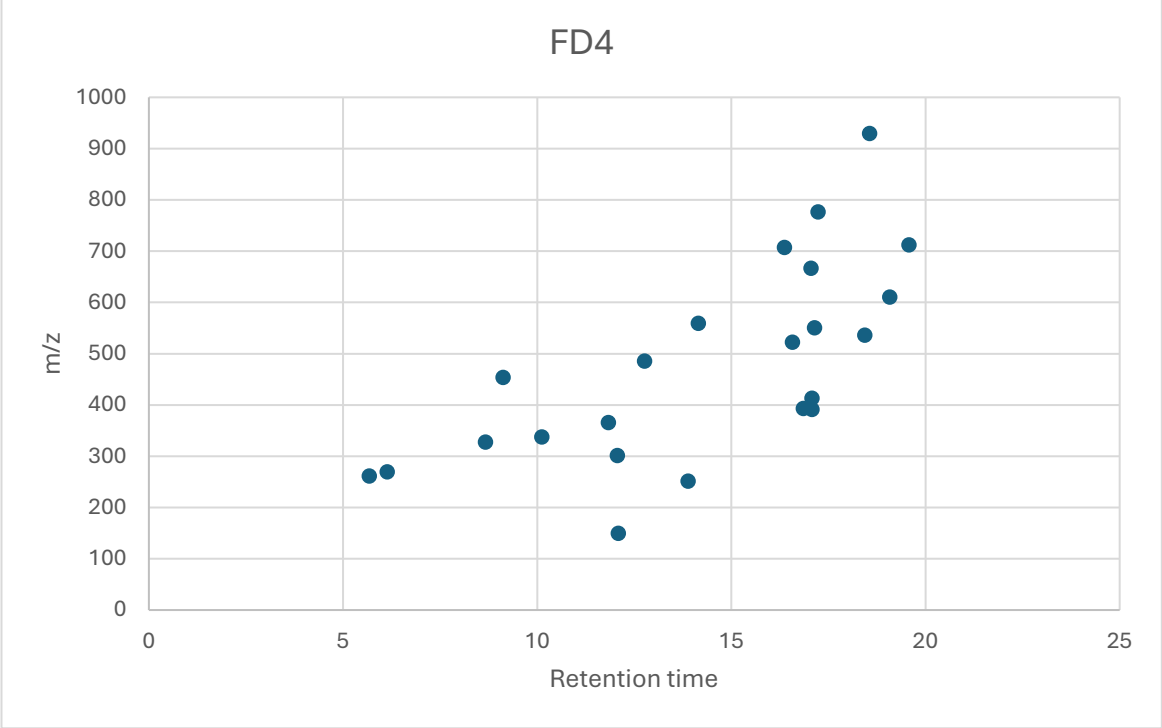

Figure A 12 shows the scatter plot of ion peaks in the FD4 fraction of retention time against m/z using the ACD lab software.

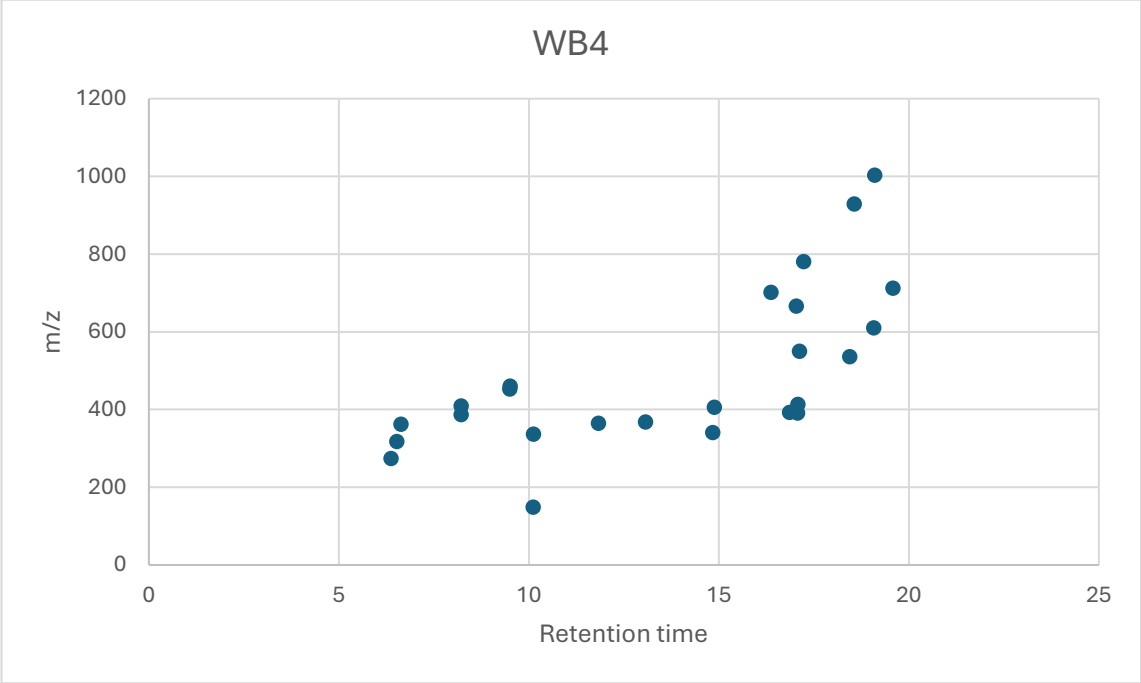

Figure A 13 shows the scatter plot of ion peaks in the WB4 fraction of retention time against m/z using the ACD lab software.

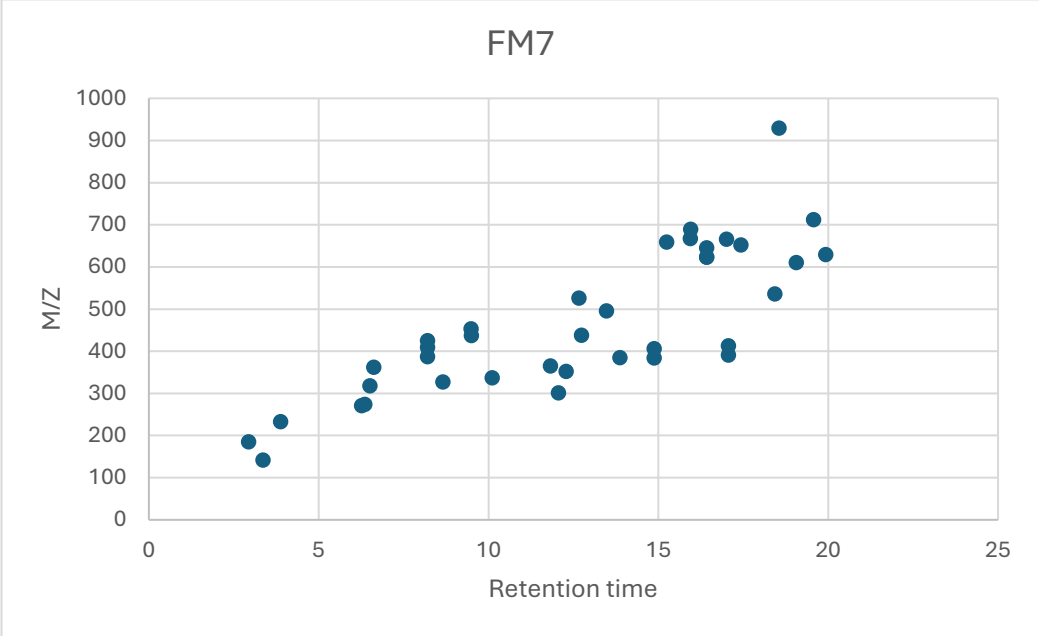

Figure A 14 shows the scatter plot ion peaks in the FM7 fraction of retention time against m/z using the ACD lab software.

4.0 NMR

4.1 1D and 2D NMR spectrum of compound FH4.

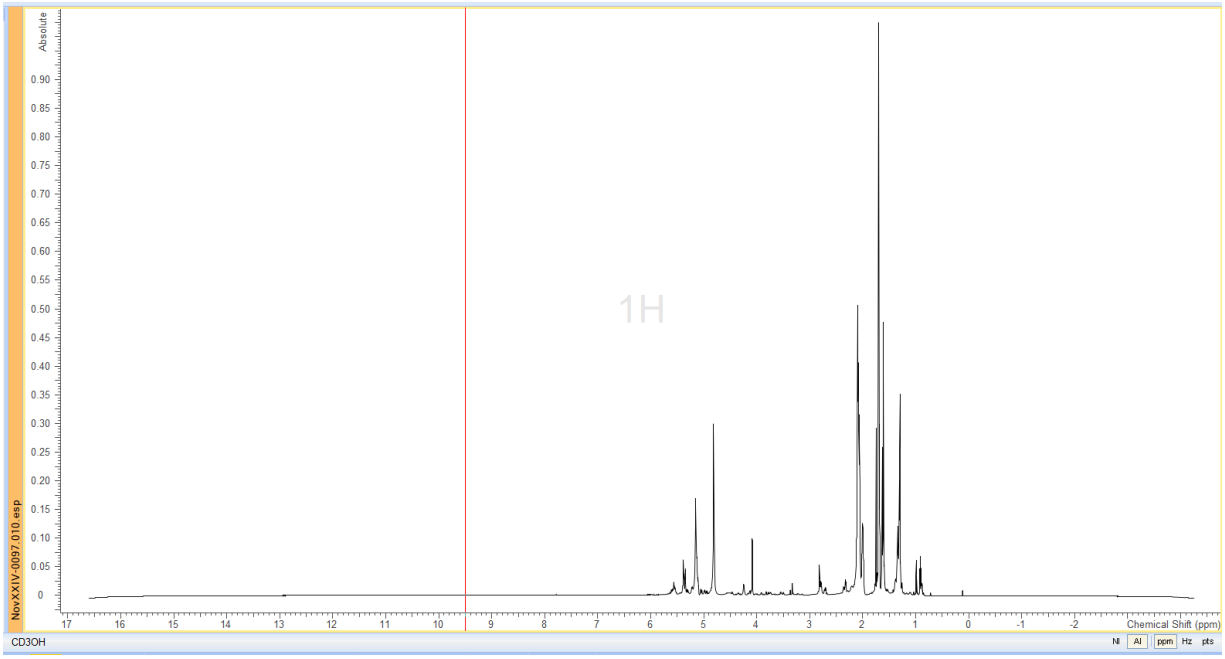

Figure A 15 shows the ^{1}H NMR spectrum of the FH4 compound at 800 MHz in CD_3OD.

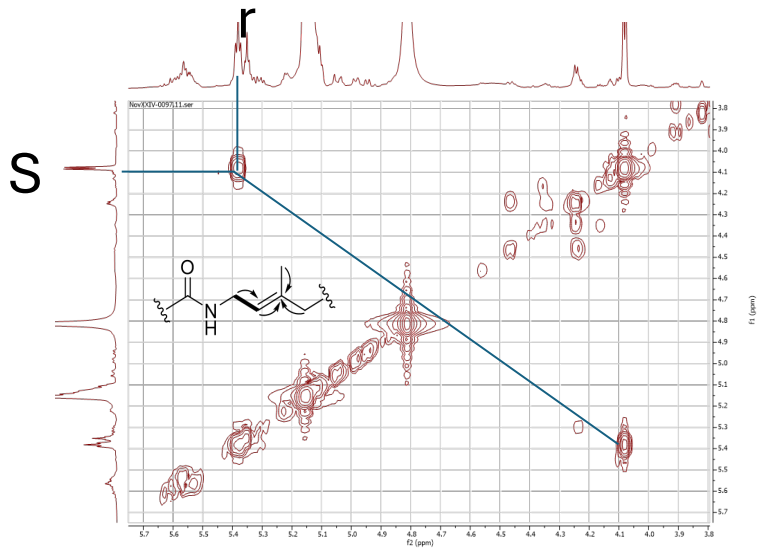

Figure A 16 COSY spectrum corelations between the CH_2 group (S2) and the vinyl proton (r).

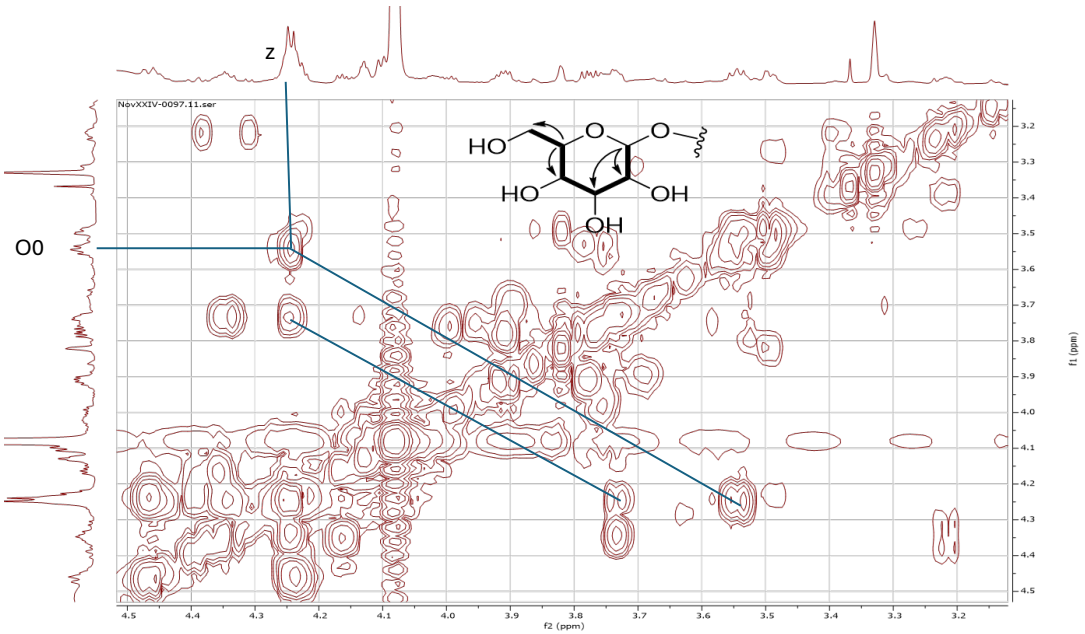

Figure A 17 COSY spectrum showing anomeric proton correlations to neighbouring proton.

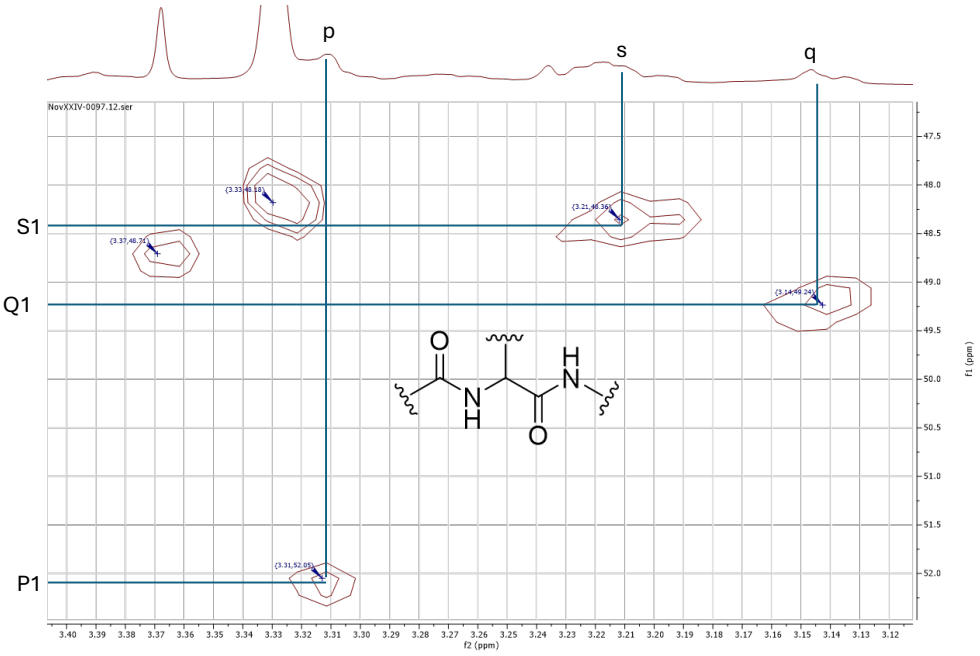

Figure A 18 HSQC spectrum showing chemical shifts of protons possible associated to peptides/amino acids.

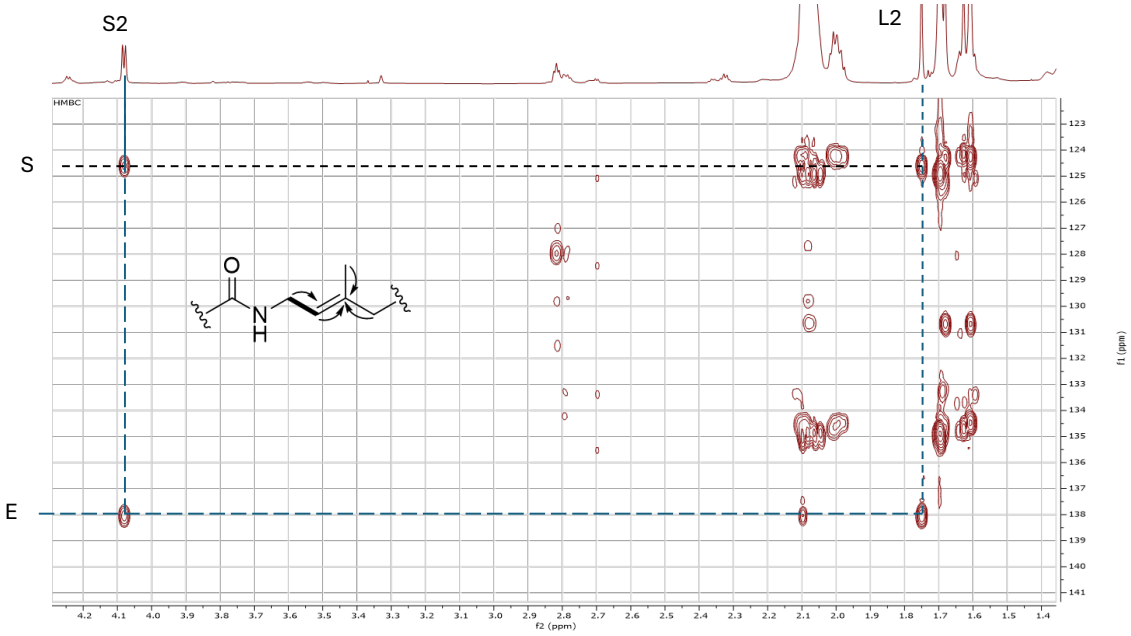

Figure A 19 HMBC spectrum corelations showing correlations between the methyl group (L2) and the CH_2 group (S), and the quaternary carbon to both the methyl group and the CH_2 group confirming this existence of this substructure.

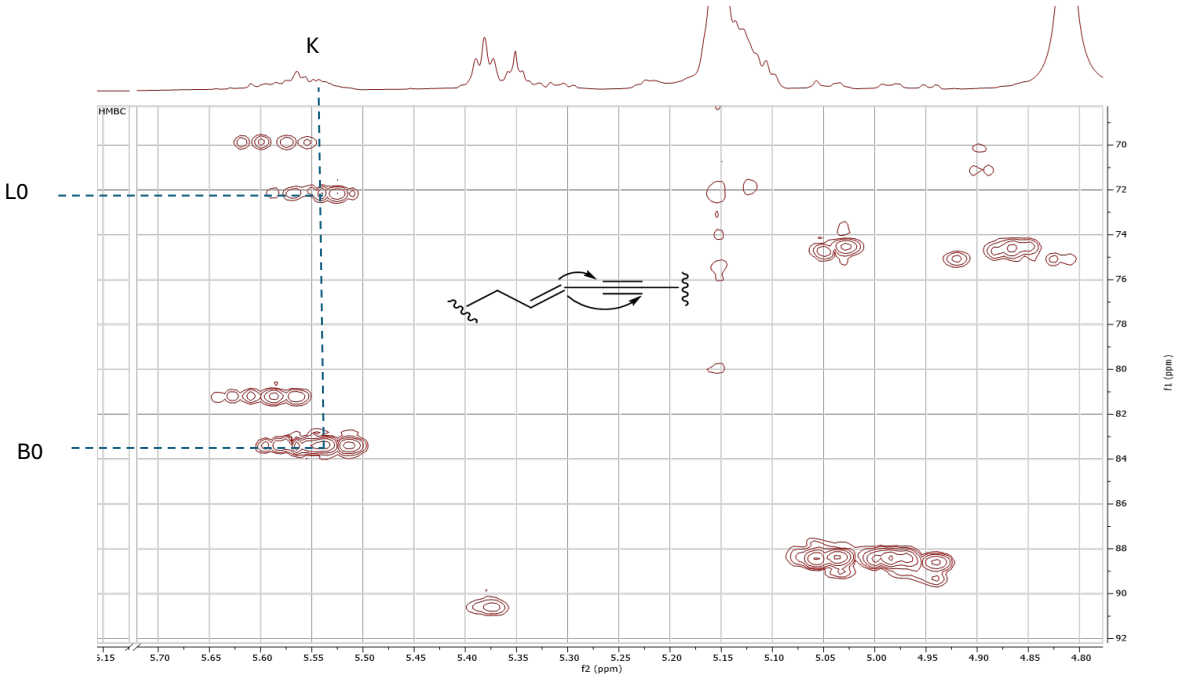

Figure A 20 HMBC spectrum showing correlations between neighbouring alkene protons to the alkyne bond.

Table A13 shows the ^{1}H, ^{13}C, ^{1}H-^{1}H COSY, ^{1}H-C^{13}HMBC NMR Data of FH4 compound.

Carbon Position	**^{13}C (ppm)**	**C type**	**^{1}H/ppm proton count**	**COSY H-H**	**HMBC H to C**
A	173.8	C			
B	173.4	C			
C	173.2	C			
D	172.9	C			
E	138.02	C			
F	137.49	CH	5.54, 1H, Multiplet	j	J2, E2
G	135.55	CH	5.61, 1H, Multiplet		
H	134.67	CH	5.56, 1H, M		F2, X1
I	134.15	CH	5.57, 1H, M		X1, M2
J	131.51	CH	5.39, 1H, M	f	L2
K	129.75	CH	5.37, 1H, M		
L	127.99	CH	5.53, 1H, M		Y1
M	126.94	CH	5.31, 1H, M		
N	125.53	CH	5.22, 1H, M		
O	125.45	CH	5.22, 1H, M		
P	125.00	CH	5.54, 1H, M		P2
Q	124.96	CH	5.12, 1H, M	a2	V1, X1, O2
R	124.89	CH	5.38, 1H, M		
S	124.62	CH	5.38, 1H, M		A2

T	124.30	CH	5.18, 1H, M		F2
U	124.29	CH	5.12, 1H, M		
V	124.12	CH	5.15, 1H, M	i2	
W	113.20	CH_2	4.94, overlap		
X	111.58	CH_2	A: 5.04 bd B: 4.98 bd		A0
Y	108.96	CH_2	A: 5.02 bd B: 4.86 bd		
Z	104.08	CH	4.24, overlap		C2
A0	90.55	CH	bm (broad multiplet)		Xa, Xb
B0	83.44	CH	4.24, bm		
C0	79.12	CH	3.53		
D0	76.48	CH	3.39, bm		
E0	76.48	CH	3.31, bm		
F0	75.25	CH	3.53, bm		
G0	75.08	CH	3.99, bm		
H0	74.90	CH	3.59, bm		
I0	74.35	CH	4.01, bm		
J0	73.50	CH	3.22, bm		
K0	73.32	CH	3.50, bm		
L0	72.30	CH	3.73, bm		
M0	71.91	CH	3.56, bm		
NO	71.74	CH	4.05, bm		

O0	70.86	CH	3.54, bm		
P0	70.68	CH	3.26, bm		
Q0	70.16	CH	3.75, bm		
R0	70.16	CH	3.31, bm		
S0	70.33	CH	5.29, bm		
T0	70.16	CH	3.75, bm		
U0	69.63	CH	3.93, bm		
V0	69.29	CH	5.28, bm		
W0	68.93	CH	3.82, bm		
X0	68.75	CH	3.86, bm		
A1	67.69	CH_2	A: 3.91, overlap B: 3.78, overlap		
B1	67.46	CH_2	A: 3.97, overlap B: 3.76		
C1	66.99	CH	4.03, overlap		
D1	66.29	CH_2	A:3.91 B:3.70		
E1	64.98	CH_2	4.16, bm		
F1	64.62	CH_2	4.13, bm		
G1	63.68	CH_2	4.39, bm		
H1	63.54	CH_2	A: 4.34, bm B: 4.24, bm		
I1	62.59	CH_2	A: 4.35 B: 4.13		

J1	62.00	CH_2	A: 4.35 B:4.13		
K1	61.82	CH_2	3.53, bm		
L1	61.42	CH_2	3.73, bm		
M1	61.33	CH_2	3.89, bm		
N1	60.90	CH_2	3.76, bm		
O1	60.22	CH_2	3.67, bm		
P1	52.05	CH	3.31, bm		
Q1	49.24	CH	3.14, bm		
R1	48.71	CH_3	3.37, bm		
S1	48.36	CH	3.21, bm		
T1	48.18	CH_2	3.33, bm		
U1	42.56	CH_2	2.70, bm		
V1	39.57	CH_2	2.00, bm		Q, O2, E2
W1	37.99	CH_2	1.60, bm		N2
X1	35.52	CH_2	1.99, bm		I, Q, H
Y1	34.82	CH_2	2.79, bm		L
Z1	33.77	CH_2	2.13, bm		
A2	32.01	CH_2	2.06, bm	q, i2	S, J2, L2
B2	31.83	CH_2	1.29, bm		
C2	29.55	CH_2	A:1.39 B:1.30		Z
D2	29.02	CH_2	1.32, bm		
E2	26.91	CH_3	1.26, bm		F, V1

F2	26.38	CH_2	2.10, bm	l2	T, H
G2	24.99	CH_3	1.68, bs (broad singlet)		
H2	24.80	CH_2	1.63, bm		
I2	22.87	CH_3	1.70, bs	v, a2	A2
J2	22.84	CH_3	1.75, bs		F
K2	22.34	CH_2	2.01, bm		
L2	22.16	CH_3	0.90, bt (broad triplet)	f2, m2	J, A2
M2	21.28	CH_3	1.32, overlap	l2	I
N2	19.35	CH_3	0.88, bt		W1
O2	16.89	CH_3	1.61, bt		Q, V1
P2	15.31	CH_3	1.62, bs		Q
S2	58.03	CH_2	Broad multiplet		

4.2 1D and 2D NMR spectrum of compound FM7

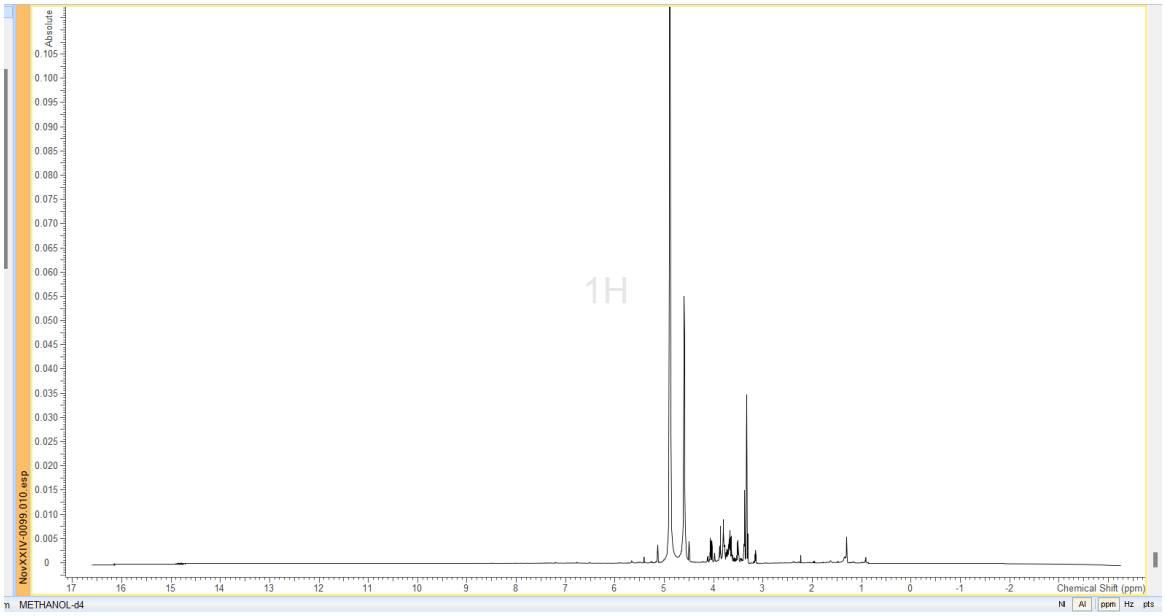

Figure A 21 shows the ^{1}H spectrum of FM7 compound at 800 MHz in CD_3OD.

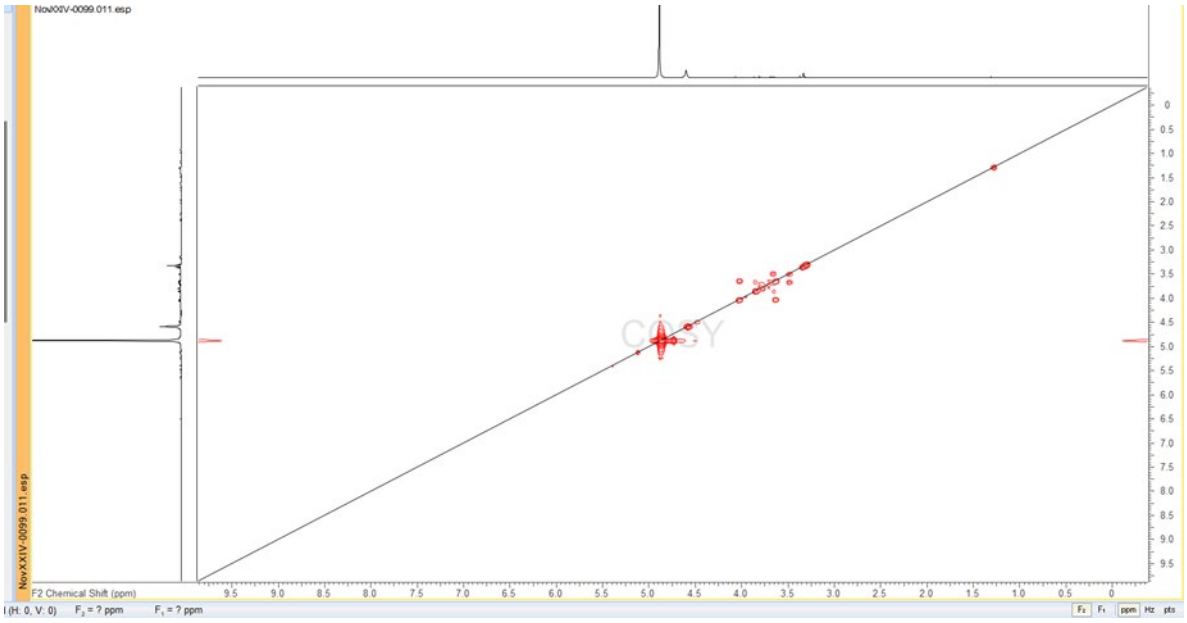

Figure A 22 shows the COSY of FM7 compound.

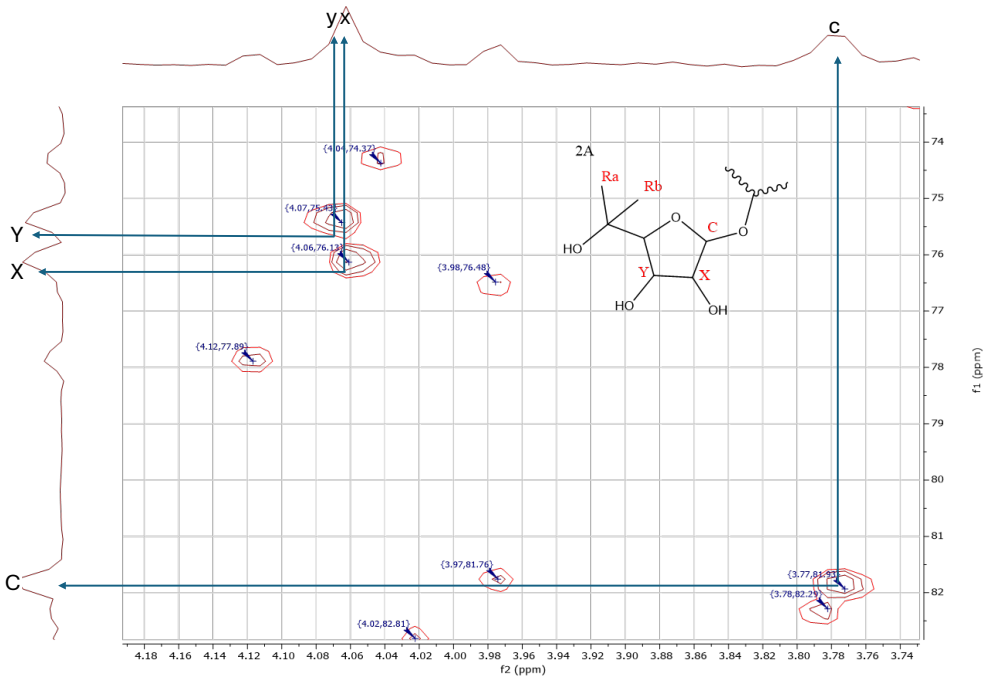

Figure A 23 shows the HSQC spectrum showing chemical shifts of protons possible associated to the five membered sugar ring.

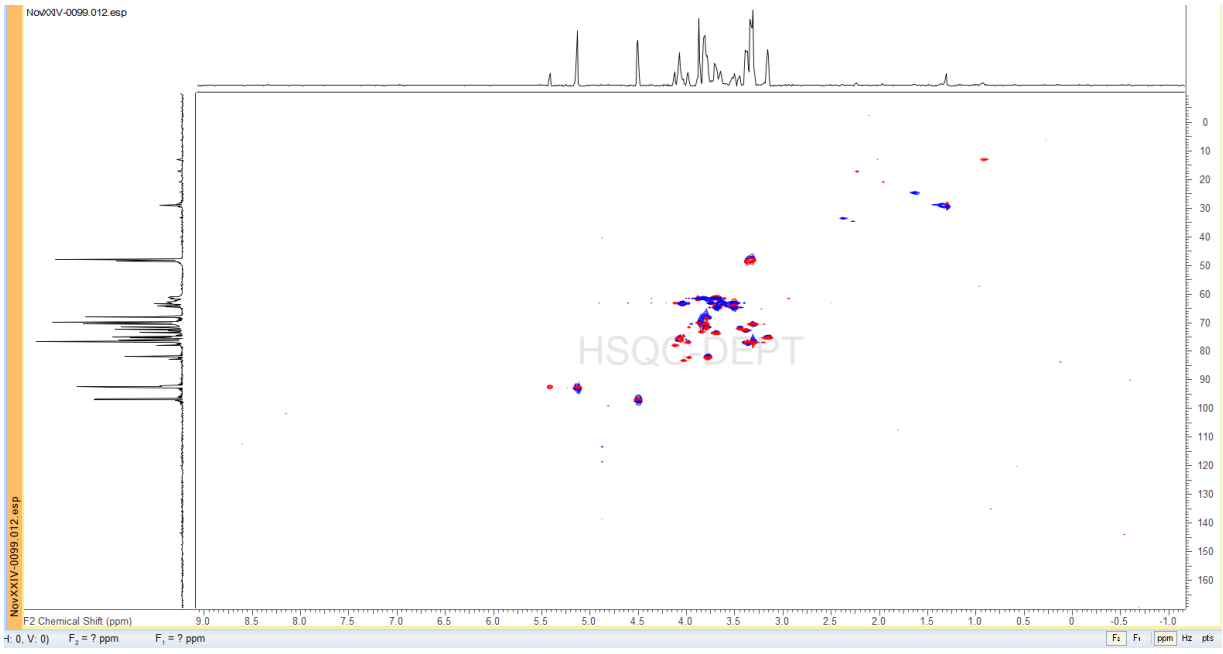

Figure A 24 shows the HSQC-DEPT of FM7 compound.

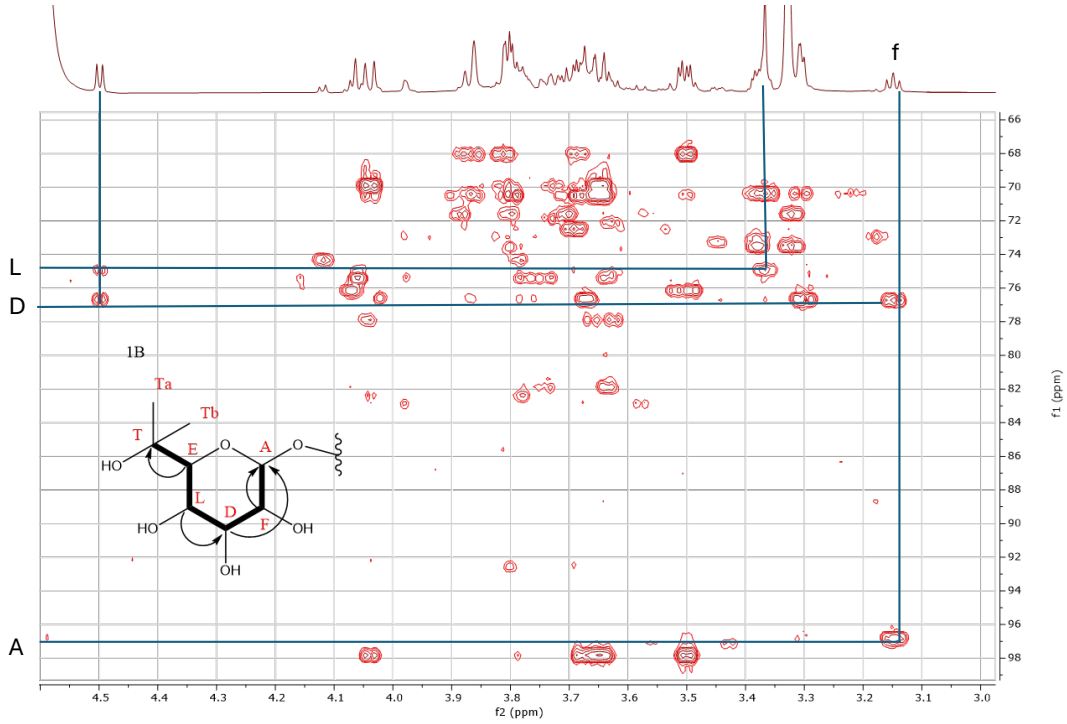

Figure A 25 shows the selected HMBC correlations for proposed structure of the partial structure of FM7.

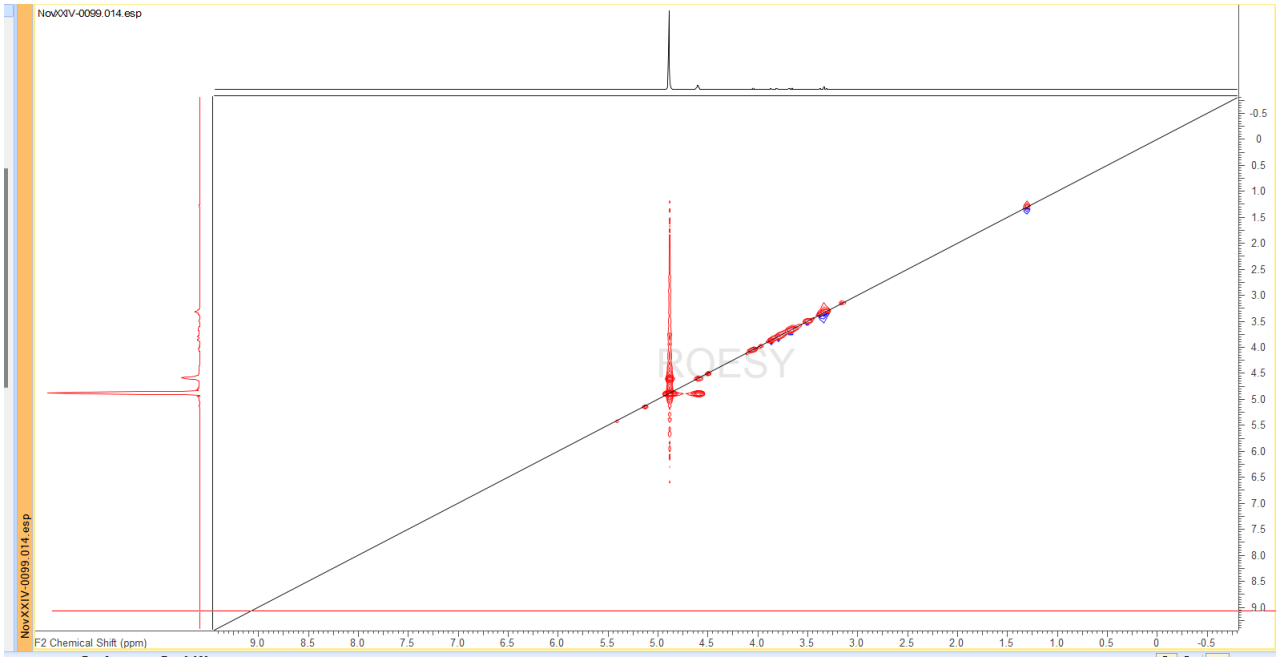

Figure A 26 shows the ROSEY of FM7 compound.

Table A14 shows the ^{1}H, ^{13}C, ^{1}H-^{1}H COSY, ^{1}H-C^{13}HMBC NMR Data of FM7 compound.

Carbon Position	**^{13}C (PPM)**	**C-type**	**^{1}H/ppm proton Count**	**COSY H-H**	**HMBC H to C**
A	96.83	CH	4.50, 1H, d, 7.8	f	D
B	92.56	CH	5.13, 1H, d, 3.6	h	H, I
C	81.87	CH	3.77, 1H, overlap	x	Y
D	76.67	CH	3.36, 1H, overlap	f, l	A, L
E	76.61	CH	3.30, 1H, overlap	d, l, t	T
F	74.89	CH	3.15, 1H, t, 8.7, 8.6	a,d	A, D
G	73.49	CH	3.69, 1H, overlap	h, k	B
H	72.40	CH	3.38, 1H, overlap	b, g	G
I	71.57	CH	3.80, 1H	g, u	B, G
J	70.43	CH	3.81, 1H	-	-
K	70.51	CH	3.32, 1H	g, i	I, G
L	70.33	CH	3.30, 1H	d, e	D
M	69.83	CH	3.86, 1H	n	N
N	67.99	CH	3.80, 1H	m, p	M
O	64.50	CH_2	A: 3.68, 1H, overlap	q	I

			B: 3.50, 1H		
P	63.15	CH_2	A: 4.04, 1H B: 3.65, 1H	m	M
Q	63.06	CH_2	A: 3.64, 1H B: 3.51, 1H	o	M
R	62.79	CH_2	A: 3.73, 1H B: 3.63, 1H		C, X, Y
S	61.97	CH_2	3.78, overlap	-	-
T	61.45	CH_2	A: 3.87, 1H, overlap B: 3.67, 1H	e	D
U	61.36	CH_2	A: 3.80, 1H B: 3.71, 1H	i	K
X	76.09	CH	4.06, 1H, d	c, y	Y
Y	75.33	CH	4.06, 1H, d	x,	X